TAMPEREEN TEKNILLINEN YLIOPISTO
TAMPERE UNIVERSITY OF TECHNOLOGY

Elisa Isotahdon

Corrosion Losses, Mechanisms and Protection Strategies for Sintered Nd-Fe-B Magnets

Julkaisu 1459 • Publication 1459

Tampere 2017

Tampereen teknillinen yliopisto. Julkaisu 1459
Tampere University of Technology. Publication 1459

Elisa Isotahdon

Corrosion Losses, Mechanisms and Protection Strategies for Sintered Nd-Fe-B Magnets

Thesis for the degree of Doctor of Science in Technology to be presented with due permission for public examination and criticism in Festia Building, Auditorium Pieni Sali 1, at Tampere University of Technology, on the 3rd of March 2017, at 12 noon.

Tampereen teknillinen yliopisto - Tampere University of Technology
Tampere 2017

ISBN 978-952-15-3911-4 (printed)
ISBN 978-952-15-3920-6 (PDF)
ISSN 1459-2045

ABSTRACT

The need for permanent magnets has increased with the advances in modern renewable energy technologies and electric vehicles. Sintered Nd-Fe-B magnets are, so far, the best alternative for light constructions, since their energy density is superior compared to other permanent magnet materials. They have good magnetic properties, but the stability under elevated temperatures and in humid environments is limited.

The aim of this thesis was to gain a deeper understanding of the corrosion behavior of sintered Nd-Fe-B magnets and to provide a basis for selecting a proper corrosion protection method. Typical methods for the improvement of the corrosion resistance include cobalt alloying and the use of coatings and surface treatments, all of which were investigated in this work. Furthermore, the objective was to correlate losses in the magnetic flux with the weight losses during the corrosion tests.

The microstructure of the magnets was characterized before and after the corrosion tests to reveal the degradation mechanisms in different environments. Accelerated cabinet testing and electrochemical measurements were utilized. Electron microscopy studies were used to discover the mechanisms and to estimate the relationship between accelerated corrosion tests and applications.

Corrosion tests were performed in the presence of water as vapor and pressurized vapor, immersed in water, in salt spray and under immersion in saline solution. Pressurized water vapor was found to be the most aggressive corrosion environment among the studied cases. It introduced both inter-granular corrosion, i.e., pulverization, and general corrosion of the $Nd_2Fe_{14}B$ phase. Cobalt alloying inhibited the pulverization tendency of the magnets. Pressurized heat-humidity tests measured well the tendency for pulverization but did not reveal the tendency for general corrosion of the magnetic phase. Immersion in pure water introduced a new type of degradation mechanism in the microstructure of sintered Nd-Fe-B magnets, where the matrix phase of the magnet was preferentially corroded.

In mild heat-humidity environments, the uncoated magnets benefit from modified surface finish so that the initiation of corrosion on the surface of the magnet is hindered. In the case of coated magnets, the principal factor influencing the corrosion performance was the quality of the metallic coating.

The most efficient method to evaluate the overall corrosion performance of a permanent magnet material was to perform accelerated tests so that the specimens are magnetized and

the losses in weight and magnetic flux are measured simultaneously. The results from the corrosion tests on magnetized specimens showed that the microcrystalline anisotropy of the sintered magnets resulted in heterogeneous corrosion, where the pole faces degraded preferentially to the side faces. However, the geometry of the magnet affected the resulting losses also by another way – the self-field of the magnet contributed to the second stage of corrosion, i.e., the detachment of the magnetic grains when the gluing grain boundary phase had dissolved. Due to the differences in the initiation rate of corrosion, the measured flux losses varied between parallel specimens. However, the corresponding percentage weight losses were always smaller than the flux losses indicating that the flux losses do not originate from the material losses only.

PREFACE

This work was carried out at the Department of Materials Science, Tampere University of Technology, during the years 2012-2016. The work was supervised by Professor Veli-Tapani Kuokkala and Docent Elina Huttunen-Saarivirta, to whom I would like to address my gratitude. Dr. Martti Paju, former Director of Prizztech Magnet Technology Centre, is also acknowledged for the interesting topic and guidance into the world of permanent magnets.

I am grateful for the financial support for this work that I got from multiple sources. The idea of the thesis was found in a research project coordinated by Prizztech Magnet Technology Centre funded by Satakunta Centre of Expertise. The main part of the thesis work was funded by a three-year personal grant from Jenny and Antti Wihuri Foundation that enabled me to focus on the experiments and writing of the publications. The last phase of the work, the writing of this dissertation was supported by K.F. and Maria Dunderberg Foundation grant. Neorem Magnets Oy is acknowledged for providing the sample materials and the possibility to use their laboratory facilities during the work. The City of Tampere Science Foundation funded the printing costs of this thesis.

Finally, I would like to thank my colleagues, friends and family for their support and encouragement over the years.

Tampere, February 2017

Elisa Isotahdon

TABLE OF CONTENTS

ABSTRACT

PREFACE

TABLE OF CONTENTS

LIST OF PUBLICATIONS

AUTHOR'S CONTRIBUTION

LIST OF TERMS AND ABBREVIATIONS

1 INTRODUCTION 1

1.1 Motivation 1

1.2 Corrosion 2

1.3 Sintered Nd-Fe-B magnets for motor and generator applications 3

1.3.1 Research and development trends 4

1.3.2 Microstructure 5

1.3.3 Alloying elements 7

1.3.4 Protective coatings 8

1.4 Corrosion losses in permanent magnets 10

1.4.1 Corrosion mechanisms of sintered Nd-Fe-B magnets 11

1.4.2 The nature of losses in permanent magnets 12

1.4.3 Measurement and detection of corrosion 12

2 THE AIM AND SCHEME OF THE THESIS 15

3 EXPERIMENTAL PROCEDURES 18

3.1 Materials 18

3.2 Corrosion tests 20

3.2.1 Corrosion exposures 20

3.2.2 Electrochemical measurements 22

3.3 Material characterization 22

3.3.1 Microscopy and profilometry 23
3.3.2 Contact angle analysis 23
3.4 Measurement of losses in the magnetic flux 24
3.4.1 Stabilization heat treatment 24
3.4.2 Losses in the magnetic flux 24
3.4.3 Demagnetization 26
4 RESULTS AND DISCUSSION 27
4.1 Corrosion protection strategies and the microstructure 27
4.1.1 Composition 28
4.1.2 Surface finish 35
4.1.3 Coatings 39
4.1.4 Summary of the corrosion protection 44
4.2 Corrosion mechanisms and rates 45
4.2.1 Different mechanisms observed under heat-humidity exposure 45
4.2.2 Immersion 48
4.2.3 Summary of the corrosion mechanisms 54
4.3 Degradation of the magnetic properties due to corrosion 56
4.3.1 Thermal stabilization treatment 57
4.3.2 Corrosion of magnetized specimens 58
4.3.3 Development of the losses in the magnetic flux 62
4.3.4 Summary of the flux losses 63
5 CONCLUDING REMARKS 65
5.1 Novel scientific conclusions 65
5.2 Research questions revisited 66
5.3 Suggestions for future work 68
REFERENCES 69

APPENDIX: ORIGINAL PUBLICATIONS

LIST OF PUBLICATIONS

The thesis is based on the work reported and discussed in the following publications, which will hereafter be referred to as follows:

I Corrosion behaviour of sintered Nd-Fe-B magnets
Elisa Isotahdon, Elina Huttunen-Saarivirta, Veli-Tapani Kuokkala, Martti Paju, Materials Chemistry and Physics 135(2012) pp. 762-771

II Corrosion protection provided by electrolytic nickel and tin coatings for Nd-Fe-B magnets
Elisa Isotahdon, Elina Huttunen-Saarivirta, Veli-Tapani Kuokkala, Laura Frisk, Martti Paju, Journal of Alloys and Compounds 585(2014) pp. 203-213

III Corrosion mechanisms of sintered Nd-Fe-B magnets in the presence of water as vapour, pressurized vapour and liquid
Elisa Isotahdon, Elina Huttunen-Saarivirta, Saara Heinonen, Veli-Tapani Kuokkala, Martti Paju, Journal of Alloys and Compounds 626(2015) pp. 349-359

IV Development of Magnetic Losses During Accelerated Corrosion Tests for Nd-Fe-B Magnets Used in Permanent Magnet Generators
Elisa Isotahdon, Elina Huttunen-Saarivirta, Veli-Tapani Kuokkala, CORROSION 72(2016)6, pp. 732-741

V Corrosion Losses in Sintered (Nd, Dy)–Fe–B Magnets for Different Geometries
Elisa Isotahdon, Elina Huttunen-Saarivirta, Veli-Tapani Kuokkala, Martti Paju, IEEE Magnetic Letters 7(2016), no. 5500504

VI Characterization of the microstructure and corrosion performance of Ce-alloyed Nd-Fe-B magnets
Elisa Isotahdon, Elina Huttunen-Saarivirta, Veli-Tapani Kuokkala, Journal of Alloys and Compounds 692(2017) pp. 190-197

AUTHOR'S CONTRIBUTION IN PUBLICATIONS

Elisa Isotahdon is the main author of all the six Publications (I-VI). She planned, organized and carried out the corrosion experiments, analyzed the results presented in each publication, and prepared the manuscripts. She also conducted most of the electron microscopy studies.

In all the publications, Professor Veli-Tapani Kuokkala and Docent Elina Huttunen-Saarivirta gave advice and commented the manuscripts. Elina Huttunen-Saarivirta participated also in the planning of the electrochemical measurements and provided guidance with the interpretation of the results of the corrosion tests. She also conducted the electron microscopy in Publication I. In Publications I, II, III, V and VI, Dr. Martti Paju and Prizztech Magnet Technology Centre participated in the planning and conducting of the magnetic measurements. Magnet manufacturers contributed to the study by providing the sample materials. In Publication III, the contact angle experiments and analyses were carried out with the help of M.Sc. Saara Heinonen. She also helped with the EDS mapping in Publication IV. Dr. Laura Frisk contributed to the environmental testing in Publication II. All manuscripts were commented by all the co-authors.

LIST OF TERMS AND ABBREVIATIONS

AC	Alternating current
Ag/AgCl	Silver/Silver chloride (electrode)
ASTM	American Society for Testing and Materials
B	Boron
BCT	Bulk Corrosion Test, ASTM standard A1071 / A1071M-11 (2015)
$(BH)_{max}$	Maximum energy product, energy density of permanent magnet
BSE	Backscattered electron
Ce	Cerium
Ce-alloy	Cerium-substituted magnet grade, also denoted as M9
Co	Cobalt
Coercivity	Ability (of a magnet) to resist demagnetization
Curie temperature	Temperature at which a ferromagnetic material becomes paramagnetic
DMF	Demagnetization factor
Dy	Dysprosium
EA	Easy-axis of a magnet, i.e., the energetically favorable direction of spontaneous magnetization
E_{corr}	Corrosion potential
EDS	Energy Dispersive X-ray Spectrometer
EIS	Electrochemical Impedance Spectroscopy
Fe	Iron
$Fe(OH)_3$	Iron hydroxide
FEG-SEM	Field emission gun scanning electron microscope
FEM	Finite Element Method
GB	Grain boundary
H_2	Hydrogen
H_2O	Water
HAST	Highly Accelerated Stress Test
HD	Hydrogen Decrepitation (process)
HDDR	Hydrogenation Disproportionation Desorption Recombination (process)
HH	Helmholz coil measurement
HRE	Heavy Rare Earth element
IC, ICR	Magnet grade with Improved Corrosion Resistance due to Co alloying, also denoted as M7
i_{corr}	Corrosion current density
ICP	Inductively coupled plasma

IS	Magnet grade with Improved Stability due to Dy alloying, also denoted as M3
KCl	Potassium chloride
Nd	Neodymium
$Nd_2Fe_{14}B$	Composition of the hard magnetic phase in sintered Nd-Fe-B magnets, also called the matrix phase
$Nd_{1.11}Fe_4B_4$	Composition of the boron-rich secondary phase
NdH_3	Neodymium trihydride
NdO	Neodymium (II) oxide
Nd_2O_3	Neodymium (III) oxide
$Nd(OH)_3$	Neodymium hydroxide
Ni	Nickel
O	Oxygen
OCP	Open Circuit Potential
P_C	Permeance coefficient
PCT	Pressure Cooker Test
PM	Permanent magnet
Pr	Praseodymium
PTFE	Polytetrafluoroethylene, brand name Teflon
R_a	Arithmetic mean surface roughness
Ref-A	Standard magnet grade, also denoted as M1
Ref-B	Co-alloyed magnet grade, also denoted as M8
RH	Relative humidity
SE	Secondary electron
SG	Standard grade magnet (i.e., non-alloyed), also denoted as M1 and Ref-A
SEM	Scanning Electron Microscope
Sn	Tin
T	Temperature
T_C	Curie temperature
TRE	Total rare-earth (content) including cerium, praseodymium, neodymium, terbium and dysprosium
wt.%	Percentage by weight
XRF	X-ray fluorescence spectrometry

1 INTRODUCTION

Permanent magnets (PM) play an important role in improving the efficiency and performance of many consumer electronics and industrial devices. The markets of PMs are dominated by two types of magnets: ferrites and rare-earth magnets. Ferrite magnets are cheaper and the production volumes are much higher than those of the rare-earth magnets, but their share of the market is quite equal [1]. Rare-earth magnets' development in the early 1980's resulted in an increasing need for finding a good alternative alloy for strong permanent samarium-cobalt magnets, since the raw materials for them were scarce. In 1984, a new revolutionary permanent magnet material based on the alloy of neodymium, iron and boron was discovered [2]. Sintered Nd-Fe-B magnets had outstanding magnetic properties, being the strongest among the permanent magnet materials in terms of their saturation magnetization and energy density of the material. Therefore, the Nd-Fe-B magnets provide an advantage in terms of smaller size and weight as compared to other permanent magnet materials, as smaller volumes can be used to provide the required magnetic field [3]. Applications for PMs can be found for example in electric power generation and conversion, automotive engineering and sensors, magnetic resonance imaging, and magnetic bearings and couplings [4]. One of the key limiting factors in using Nd-Fe-B magnets is their corrosion resistance, which is the topic of this doctoral thesis.

This thesis is a compilation dissertation based on six scientific publications in the area of the corrosion behavior of sintered Nd-Fe-B magnets. This first part of the dissertation comprises a short theoretic background (Chapter 1) of the studied materials, the methods to improve their corrosion resistance, and the nature of the corrosion losses. The aim and scheme of this study, including the research questions stated, are presented in Chapter 2. The experimental procedures selected to characterize the microstructure and evaluate the corrosion performance of the magnets are presented in Chapter 3. The most important results obtained are collected from the publications and presented and discussed in Chapter 4. Finally, the concluding remarks are stated in Chapter 5. The original publications including all the experimental results are provided as Appendices at the end of the thesis.

1.1 Motivation

The well-known and established applications of permanent magnets include consumer electronic gadgets, hard disc drives and loudspeakers, where corrosion has not been a significant issue due to the dry environments. In the near future, the PM motors are expected to replace most of the electric motors due to the obvious advantages, such as higher torque

and reliability. As motors in general are regarded as devices with the largest energy-saving potential, the growth of PM motors is promoted by energy-saving regulations that result in minimum efficiency standards for motors [5]. Besides regulations for motors, the use of magnets has recently grown due to their increasing use in industrial generator applications, in particular in the area of renewable energy. For example, wind turbine generators are among the fastest-growing application areas of PMs. The role of renewable energy applications for PMs will probably become even more important in the future with the expansion in the wind energy sector, but possibly also in other new energy harvesting systems, such as ocean and tidal energy devices based on permanent magnets [6,7].

In order to serve the desired lifetime as a component of an electric motor or a generator, the magnet materials need to be reliable. One of the key challenges in the use of sintered Nd-Fe-B magnets is their limited stability at elevated temperatures and in humid environments. The corrosion behavior of magnets has been studied by several research groups already from the early 90's, and improvements in the microstructure and good protective coating materials have been presented to decrease the corrosion risks [8,9]. However, now that the potential applications of sintered Nd-Fe-B magnets are expanding from electronics to larger scale industrial motors and generators and the surrounding environment changes from dry air to sea water atmosphere with the possibility of condensation, the corrosion evaluation approach must simultaneously be updated. The differences between these two application areas can be found in the size, shape and composition of the used magnets as well as in the environments they are exposed to during service. Magnets used in hard disc drives and similar applications are designed to withstand mainly dry indoor environments or are even encapsulated hermetically, whereas the motors and generators may be exposed to rough environments and aggressive chemical species, such as chlorides in the offshore conditions. This work has a unique viewpoint, questioning the applicability of the existing knowledge on the evaluation of the corrosion risks of Nd-Fe-B magnets in potential motor and generator applications.

1.2 Corrosion

Corrosion may be defined as a chemical or, more commonly, electrochemical reaction between the metal or alloy and the surrounding environment [10,11]. Electrochemical corrosion necessitates the presence of anodic (electron releasing) and cathodic (electron receiving) reactions, with the anodic oxidation reaction(s) being often of interest in the corrosion studies. Corrosion research, similarly to many other areas of materials science, is a combination of electrochemistry, physics, thermodynamics, surface science, and modeling. The goal of the corrosion studies is to gain understanding on the rates and mechanisms of interaction in order to predict the behavior of a certain type of material in a defined environment. Therefore, this

study includes plenty of material characterization and microscopy of corroded magnets to reveal the corrosion mechanisms.

Corrosion studies are usually motivated by savings and safety. The greatest efforts to avoid corrosion are typically seen in places where metallic structures are holding huge loads or material failures may lead to dramatic accidents, even at the expense of human lives. In factories, the corrosion damage may result in interruptions in the plant operation, which is, again, very costly, and thereby more effort is put on material reliability. Besides the critical applications, the world is full of materials corroding evenly at a slow speed, and in most cases the controlled rusting is acceptable.

The economic costs of corrosion can be divided into direct and indirect costs. Direct costs can be measured by, e.g., replacement costs of the corroded part. Indirect costs are more difficult to measure, since they include the losses of downtime in plants and all sorts of design costs. For example, the cost of a new magnet block for a wind generator would most likely be only a small part of the total corrosion costs, including installation and downtime-costs of the wind turbine. Costs can be considered in terms of money but also through the possible effects on the environment by poisonous leakages, or on safety by fatal accidents [12]. In terms of financial losses, it is said that corrosion is costlier than all other natural disasters combined. For instance, the annual estimates only for the losses in the United States are hundreds of billions of dollars, and generally the estimates of the total costs range from 1 to 5 % of the GNP of each country [13]. In a wider perspective, the unconcern of corrosion protection can be seen as an unnecessary use of natural resources. All in all, numerous studies and statistics show that the costs due to corrosion are significant, independently of how they are calculated.

1.3 Sintered Nd-Fe-B magnets for motor and generator applications

Two well-established techniques are nowadays used for the manufacturing of Nd-Fe-B magnets: powder metallurgical route (sintering) and plastic bonding of magnet powder [14]. The powder metallurgical route is based on the sintering of compositionally heterogeneous fine powder produced by hydrogen decrepitation (HD) and jet-milling that produces anisotropic fully dense magnets. Melt-spinning and hydrogenation-disproportionation-desorption-recombination (HDDR) are the more commonly used methods to produce raw material powder for polymer-bonded magnets. Polymer-bonded magnets are typically isotropic and due to the presence of the non-magnetic polymer binder, they exhibit significantly lower energy densities than the sintered Nd-Fe-B magnets. Therefore, the magnets utilized in motor and generator applications are typically sintered grades, and this work focuses on them.

All Nd-Fe-B magnets have a relatively low Curie temperature, about 310°C, which restricts their use at higher temperatures. The actual maximum operating temperatures of the commercial magnet grades vary between 60°C and 200°C. At higher temperatures, for example samarium-cobalt magnets may be employed, as they may be used up to operating temperatures of 350°C [15]. The energy product of the magnet is calculated based on the remanence and coercivity of the magnet material and often used as a key indicator of the performance or strength of permanent magnets. The maximum energy product $(BH)_{max}$ for a typical Nd-Fe-B magnet is 350 kJ/m^3 at room temperature. For an isostatically pressed sintered Nd-Fe-B magnet it amounts to 415 kJ/m^3 [16]. For comparison, the typical energy product of ferrite magnets is about 34 kJ/m^3 and that of samarium-cobalt magnets 150-220 kJ/m^3[1].

In some applications, also the mechanical properties may become important [16]. Sintered magnets are generally hard and brittle, and the brittleness makes machining and handling of the components laborious and expensive [17]. Sintered Nd-Fe-B magnets always contain some porosity due to the powder metallurgical fabrication method, the density of the magnet depending primarily on the sintering temperature [18]. The magnet composition may also contribute to the density, since a higher rare-earth content and particularly the presence of alloying elements may result in a greater relative amount and better liquid phase sintering properties of the GB phase [19–21].

1.3.1 Research and development trends

The material development in the area of sintered Nd-Fe-B magnets has been constant during the last 30 years, as the production methods have been modernized and new manufacturing routes have been established, and their connection to the microstructure and the key magnetic properties have been recognized. Yet there is a constant need to fill the gap between ferrite and Nd-Fe-B magnets by the discovery of alternative magnetic materials for the fairly expensive Nd-Fe-B magnets, or at least an intermediate permanent magnet material in terms of energy density [22]. The search for alternative alloying elements or new alloys was again peaked when the permanent magnet industry faced a “rare-earth crisis” with the raw material prices escalating significantly in 2011 [23]. Neodymium, dysprosium, praseodymium and terbium are all rare earth elements (REE) used in Nd-Fe-B magnets. European Commission has categorized REEs as critical raw materials not only due to their limited availability but also because of the environmental issues in their extraction process [24]. These facts have directed the research to searching for modified compositions and options for using less expensive and less polluting elements. Still, the superior magnetic properties of Nd-Fe-B magnets are the reason why their use is growing all the time.

During the past few years, the emphasis of the research on sintered Nd-Fe-B magnets has been on modifying the chemistry and distribution of the grain boundary (GB) phase [3,14]. The

GB phases and the areas of the matrix phase $Nd_2Fe_{14}B$ grains near the grain boundaries are critical to ensure high coercivity, i.e., the ability of the magnet to withstand demagnetization. Demagnetization may arise from thermal demagnetization or electric or magnetic circuits present. The push towards the use of hybrid and electric vehicles has promoted the use of strong permanent magnets in motors, where magnets need to withstand both of the above-mentioned demagnetizing factors [3]. The operational temperatures, where the magnets do not demagnetize can be increased closer to the Curie temperature by modifying the microstructure. Alloying by dysprosium has been the primary method to ensure the thermal stability. In order to withstand temperatures up to 200°C, as needed for example when used in the motors of electric vehicles, approximately one third of the neodymium in the alloy needs to be replaced by dysprosium [25]. However, dysprosium is one of the most expensive and critical heavy rare earth (HRE) elements, the use of which should be avoided if possible [26]. The attempt to decrease the overall HRE content of the magnets without sacrificing the thermal stability has been approached in the literature by using a diffusion processing of the grain boundaries, reduction of the grain size, and the use of other alloying elements to replace the HREs [27–29].

Recently, the use of cerium as the substituent for neodymium and dysprosium in Nd-Fe-B magnets has shown promising results [30–32]. Cerium is the most abundant rare-earth element and thus a much cheaper element than dysprosium, but it can occupy the same atomic sites as neodymium and dysprosium. Magnets with cerium substitution are not expected to reach as good magnetic properties as those based on neodymium and dysprosium, but they are predicted to be good commercial alternatives for less demanding applications.

Besides the studies on replacing the expensive raw materials in the magnets, much research interest has been lately directed towards the recycling of existing old magnets due to the high raw material prices, since there could be potential to return the expensive materials back to use. Hydrogen decrepitation (HD) process, which is actually used in the production process of sintered alloys to bring the starting alloy into small particles, is now proposed as a promising method to separate the components of the magnets [33]. The hydrogen decrepitation resembles the intergranular corrosion mechanism of the magnets. Therefore, the information gained on the corrosion mechanism research could also have implications on the research concerning the recycling processes [34].

1.3.2 Microstructure

The strongest Nd-Fe-B magnets are produced by powder metallurgy to achieve a well-defined microstructure [16]. The manufacturing process of sintered magnets includes several steps: melting of the nominal alloy, crushing and milling, alignment of the powder in the magnetic field, and then pressing it before the actual sintering [16]. After sintering, several annealing

procedures may be used, followed by machining, coating, and finally magnetizing. This multi-step process results in a microstructure with several phases. Besides processing parameters, also the amount and type of the alloying elements modify the microstructure and properties of the magnet.

The microstructure of sintered Nd-Fe-B magnets is a multiphase system. The $Nd_2Fe_{14}B$ phase is also called the matrix phase as it covers the majority of the microstructure. The phase is a rare-earth intermetallic phase with a high uniaxial anisotropy. The crushed alloy to be sintered consists of single grain particles. Sintering of the aligned finely milled particles is performed at a temperature where the Nd-rich liquid phase densifies the structure. The formation of the Nd-rich GB phase is necessary because it magnetically decouples the $Nd_2Fe_{14}B$ grains [19]. As a result, a structure with the grains of hard ferromagnetic $Nd_2Fe_{14}B$ phase being surrounded by a heterogeneous Nd-rich GB phase is formed. The Nd-rich phase is located as thin layers between the $Nd_2Fe_{14}B$ grains and as larger deposits at the $Nd_2Fe_{14}B$ grain triple junctions. Typical microstructures in a schematic illustration (Figure 1a) and a SEM-BSE image of a fractured magnet (Figure 1b) show the morphological features of the magnets. The grain size of the matrix phase in the sintered Nd-Fe-B magnets is above 1 µm, typically from 5 to 10 µm in modern commercial magnet grades [19]. Most of the grains have an angular shape and from five to seven corners [35].

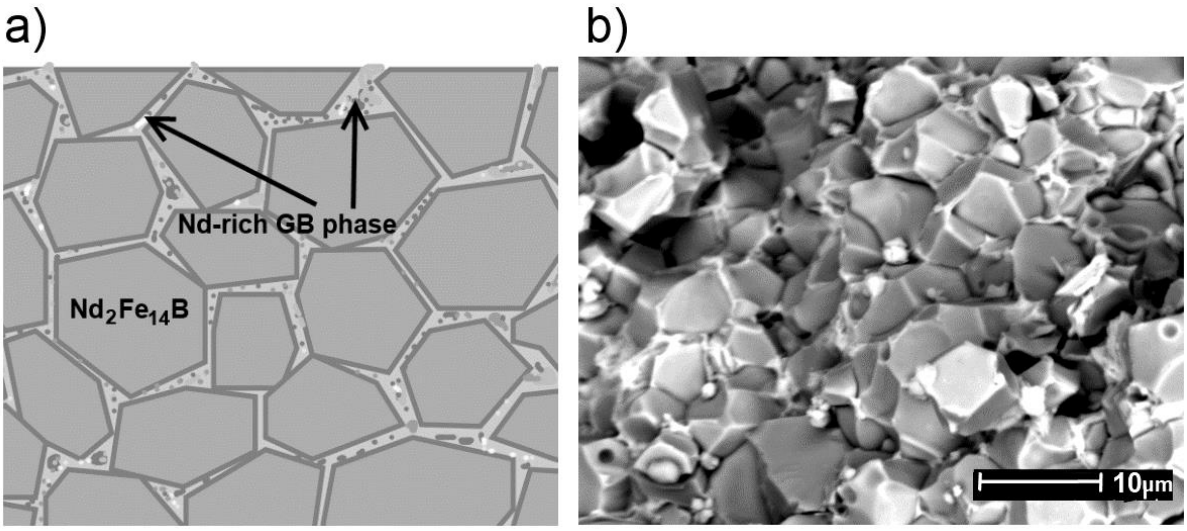

Figure 1. a) Schematic picture of the microstructure of a sintered Nd-Fe-B magnet and b) SEM BSE image of a fractured Nd-Fe-B magnet.

The GB phase is very heterogeneous and can be divided into sub-types [36,37]. It includes both metallic and oxide constituents that may be crystalline or amorphous [38,39]. The triple junction areas of the GB phase consist typically of neodymium oxides Nd_2O_3 and/or NdO, whereas the thin intergranular sections are metallic neodymium [40]. The intergranular Nd-rich

sections less than about 2 nm in thickness are found to be amorphous [41]. According to the phase diagram of Nd-Fe-B [42], also another ternary phase, a boron-rich phase $Nd_{1.11}Fe_4B_4$ may be formed at the sintering temperature. The boron-rich phase has a detrimental influence on the magnetic properties, and the amount of it is minimized with modern manufacturing processes [41]. When present, the boron-rich phase is also located at the GB areas between the matrix phase grains. However, from a corrosion engineering point of view, the distribution and chemistry of the Nd-rich GB phase are the key characteristics controlling the corrosion properties of the magnets.

1.3.3 Alloying elements

Alloying is used to modify the properties of sintered Nd-Fe-B magnets. Alloying elements can be divided into substituent and dopant elements, depending on whether they substitute Nd or Fe in the existing phases or form new phases [43]. Other rare-earths, such as dysprosium and terbium, may substitute Nd atoms, whereas Fe can be substituted by cobalt, nickel or chromium. Dopant elements may partly dissolve in the matrix phase, but in the typical case of low solubility at the sintering temperature, they form precipitates or new phases in the GB areas. Dopants may also affect wetting of the liquid phase [19]. Commonly used dopant elements include, e.g., gallium, copper and niobium [44–46].

The substituent elements change the intrinsic properties, such as the Curie temperature, spontaneous polarization and magnetocrystalline anisotropy, of the magnet. If the dopant elements have solubility in the matrix phase, they also influence these properties. Most of the dopants are primary targeted to the GB phase, where they modify the coercivity and corrosion properties.

Alloying for increasing the corrosion resistance of the magnets is based on the stabilization of the metallic Nd in the GB phase by new elements. Basically all new elements and the developing phases are more noble than the metallic Nd. Cobalt is the most widely used additive in terms of improving the corrosion resistance by the stabilization of active Nd in the GB phase [8,47].

Doping by aluminum nano-particles has also been shown to decrease the corrosion tendency [48] of the magnets. The addition of alloying elements may also lead to the replacement of the Nd-rich phase by secondary phases. Many additives that form compounds with the reactive Nd have been shown to improve the corrosion resistance. New phases formed in the GB in the presence of Co alloying are, e.g., $Nd_3(Co,Fe)$ and $Nd(Fe,Co)_2$ [49]. Indeed, different mixtures of transition metal elements and rare-earth elements have been shown to improve various properties of sintered Nd-Fe-B magnets.The combined additions of Co and Al [50] and

Cu and Co [51] have shown promising results, since small additions of copper and aluminum can compensate for the drop in coercivity due to cobalt additions.

Although not an additive element, oxygen at right amounts can be beneficial to the corrosion performance. Kim *et al.* [52] showed that the corrosion rate of the magnet reached the minimum at the oxygen contents between 0.6 and 1.2 %. In the long-term corrosion tests by Kaszuwara and Leonowicz [53], the controlled oxidation of sintering powders decreased the corrosion rate at the later stages. The critical oxygen concentration required to slow down the corrosion rate without degradation in the other properties is known to be dependent on the neodymium content and the other used alloying elements and amounts in the magnet [37].

From the corrosion protection point of view, additive elements are most effective in the intergranular areas and, therefore, not wanted to dissolve in the $Nd_2Fe_{14}B$ phase. Developments in the manufacturing techniques have made the additions more effective since the desired additive can be selectively added into the targeted regions of the microstructure. Recently, powder blending methods and grain boundary diffusion treatments have been successfully applied to control the distribution of the alloying elements [20,54,55].

This work does not suggest new additive elements or new chemical combinations. Here, the experimental part is conducted using commercial grade magnets. In terms of using alloying elements, the focus of this work is to evaluate the economical and reasonable use of cobalt in the magnet corrosion protection and to compare the effects of cerium alloying with the alloying by cobalt. These are unique approaches, which have not been reported in the literature before.

1.3.4 Protective coatings

Often the corrosion issues of sintered Nd-Fe-B magnets are considered to be easily solved by applying a protective coating as a barrier between the magnet and the environment. Use of a coating, however, introduces a new step in the magnet manufacturing process and another at the end of its lifetime, and adds new challenges to the recycling processes.

The surface of a sintered Nd-Fe-B magnet is demanding for some coating materials. In general, to achieve a good adhesion between the substrate and the coating, pretreatments are used. However, for sintered magnets, the pretreatments usually applied to steel or other common structural materials may be too harsh or ineffective, as many chemicals cause corrosion of the magnet.

The suppliers of Nd-Fe-B magnets generally provide a wide range of different coatings to protect their products against corrosion. For example, epoxy, polytetrafluoroethylene (PTFE, Teflon), nickel-copper-nickel multilayer, nickel, zinc, gold, silver, tin, titanium, chrome, phosphating and combinations of these platings are used commercially [56]. The most

common metallic coating material for Nd-Fe-B magnets is nickel because of the ease of mass production, economical processes, and durability [57]. However, electrochemical nickel plating is a multi-stage process, which may account for as much as 8% of the total production costs of the magnet [58].

The broad selection of available coating materials does not provide a simple solution for the corrosion protection of the magnets. Selection of the coating material is naturally based mostly on the operating conditions [59], but information on the performance of various coatings in the operating environments of the magnets is not widely available. Therefore, selection of the most effective corrosion protection for a specific environment is not always possible. In the literature, advanced coating materials, such as sputtered multilayers [60] or composite coatings [61], are found to show excellent anticorrosive properties, but they are still costly for the commercial use due to the rather low production efficiency. Literature has presented many protective multilayer coatings for the corrosion protection of sintered Nd-Fe-B magnets. Many of the multilayers combine nickel with other metallic layers [62,63], but also SiC-Al and AlN-Al bilayers have shown good results [64,65]. In addition, separate sealing treatments applied on the metallic coatings have shown improvement in the long-term corrosion resistance [66–68]. Various publications have presented good coating solutions [62,69–71], but the studies are mainly comparing the corrosion resistance of a few coating types with the uncoated magnet and not explaining what makes the coating particularly suitable or unusable for sintered Nd-Fe-B magnets. The most widely used coating materials can be roughly divided into groups of metallic and organic coatings. The corrosion protection mechanisms of these coating types are different.

Metallic coatings may protect the substrate material in two ways: firstly, by providing a barrier between the magnet and the environment and secondly, by galvanic protection. The latter occurs when the coating material is more electronegative than neodymium. The standard electrode potential for neodymium is E_0=*-2.323 V*, which is among the lowest values in the electrochemical series [72]. In principle, there are no metallic coatings that could provide galvanic protection to pure neodymium in the GB phase. Achieving an anodic coating to the Nd-Fe-B magnet would be possible, if all the Nd-rich phase could be first removed from the surface. In that case, a coating material with a lower electrode potential than that of the matrix phase should provide cathodic protection. Nevertheless, there are no reports of this approach.

In theory, a defect-free metallic coating is very protective and is typically not easy to deteriorate mechanically, if well attached to the substrate. However, once a cathodic coating is deteriorated, it may form a galvanic couple with the magnet as an anode, a situation which may even accelerate the corrosion of the magnet [66].

Organic coatings, such as epoxies, are electrochemically inert and do not participate in the galvanic reactions. Commercial epoxy coatings for the magnets are numerous [73]. The mechanical properties and thermal and corrosion stability of epoxy coatings for the Nd-Fe-B magnets can be improved by using nanofillers, such as titania particles [74]. Organic coatings can be applied also after assembling the magnets into the motor by impregnation with polymers [59]. However, all organic coatings absorb water, at least to some degree [75]. As a result, moisture and oxygen may penetrate through the coating with time. Thereby, the thickness of the organic coating layer may be used to control the moisture permeation. The corrosion resistance of epoxy films in a salt spray test has been systematically higher than that of the corresponding metallic coatings on Nd-Fe-B magnets [76–78]. For example, in a salt spray study by Codescu *et al***.** [76], metallic zinc and nickel coatings applied on Nd-Fe-B magnets suffered visible corrosion damage within only 24 h, whereas epoxies, depending on the type, showed no evidence of degradation or the formation of corrosion products until 144 h to 200 h of exposure. In addition, Codescu *et al*. [76] studied epoxy resins with different additions of zinc and aluminum powders and found them one of the most resistant coating materials for the protection of Nd-Fe-B magnets against the salt spray environment. As compared to the metallic coatings, organic coatings also have some advantages not related to corrosion. For example, they are electrically insulating and may thus reduce eddy currents in the alternating magnetic fields [59].

As long as the coating on the sintered Nd-Fe-B magnet is undamaged and moisture cannot penetrate to the magnet surface, both coating types behave quite similarly. In the case of a damaged coating layer, different corrosion mechanisms will dominate depending on the selected coating type. This study takes into consideration also the mechanisms and risks of the damaged coating layer, because if the magnet will be installed to, e.g., a rotating machine, the possibility of a mechanical damage, such as scratches, is real.

1.4 Corrosion losses in permanent magnets

In order to prevent the corrosion of sintered Nd-Fe-B magnets, the corrosion mechanisms and extent of losses in different cases must be known. Commonly, accelerated corrosion tests are used for evaluating the uniform corrosion of a material and thereby evaluating the corrosion risks in real (non-accelerated) environments. The test procedures are simple and the results are reported as weight loss per area and often converted to thinning rates, e.g., millimeters per year [79]. There is a constant effort to design corrosion tests that would simulate realistically the actual service conditions of materials and components [80]. Sintered Nd-Fe-B magnets differ from construction materials in their basic physical function. Also the multiphase microstructure combined with the strict microstructural hierarchy is unique in the magnets. In

order to choose or identify the best test methods for evaluating the performance of magnets under real operating conditions, the nature of losses has to be defined. This chapter first presents the corrosion mechanisms of sintered Nd-Fe-B magnets. The origins of polarization losses are then briefly discussed and, lastly, the used methods to evaluate the corrosion of Nd-Fe-B magnets are discussed with respect to losses in the magnetization.

1.4.1 Corrosion mechanisms of sintered Nd-Fe-B magnets

The driving force for corrosion and the reason for the low corrosion resistance of sintered Nd-Fe-B magnets is the potential difference of the phases. The Nd-rich GB phase is compositionally very heterogeneous, but in all cases its potential is lower than that of the matrix phase. The relative amounts of the phases in the magnet, i.e., the smaller volume fraction of the GB phase compared to the matrix phase, thus results in an unfavorable anode-cathode relation, causing rapid corrosion of the anodic GB phase.

Selective corrosion of the Nd-rich GB phase occurs when the magnet is exposed to humidity. Chemical reactions that describe the intergranular corrosion process are here denoted as Equations (1)-(3). Water vapor reacts with the metallic neodymium of the GB phase forming neodymium hydroxide, $Nd(OH)_3$, and hydrogen (Equation 1) [81,82]. The formed hydrogen diffuses along the grain boundaries and further reacts with the neodymium causing volume expansion due to the formation of neodymium trihydride, NdH_3 (Equation 2). Neodymium-hydrides are not stable and they react further with water vapor and are finally transformed into neodymium hydroxides (Equation 3) [82]. The volume expansion by the corrosion product formation accelerates the detachment of the matrix grains.

$$3H_2O + Nd \rightarrow Nd(OH)_3 + \frac{3}{2}H_2 \qquad (1)$$

$$\frac{3}{2}H_2 + Nd \rightarrow NdH_3 \qquad (2)$$

$$NdH_3 + 3H_2O \rightarrow Nd(OH)_3 + 3H_2 \qquad (3)$$

The whole process is called pulverization, as the grains of the matrix phase disintegrate from the magnet surface.

Although the pulverization of magnets has been acknowledged as the primary and the most destructive corrosion mechanism in hot and humid atmospheres, it is not necessarily the only corrosion mechanism the magnet undergoes. In the literature [82] the formation of red rust due to the corrosion of the iron-rich matrix phase is acknowledged, but the mechanism is poorly studied and the conditions under which it occurs are not explored thoroughly. As more than 60 wt.% of the Nd-Fe-B magnet consists of iron, the corrosion of the matrix phase is estimated to

correspond to that of iron and the formation of iron hydroxides $Fe(OH)_3$ being formed in the process [59].

1.4.2 The nature of losses in permanent magnets

Corrosion in general terms is defined as the environmental degradation of a material and typically measured as a weight loss that enables the determination of the corrosion rate. However, what really matters and should be measured in the case of permanent magnets are the losses in the magnetic flux that the magnet is designed to produce. Weakened magnetic flux can result in the malfunction of the component.

Losses in the magnetic flux can be divided into three types of losses: reversible, irreversible, and permanent losses [83]. Reversible losses due to an increase of temperature can be taken into account using the temperature coefficient of remanence. Reversible losses occur as the temperature rises, but the flux is recovered as the temperature decreases. Irreversible losses occur, similarly, when the temperature is increased, but they do not return to the original level when the temperature decreases. Some of the irreversible losses are recoverable by remagnetization of the magnet, whereas some are permanent. Corrosion losses are permanent losses, because they damage the microstructure and thus the properties do not recover with magnetization.

The long-term stability of a permanent magnet is considered as its ability to resist demagnetization. Demagnetization may arise from demagnetizing fields, exposure to high temperatures, or environmental degradation by corrosion [83]. The irreversible losses due to the temperature dependence of coercivity can be taken into account in the design for a specific application, but corrosion introduces material losses that are more complex to model.

Due to their high coercivity, the Nd-Fe-B magnets are designed as thin components, which means that they have relatively great amount of surface area compared to the total volume [84]. This further emphasizes the corrosion risks.

1.4.3 Measurement and detection of corrosion

General practices of testing and ranking sintered Nd-Fe-B magnets in terms of their corrosion resistance are based on the highly accelerated stress test, HAST, which is adapted from the electronics industry and has become a standard used in several literature references [47,82,85]. HAST was originally a test for the reliability of electronic components in severe climates [86,87]. The difference to other chamber corrosion tests and the original idea behind HAST is to use unsaturated autoclave with precision temperature and humidity control to calculate the total acceleration factor for each test. For some reason, the permanent magnet industry simplified the test method but continued to use the name for an unsaturated autoclave

test. Often the term is mixed for example with the Pressure Cooker test (PCT). Some of the PCT tests refer to a standard, but several interpretations are reported, with temperatures typically varying between 125-130°C and relative humidities in the range of 85-100% [88,89]. Some references also report testing in milder heat-humidity conditions, such as at the temperature of 85°C and the relative humidity (RH) of 85 % [90]. In 2011, ASTM released a standard for a test method to evaluate the hygrothermal corrosion resistance of permanent magnet alloys [91], which is very similar to PCT but now called the bulk corrosion test, BCT. This was the first test standard aimed specially at the corrosion testing of permanent magnet materials. However, to the best of our knowledge, the test results from the BCT tests cannot yet be found in open literature apart from Publication VI of this thesis.

Long-term corrosion test results for the sintered Nd-Fe-B magnets are rare in open literature, but a two-year exposure by Kaszuwara and Leonowicz has been published in 1999 [53]. Magnets were kept in dry air at a laboratory atmosphere, which was considered as the operation environment of the magnets at the time of publishing the article. However, nowadays the magnets are placed in more demanding environments. Application-oriented test routines have been used, such as the one by Moore *et al.* [92], which combined several cycles of pre-immersion of the magnets in a salt solution, autoclave testing in a gearbox oil heated to 130 °C, and cooling down to room temperature in air. Some magnet manufacturers use the 85/85 test, the autoclave test, or the salt spray test for evaluating the corrosion resistance of the coated magnets [59]. Still the comparison between the magnet grades is based mainly on the weight losses in HAST or a similar accelerated autoclave test.

Measuring of the weight losses during an accelerated corrosion test is one of the most common tools to estimate and compare the corrosion resistance of materials. In the case of structural materials, such as construction steels, the corrosion rate can even be given only as a value of thinning of the material. However, in the case of permanent magnets, the basic function of the component is entirely different. Permanent magnets used in electric motors and generators must fulfill their basic function: provide the designed magnetic flux. A defined volume of the magnet material is designed to produce a certain field intensity and, therefore, the most interesting losses are not the ones in weight but those in the magnetic flux that the magnet can produce. In order to measure the flux losses, the corrosion tests should be conducted using the specimens in a magnetized state.

Most of the corrosion evaluation of sintered Nd-Fe-B magnets is still done similarly as in the case of other metals, using tests resulting in weight losses, visual and microscopic observations, as well as the electrochemical response of the surface (electrochemical measurements). The common tests, such as salt spray, immersion and heat-humidity exposures, are used to determine the degree of corrosion measured by weight loss. For practical reasons, the tests are basically always conducted for magnets in a demagnetized

state, since the magnetized Nd-Fe-B magnets are challenging to handle. Indeed, most of the experimental work is still conducted using demagnetized specimens; only a few of the studies published in open literature were conducted using magnetized specimens [92–94]. These studies showed that the magnetization state has an effect on the corrosion mechanism and, thereby, also on the extent of losses. Nevertheless, the measured variable should be losses in the magnetic flux rather than (or together with) weight losses in order to predict better to performance of the magnet under the operating conditions.

In the future, corrosion monitoring could be included also in the maintenance program of permanent magnet machines. Detection of the early stages of corrosion in a magnet attached to a motor or even the corrosion under a protective coating or embedding resin is difficult. When the use of traditional laboratory corrosion measurement techniques is not possible, the main approach could be the measurement of the losses in the magnetic flux. Although that may be challenging or even impossible in some cases, it is theoretically the best detection method as it is a non-destructive and doesn't require a direct contact with the magnet. In addition, as will be shown later in this work, the losses in the magnetization can be detected prior to other physical changes, such as weight losses or changes in the appearance [Publication IV]. In order to develop a method for measuring the magnetic losses to characterize the corrosion damage, the theory behind the corrosion mechanisms of magnetized magnets must be studied. In addition, the knowledge needed to separate the other irreversible losses from those originating from corrosion must be developed.

2 THE AIM AND SCHEME OF THE THESIS

The aim of this study is to investigate the corrosion performance of sintered Nd-Fe-B magnets used in motor and generator applications in order to achieve a deeper understanding of their corrosion behavior under operation conditions and to provide a basis for selecting a proper corrosion protection method for the magnets. Another goal is to achieve more knowledge on the corrosion mechanisms of uncoated and coated magnets. Furthermore, also an important goal of this work is to correlate the material losses due to corrosion with the losses in magnetization to understand how the corrosion risks of the magnets should be evaluated.

The research questions of the thesis are as follows:

1. What corrosion protection method should be prioritized in motor and generator applications?
2. What are the relevant corrosion mechanisms in sintered Nd-Fe-B magnets in typical applications?
3. What are the parameters that would best represent the true corrosion losses and could be reliably measured when evaluating the corrosion resistance of magnets?

In order to answer these questions, the corrosion mechanisms of several magnet grades with varying surface topography and different types of coatings were studied. Figure 2 shows a flow chart of the included publications I-VI. The research work started with a screening-type corrosion study including magnets with different compositions [Publication I] and testing of magnets with different types of protective coatings [Publication II]. The goal was to achieve more scientific knowledge on the key characteristics of the coating materials that is needed for a proper corrosion protection of Nd-Fe-B magnets. The obtained results raised a question about the prevailing corrosion mechanisms and criticism against the commonly used corrosion test procedures. In Publication III, these questions were answered, with the scope being limited to the corrosion environments of water, water vapor (humidity), and pressurized water vapor. One of the research hypotheses was that there are measurable threshold values for heat and humidity for each magnet type, where the corrosion mechanism changes from the general corrosion (of the iron rich $Nd_2Fe_{14}B$ phase) to the intergranular corrosion. Naturally, modification of the microstructure and alloying of the Nd-Fe-B magnet influence these values and, therefore, a universal model cannot be discovered. Another hypothesis was that cobalt additions improve the magnet's resistance to intergranular corrosion, but not necessarily the overall corrosion resistance of the sintered Nd-Fe-B magnet. These hypotheses are tackled in Publication III. Publications IV & V concentrated on measuring the losses in the magnetic flux, approaching the fundamental question of true losses due to corrosion and possible losses in the magnetization that the magnets may experience. The formation of corrosion products and

detachment of the magnet material may damage the PM machine, but also the losses in the magnetization are vital with respect to the magnet's functionality. A unique approach of this work is the correlation of the weight and flux losses formed during the corrosion tests of the Nd-Fe-B magnets.

In addition, the current need for the development of heavy rare-earth free magnet grades was taken into account by including a corrosion study of a Ce-alloyed magnet grade in this thesis [Publication VI].

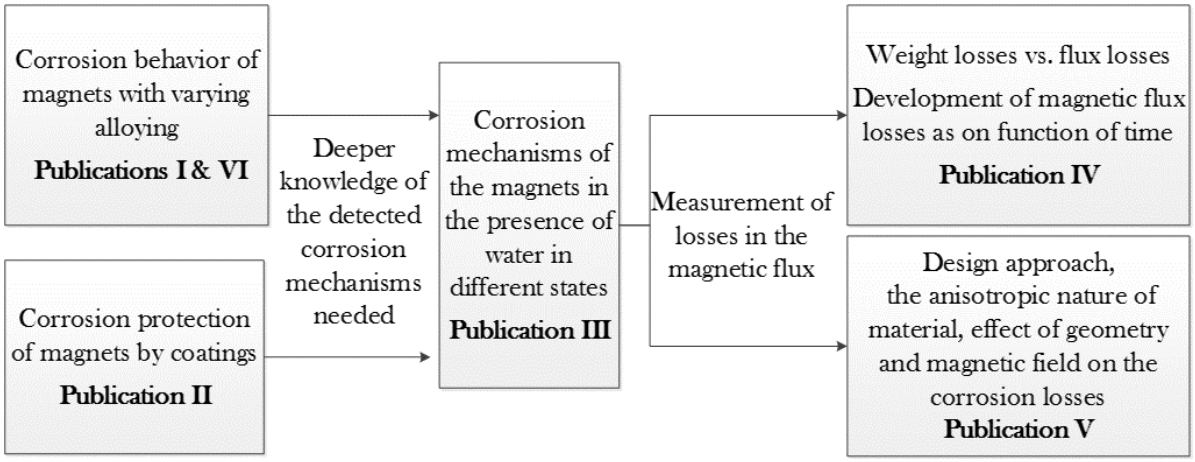

Figure 2. Structure of the thesis work based on the interrelation between publications I-VI.

This thesis will summarize the main findings of the attached six scientific publications and combine the information gained in each article into a coherent entity. The scientific novelty of the work arises from the progressive nature of the corrosion investigation. The research evolved from the comparison of different alloys to criticizing the common measurement techniques and suggesting improved approaches.

The main scientific contributions of this work are:

- Conduction of a wide range of corrosion studies on sintered Nd-Fe-B magnets taking into consideration several methods for improving the corrosion resistance, and resulting in important new knowledge of different alloys and coatings and, particularly, of their joint influence on the overall corrosion performance of the magnets.
- Improvements in the theoretical understanding of the corrosion mechanisms of sintered Nd-Fe-B magnets, with an important addition of the magnet's self-field taken into consideration.
- Comparison of the magnetic and weight losses due to the corrosion of the magnets and observations on the evolution of the magnetic losses as a function of time.

The corrosion mechanism studies and evaluation of the effect of different dopants used in commercial grade magnets formed an essential base for assessing what are the main corrosion mechanisms and which tests and measurements would give the most usable information. As a result, a novel combination of measurements comparing the percentage losses in the weight and in the magnetic flux produced by the magnet was put into practice. The measurement systems in Publications IV and V gave new perspective to the corrosion mechanisms of magnetized samples. Throughout the work, the potential of utilizing the results of this study in the industry by the end-users was promoted by using commercial grade magnets.

3 EXPERIMENTAL PROCEDURES

This chapter describes the experimental procedures used in this thesis. The sintered Nd-Fe-B magnets differing in terms of their composition, manufacturing route, and properties were received from the manufacturers. Two types of metallic coatings and their corrosion protection properties on sintered Nd-Fe-B magnets were also studied. For examining the corrosion behavior of the magnet materials, various heat-humidity tests were employed. The electrochemical nature of corrosion was further studied using electrochemical measurements, where the magnets were immersed in an electrolyte. The test procedures were adjusted partly to investigate the factors causing component failures in real applications, e.g., some of the coatings were intentionally scratched prior to corrosion exposures.

3.1 Materials

Table 1 provides a summary of the studied magnet grades in terms of the most important parameters in their chemical composition and surface condition. The chemical compositions were determined by XRF and ICP measurements. The total rare-earth TRE content is given as it may be considered as a rough indicator of the ratio of the rare-earth rich grain-boundary phase and the amount of the magnetic phase. As Table 1 shows, TRE varied from 30.9 to 32.3 wt.%. The cobalt and dysprosium contents are listed in the table, since they are the best-known alloying elements for the improvement of coercivity, corrosion resistance, and thermal stability. The cobalt content in the studied magnet grades varied from 0 to 2.5 wt.% and dysprosium from 0 to 7.3 wt.%. Some of the specimen types have several abbreviations: SG stands for Standard Grade magnet with minimal alloying (0% Co and 4.1 wt.% Dy), IS for the grade with Improved Stability and IC(R) for Improved Corrosion Resistance due to the high Co-alloying. Specimens used in Publications IV and V were tested also in the magnetized state; otherwise the magnet specimens were in a non-magnetized state, because the magnetic field would cause difficulties with the measurements and electron microscopy. A few different sizes of magnet specimens were used because of different manufacturing batches, but the most widely used size was 24 mm x 24 mm x 4 mm (the last one is the direction of the easy-axis, EA). In each case, the specimens had a shape of a rectangular prism (parallelepiped) so that the large faces were the pole faces of the magnet. The exceptions to the above-mentioned specimen sizes were the magnets in Publications I and V, where the sizes of 10 x 10 x 10 (EA) mm and 10 x 10 x 5 (EA) mm were used.

Table 1. Specimens used in this study. The surface finishes tested for each magnet type are denoted as passivated (Pa), ground (G), polished (Po), and coated (Coat).

Specimen	TRE [wt.%]	Co [wt.%]	Dy [wt.%]	Surfaces	Publications
M1, SG, Ref-A	32.2-32.3	0.0	4.1	Pa, G, Po, Coat	I, II, III, VI
M2	31.7	0.0	3.6	Pa	I
M3, IS	31.7	0.0	7.3	Pa, G, Po	I, III, IV, V
M4	31.2	1.0	7.0	Pa, Po	I
M5	30.9	1.0	6.5	Pa, Po	I
M6	31.8	2.5	6.0	Pa, Po	I
M7, IC or ICR	31.2-31.7	2.0-2.5	7.2	Pa, G, Po	I, III, IV, VI
M8, Ref-B	31.3	1.0	1.3	Coat	II
M9, Ce-alloy	31.3	0.3	0.0	G, Po	VI

The surface finishing was either ‘ground’ (G), ‘polished’ (Po), ‘passivation treated’ (Pa), or ‘coated’ (Coat). Ground is the loosest specified surface condition aiming to imitate the most common case where no particular surface treatment is applied. The sample was sawn from a bigger block and the surface was finished by grinding down to grit #240 SiC abrasive paper. In the polished magnets, the surface was first ground and then polished using a diamond product down to 1 µm in size in order to achieve as smooth surface as possible. Such polished mirror-like surfaces are ideal for the microstructural characterization by SEM and they yield easy-to-examine surfaces for surface-sensitive measurements, but they are not a realistic reproduction with respect to the industrial applications. Therefore, specimens with a more realistic surface finish treatment were also tested. The passivation-treated surface was the standard finishing procedure of the manufacturer at the time when the samples were produced. The surface of the magnet was first glass-bead blasted and then treated with a commercial iron phosphating agent to passivate the surface, resulting in a surface roughness of R_a=0.9 µm.

Protective coatings and their ability to protect the Nd-Fe-B magnets from corrosion were examined in Publication II. Within the wide variety of coatings available commercially, electrodeposited nickel and tin coatings were selected for this study. For the magnets to be coated, acid pickling was used as an activation treatment prior to applying an electrolytic coating. The nickel coating was deposited from a semi-bright acidic (pH 4.3) nickel bath, while the tin coating was applied in a sulphuric acid based sulphate bath. The resulting coating thicknesses were 13±2 µm and 17±2 µm for the nickel and tin coatings, respectively.

3.2 Corrosion tests

The corrosion performance of the magnets was studied using accelerated heat-humidity corrosion tests and immersion studies. The electrochemical behavior and reactions were approached using electrochemical measurements.

3.2.1 Corrosion exposures

In order to investigate the corrosion of the magnets, several test methods with various corrosive factors were used. These included exposing the magnets to elevated temperatures, water, humidity, and a NaCl-solution. A summary of the test methods with the relevant temperature, humidity, duration and publication number is presented in Table 2. Before exposing the magnets to the tests, they were cleaned with ethanol and dried carefully. In the HAST and BCT tests, the magnets were weighed to the nearest 0.01 g prior to testing and again after the tests, when the corrosion products formed during the tests were removed. Visual and microscopical inspection was performed on all types of exposed magnets.

The corrosion resistance of uncoated and coated magnets in the heat-humidity environment was studied with the so-called 85/85 steady-state test utilizing the temperature of 85°C and the relative humidity of 85% [95]. The tests were performed in a temperature-humidity chamber ESPEC PR-1 for the durations of 500 and 1000 hours for the coated magnets, and for the duration of 96 hours for the uncoated magnets with passivated, ground, and polished surfaces.

The Bulk Corrosion Test, BCT (also called the Pressure Cooker Test, PCT), exposes the specimen to saturated water vapor. The tests were conducted using Parr 4748 pressure vessels partially filled with water. The specimens were placed in the vessels during the tests so that they were above the water level and the large (pole) faces were in a vertical position. The closed vessels were placed in a thermal chamber heated to 120°C in order to generate pressurized water vapor inside the vessel for the desired duration. In this test configuration, the specimens were not immersed in the water but the surfaces may have wet due to the condensation of the water vapor. In the BCT test of Publication VI, the ASTM standard A1071M [91] was followed and grading of the tested magnets was performed. Therefore, the surface areas of each specimen were determined by precision measurements prior to testing. Weighting was performed prior to the test and after the exposure, when the specimens were first cleaned under a water stream and ethanol and dried. Grading was based on the scale from A to F so that a BCT grade A refers to the best corrosion resistance category with the weight losses of 1.0 mg/cm^2 or less, while a BCT grade F refers to a poor corrosion resistance category with the weight losses of 36 mg/cm^2 or more. The grades B to E fall between these values.

The Highly Accelerated Stress Tests, HAST, were conducted using two different test devices. In Publication I, the tests were conducted with a specially designed and built device where the desired humidity was obtained manually by adding water into the chamber. The condensation of water on the specimens was avoided by introducing a cooled lid (to facilitate condensation onto the lid instead of the specimens). In Publications I, II, IV and V, the HAST tests were conducted with a commercial equipment Espec EHS-211, which is an automatically controlled corrosion test device. Here, the most significant difference as compared to the BCT tests was that the humidity was kept at 95% (instead of 100%) and the condensation of water on the surface of the specimen was avoided. The test durations of 96 and 240 hours were used.

The immersion tests in water and NaCl solution were performed simply by immersing specimens in the electrolyte for a required duration. During the tests, the specimens were placed so that the large faces were in a vertical position, similarly to the BCT tests.

The salt spray tests for the coated and uncoated magnets were performed according to the ISO 9227 standard [96] in a Liebisch Constasal salt spray chamber at 35°C with 5 wt.% NaCl. The tests were interrupted at predefined intervals to check the specimens; different exposure times ranging from 24 to 480 hours were used. The durations to failure were tracked and the specimens were removed when considered significantly damaged.

Table 2. Corrosion exposure tests.

Test name	Temperature [°C]	Prevailing water phase, relative humidity [%]	Durations [hours]	Publications
85/85	85	Vapor, 85	96, 500, 1000	II, III
BCT	120	Vapor, 100	96	III, VI
HAST	130	Vapor, 95	96, 240	I, II, IV, V
Immersion test (water)	23	Liquid, 100	96	III
Immersion test (3.5 wt.% NaCl)	23	Liquid, 100	168	II
Salt spray test (5 wt.% NaCl)	35	Vapor, liquid	24-480	II

The testing of coated magnets included steps with mechanical and thermal deterioration prior to the corrosion exposure. The mechanical deterioration was performed by scratching the coatings with a sharp blade so that the substrate was exposed for a length of 10 mm. Thermal cycling was conducted in a thermal cycling chamber where the temperature was varied from -40°C to +125°C with a ramp rate of 1.6 ºC/min and a soak time of 15 min according to standard JEDEC No 22-A104D [97]. The cycle was repeated 100 times giving the total test duration of 400 hours.

3.2.2 Electrochemical measurements

The electrochemical measurements were conducted with a computer-controlled Gamry Instruments potentiostat model G750 using a traditional three-electrode cell, which consisted of the specimen as a working electrode, a silver-silver chloride (Ag/AgCl, 3 M KCl, +0.197 V vs. standard hydrogen electrode) reference electrode, and a platinum counter electrode. Before conducting the potentiodynamic polarization or electrochemical impedance spectroscopy (EIS) measurements, the specimens were let to stabilize immersed in the electrolyte for 30 or 60 minutes. The open circuit potential (OCP) of the specimens was monitored during the stabilization period. In the potentiodynamic polarization measurements, the potential was varied from -500 mV to +500 mV vs. E_{OCP} at a scan rate of 0.5 or 1.0 mV/s. In the EIS measurements, an alternating current (AC) voltage with an amplitude of 10 mV was applied over the frequency range from 100 kHz to 5 mHz. Gamry Echem Analyst and Gamry Instruments EIS300 software were used to analyze the polarization curves. The Tafel extrapolation method was utilized to determine the corrosion potentials and corrosion current densities from the polarization curves. Some of the EIS data curves were analyzed by fitting an appropriate equivalent electrical circuit model (describing the corroding magnet or coating), resulting in the determination of the electrical parameters related to the corrosion behavior.

The electrolyte in which the electrochemical measurements were performed was 3.5 wt.% NaCl solution in Publications I, II and VI. In Publication II, the EIS measurements were performed as a function of the immersion time in the electrolyte, typically after 0, 2, 6, 24, 48, 96 and 168 hours of immersion. In Publication III, the magnets were immersed in ion-exchanged water and let to stabilize for one hour. The OCP measurements were performed during the stabilization period and then continued for 96 hours. The EIS measurements were carried out after the stabilization for one hour and again at the end of the 96 hours of immersion. All electrochemical measurements were carried out at room temperature (23±2°C) in naturally aerated and unstirred solutions.

3.3 Material characterization

Visual inspection and photographing of the samples were done after the corrosion tests. Notable corrosion damage was often detected visually. Especially the accelerated tests, such as HAST, introduced great differences between the test samples that could be detected by bare eye.

3.3.1 Microscopy and profilometry

The Scanning Electron Microscopy (SEM) studies were performed using a Philips XL-30 microscope equipped with an EDAX DX4 energy-dispersive X-ray spectrometer (EDS). Secondary electron (SE) imaging was used mainly to characterize the surface morphology and topography, whereas the back-scattered electron (BSE) mode was very useful for the observation of different phases and areas with different chemical composition. EDS spot and area analyses were conducted to identify the phases. Although the ability to detect light elements in Nd-Fe-B magnets, mainly boron and oxygen, is limited with EDS, the relative fractions of rare-earths and iron were used to identify the phases. EDS mapping in Publication IV was performed using a field emission gun (FEG) SEM, Zeiss ULTRAplus equipped with an EDS INCA Energy 350 micro-analysis system from Oxford Instruments.

The as-received passivated surfaces and polished surfaces of the magnets were studied by SEM to reveal the microstructure. Some specimens were mounted in conductive resin or non-conductive epoxy prior to grinding and polishing. Silicon carbide papers were used in the mechanical grinding followed by polishing with diamond products down to the size of 1 µm. Because the Nd-Fe-B magnets are known to corrode rapidly in the presence of water, rapid cleaning and drying immediately after each preparation step and the use of non-water based lubricants were preferred.

The cross-sectional specimens normal to the pole face were examined in the connection of the studies of the interface between the magnet substrate and the coating [Publication II] and the sub-surface crack formation during HAST [Publication IV]. The corroded surfaces of the specimens after the corrosion exposures or electrochemical tests were in many cases examined with SEM. Prior to examination, the corroded specimens were cleaned gently in ethanol and dried carefully. Loose corrosion products were collected and studied separately by attaching them into SEM specimen tubs with conductive carbon tabs.

A Wyko NT1100 optical profilometer with 2.5X objective and Vision software were used to measure the arithmetic mean surface roughness (R_a) values for the specimens with different surface finishes in Publication III. An optical profilometer Alicona Infinite Focus G5 was used for characterizing the surface profiles and heterogeneous corrosion on the pole faces after the HAST tests in Publication V.

3.3.2 Contact angle analysis

Contact angle analysis was used to characterize the morphology and wetting properties of differently finished (passivated, ground, polished) magnet surfaces in Publication III. A drop was dispensed onto a clean and dry magnet surface and an image of the drop was recorded.

The measurements were conducted using water droplets of 5 µl in volume, and the results are given as an average of five measurements.

3.4 Measurement of losses in the magnetic flux

In Publications IV and V, the magnet specimens were in a magnetized state during the corrosion exposures. Special attention was put in the planning of the flux measurement procedures with two test durations and multiple measurement points. Since the measurement procedures were not used before, observations on the specimens were made in each phase of the procedures in order to obtain as much information as possible.

3.4.1 Stabilization heat treatment

Magnetized specimens were used to measure the losses in the magnetic properties during the corrosion tests. In order to separate the time-dependent demagnetization, i.e., the thermal losses from the structural corrosion losses during the tests, all specimens were thermally stabilized. The stabilizing heat treatment, where the magnets are exposed to a temperature 10°C higher than in the following static exposure was presented by Haavisto [83]. The treatment introduces initial polarization losses, but further temperature-induced losses are detected only after about 100 hours of static exposure. In this study it was ensured by a similar type of treatment that the magnets would not suffer losses due to temperature during the 10 days in HAST (T=130°C). The practice was adapted by placing the magnets in a laboratory furnace heated to 150°C for one hour before exposing them to HAST. Afterwards the magnets were let to cool down to room temperature.

3.4.2 Losses in the magnetic flux

The corrosion induced magnetic flux losses were determined by measuring the total induction by the magnets placed in a Helmholtz (HH) coil (MS 150 by Magnet-Physik) before and after the corrosion tests. An integrated precision fluxmeter (Electronic fluxmeter EF5 by Magnet-Physik) was used for the measurements. The average flux values of three parallel measurements are reported.

The first flux values were measured immediately after the pulse magnetization (measurement point HH_1) and the second ones (HH_2) after the thermal stabilization. The third measurements were done after the corrosion test were performed and the corrosion products were cleaned. In Test series 2 in Publication IV, the measurements after the corrosion test (HH_3) were done first immediately after the corrosion exposure with the detached corrosion products still present

on the surface of the specimens due to the magnetic field, and then again after cleaning the corrosion products.

In Publication IV, two test series were conducted, differing from each other in terms of the magnet grades used, the test duration, and the specimen holder. In the first test series, two magnet grades, IS and ICR, were tested. A total of seven IS magnets (5 magnetized and 2 unmagnetized) and six ICR magnets (4 magnetized and 2 unmagnetized) were exposed to the HAST test. The test series followed the process described by the flow chart in Figure 3. Each specimen was placed in a glass beaker in the HAST chamber and the test was continued for 96 h. In addition, magnetized reference samples (two of each grade in both reference atmospheres) were similarly kept in a laboratory furnace at 130°C and at room temperature (T = 22±2°C) for the same duration as in the corrosion tests, i.e., 96 h. In total, three HH-measurement points were used, as shown in Figure 3. After the HAST test, removal of the corrosion products was performed using an adhesive tape, after which the magnets were weighed to determine the weight losses. The same was done to the magnets kept in the reference conditions.

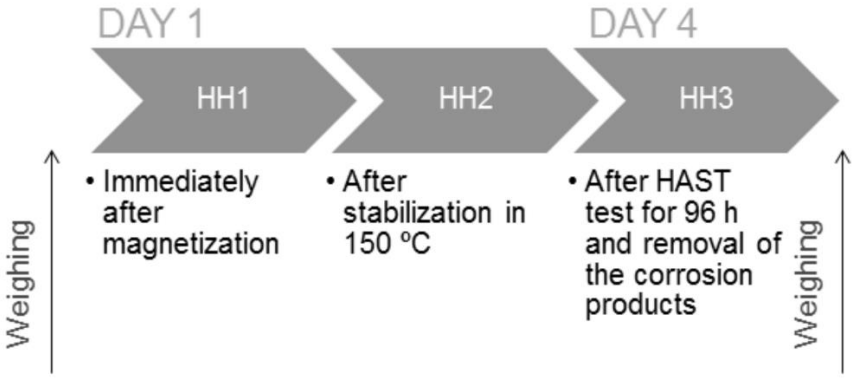

Figure 3. Test series 1 [Publication IV]. HH stands for a magnetic flux measurement point.

In the second test series of Publication IV, a total of six HH-measurement points were used, as shown in Figure 4. All 14 tested IS magnets were in a magnetized state. The samples were positioned in pairs with an air gap between them. A polytetrafluoroethylene-coated net was used to maintain an air gap between the magnets positioned in pairs and, hence, a maximum contact area between the magnets and the surrounding humidity. The test was first interrupted at 96 h, and some of the magnets were removed from the test chamber for measurements. After the HH-measurement, the magnets were returned to the test chamber with the exception of two, which were further studied with SEM. Furthermore, some of the removed magnets were left untouched (corrosion products were not removed at 96 h) until the end of exposure for 240 h, while the rest of the samples were cleaned of the corrosion products to see if there was an effect from removing the corrosion products on the corrosion behavior during further exposure.

At the end of the test period of 240 h, all magnets were subjected to the removal of the corrosion products.

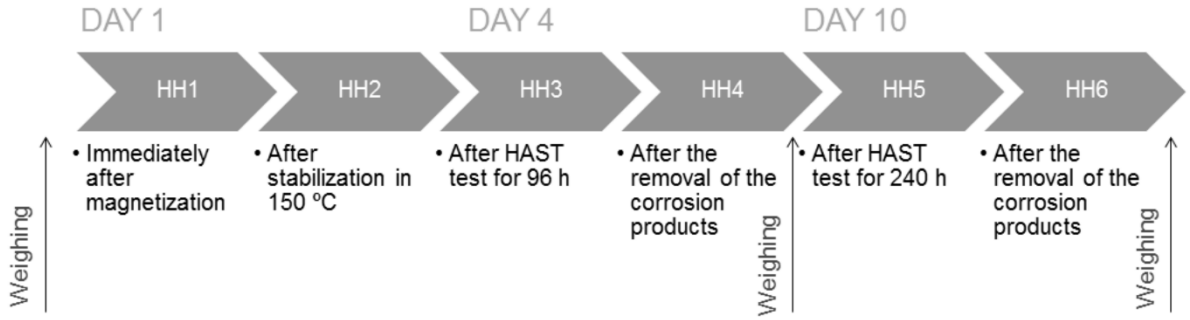

Figure 4. Test series 2 [Publication IV]. HH stands for a magnetic flux measurement point.

In Publication V, magnetized IS grade magnets with two different geometries were HAST tested with an almost similar procedure as in Test series 2 in Publication IV. A total of eight specimens of both geometries was tested. Here, the flux and mass measurements were performed at both test durations (96 and 240 hours) immediately after the loose corroded powder formed during the test was removed.

3.4.3 Demagnetization

In order to characterize the magnets corroded in the magnetized state with SEM, the selected samples were thermally demagnetized. A laboratory furnace with an inert argon gas was used to avoid oxidation of the magnets during the thermal exposure. The magnets were heated up to 350°C [Publication V] or 400°C [Publication IV], both being above the Curie point of about 310°C of the Nd-Fe-B magnets [2].

4 RESULTS AND DISCUSSION

This chapter summarizes the most important results obtained in this thesis work and presented in detail in the attached six publications. First, the aspects influencing the corrosion resistance of the magnets are analyzed through microstructural studies and the effects of these aspects on the corrosion test results are discussed. After that, the observations on the corrosion mechanisms distinguished in the magnets exposed to different conditions are reported. The last part concentrates on presenting the degradation of the magnetic properties as a function of time in the corrosion exposure, aiming at evaluating the amount of realized losses.

4.1 Corrosion protection strategies and the microstructure

A commonly used method for improving the corrosion resistance of magnets is alloying in order to make the magnet less prone to the selective corrosion of the GB phase, i.e., intergranular corrosion. A second approach is the use of protective coatings to separate the magnet from the corrosive environment. These two strategies are covered well in the literature, as shown in Chapter 1, and there is a variety of alloying elements and coating materials to efficiently improve the corrosion resistance of the magnets. Cobalt alloying is widely utilized in commercial grade magnets and it unquestionably improves the corrosion resistance, but the reasonable amount of alloying is not that clearly presented earlier. In this work, the interest is in the effective amount of cobalt alloying. The coating materials selected for this study are two types of commercial metallic coatings. This work comments the ability of these coatings to protect sintered Nd-Fe-B magnets as well as discusses how the metallic coating material may influence the corrosion of the magnet substrate.

Cerium as a substituent alloying element was included in this work as it shows potential as a future economical magnet additive but no studies on its effects on the corrosion resistance of Nd-Fe-B magnets have been done before.

Besides alloying and the use of coatings, this work reports a third means to influence the overall corrosion performance of uncoated magnets: the surface finish. In many cases, surface modifications may serve as part of the pretreatment process to improve the adhesion of coatings, but as the pretreatments found in the literature include introducing new chemical elements by conversion coatings, the effect of pure surface morphology has not been studied before.

The aim of this Chapter is to present and discuss the effects that these corrosion protection strategies have on the behavior of the magnets. Instead of focusing on searching for the best

available alloying element, surface finish, or a coating material, the joint effect of the strategies and the importance of these means are discussed. This kind of comparison studies of different strategies are rare for the sintered Nd-Fe-B magnets. The magnet grades and coatings used in this study are all commercially available and therefore the aim is rather to understand the significance and role of the alloy composition, surface finish and use of coatings in the overall corrosion performance of a magnet component than to develop the most corrosion resistant magnet type or magnet-coating pair.

4.1.1 Composition

The chemical composition of the commercial magnet grades used in this study varied in terms of several elements from one grade to another. Therefore, the challenge was to understand which of the alloying elements had a role in the stability of the material, or whether there were differences in the microstructural features that could influence the corrosion resistance. Based on an earlier experience of the manufacturer, two main compositional variables of interest were selected, the cobalt content and the TRE content.

The microstructure of all studied magnet grades was examined with SEM. BSE-SEM images revealed the contrast differences based on the distribution of elements between the main phases. Figure 5 a) shows an example of the magnet grade M4 with three different phases recognized. The highest volume fraction in the material, seen with a dark grey contrast in the BSE images and marked by (1) in Figure 5, consisted of the magnetically hard “matrix” phase $Nd_2Fe_{14}B$ grains with a diameter of about 5-10 µm. These grains were surrounded by a phase seen with a clearly lighter contrast, the rare-earth-rich GB phase. The contrast difference between these two phases in the BSE images is due to the fact that the magnetic phase is rich in iron, while the phases located at the GB areas are rich in rare-earths with a higher atomic number. Furthermore, the GB areas contained areas seen with an essentially white contrast together with the areas with a light grey contrast (marked by (2) and (3) in Figure 5), implying some compositional difference and thus a probable presence of at least two separate phases. All magnets have some small degree of natural porosity, whereas some of the porosity seen with the black contrast may also originate from the sample preparation. Thus, in principle, the basic microstructure in each of the studied magnet grades is similar to this example case.

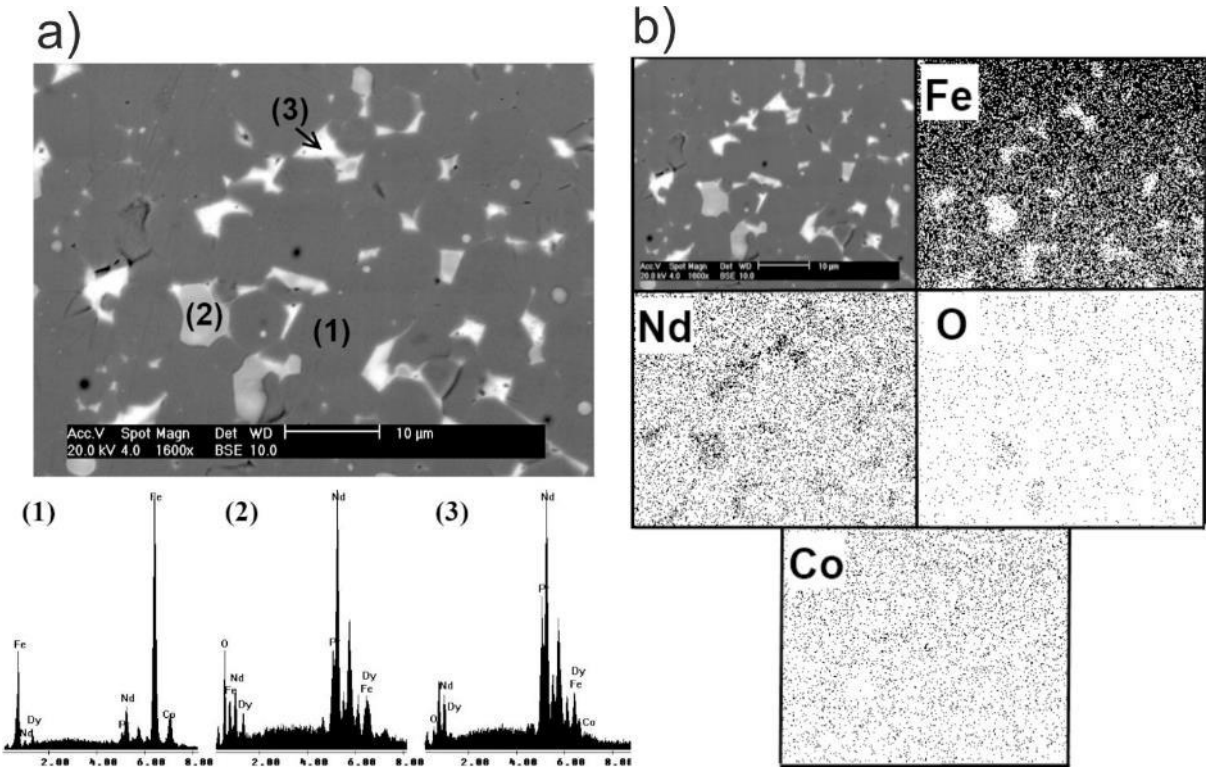

Figure 5. Microstructural study of magnet M4 with 0.9 wt.% Co-alloying, a) BSE-SEM image and EDS spectra of the phases seen in dark grey (1), light grey (2) and white (3) color, and b) EDS elemental maps [Publication I].

The phase composition and the location of the alloying elements could be studied by EDS analyses collected from individual spots and defined areas of the microstructure. The detection of light elements is limited with EDS so that boron can-not be quantified. Therefore, the main phases were identified based on the relative amounts of iron and neodymium. The EDS spectra for the characterized phases (1)–(3) are shown in connection with the SEM image in Figure 5a, and the results from the EDS spot analyses of the grade M4 magnet in Table 3. The matrix phase (1) contained iron, neodymium, dysprosium, praseodymium, cerium and cobalt. Dysprosium additions modify the magnetic properties of the magnets, but the presence of praseodymium is mainly due to properties similar to those of neodymium and a cheaper price. In terms of corrosion behavior, the standard electrode potentials of these rare-earth elements are practically equal, and thereby the expected effect on the corrosion properties of the magnet is minor [72]. Overall, the composition of the matrix phase was uniform irrespective of the studied area, whereas the GB phase had a lot of variation in the composition locally. Furthermore, in the case of M4 in Figure 5, two separate GB phases are clearly seen as they differ in terms of the oxygen content, which was higher in the phase (2) seen in a light grey color than in the phase (3) seen in a white color. In this case, the light grey phase is presumably neodymium oxide. Generally, the GB phase (3) was rich in RE elements, but included evidently

oxygen, cobalt and iron as well. Comprehensive separation of the different GB phases is unfeasible, but the observations of the heterogeneous nature agree with the results of Mo *et al.* [11] and Shinba *et al.* [12]. The composition of the phases in all magnet grades were very similar and the amount of cobalt in each phase was proportional to the overall cobalt content of the magnet. In magnet grades M6 and M7, the Co-contents of the matrix phase and the white GB phase were 3.4 and 6.7 wt.%, respectively, their overall cobalt contents being 2.3 and 2.4 wt.%. The cobalt contents of the white GB phase (3) was found to be higher than that of the matrix phase in each of the studied Co-alloyed magnet grades. Therefore, despite the challenges caused by the heterogeneous nature of the GB phases and the limited accuracy of EDS, it can be stated that cobalt is preferentially located in the GB phase(s).

The distribution of elements in the magnets was determined by EDS elemental maps. The maps for M4 are provided in Figure 5b, with the distribution of iron, neodymium, oxygen and cobalt being presented. The maps showed clearly that iron was the main element in the matrix phase and neodymium was the major constituent in the phase seen with a white contrast. The oxygen content was the highest in the GB phase in the light grey areas, which is in agreement with the EDS spot analyses. Based on the maps, the distribution of cobalt was relatively even in the matrix and in the white GB phase.

EDS maps showing the distribution of Ce and Nd in the Ce-alloyed magnet grade are shown in Figure 6. The maps revealed that cerium coexisted with neodymium in every phase but concentrated more in the GB phase than in the matrix grains, in agreement with the studies by Kablov *et al.* [98]. Again, the heterogeneous nature of the GB phase was evident, also in terms of the distribution of neodymium and cerium. Cerium was abundant in the areas of a continuous GB phase, i.e., in the thin sections between the matrix phase grains, whereas the occasional round areas in the triple junctions were mostly neodymium oxide. Although cerium is located in the GB areas, the stability of the GB phase is not considered to be improved similarly as with cobalt alloying since cerium is not known to form compounds with active neodymium.

Table 3. Results of EDS spot analyses collected from the different phases in the grade M4 magnet [Publication I].

	(1) Dark grey phase		**(2) Light grey phase**		**(3) White phase**	
	wt.%	at.%	wt.%	at.%	wt.%	at.%
Fe	69.1	84.6	9.1	11.2	16.5	28.2
Nd	16.6	7.9	53.2	27.3	53.5	38.9
Dy	7.7	3.3	11.2	5.2	2.1	1.3
Pr	4.9	2.4	15.9	8.4	24	18.1
TRE	29.2	13.5	80.4	40.9	79.6	58.3
O	-	-	10.5	47.9	1.5	9.8
Co	1.7	1.9	-	-	2.4	3.7

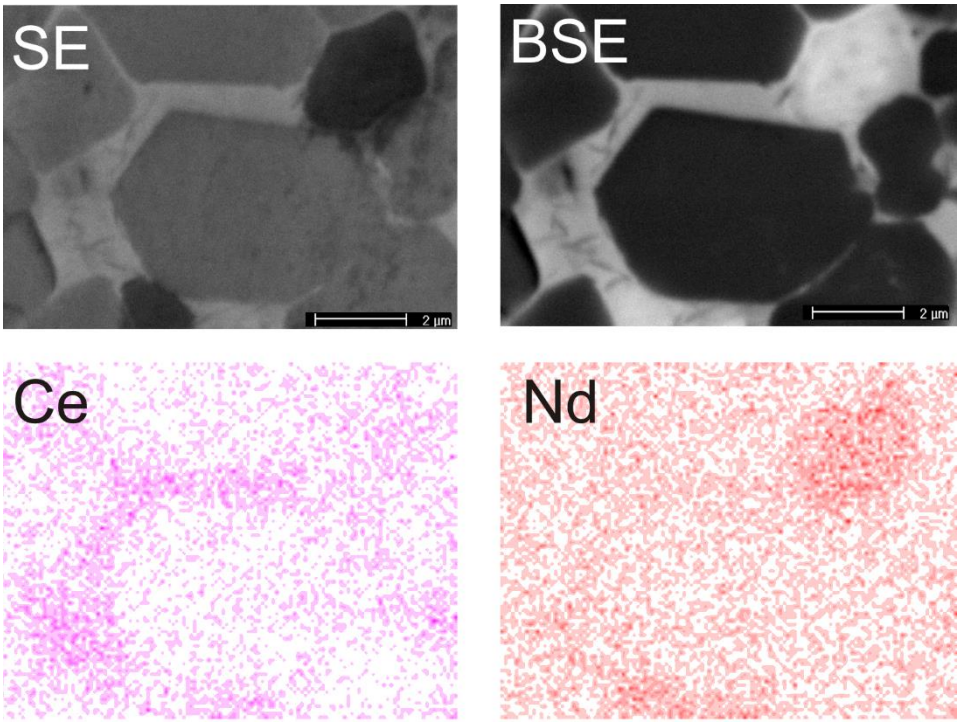

Figure 6. SEM-SE, SEM-BSE images and EDS maps showing the distribution of Ce and Nd in the Ce-doped Nd-Fe-B magnet microstructure [Publication VI].

Clear differences could be observed in the distribution and relative amount of phases between the magnet grades. Particularly the Ce-alloyed magnet differed from the other studied magnet grades (Figure 7). The GB phase in the Ce-alloyed magnets was very finely and uniformly distributed and the grains of the magnetic phase were therefore systematically separated. These findings are in agreement with the study of Huang *et al*. [31], which showed that the eutectic transformation temperature of a Ce-containing magnet is lower than that of the corresponding Nd-Fe-B magnet without cerium, resulting in better wetting characteristics and thickening of the RE-rich grain boundary phase. In the other tested magnet grades, most of the GB phase was usually concentrated in the triple junctions of the magnetic grains, i.e., they occurred as larger ‘reservoirs’, leaving the matrix grains less effectively separated than in the case of the Ce-alloyed magnet grade.

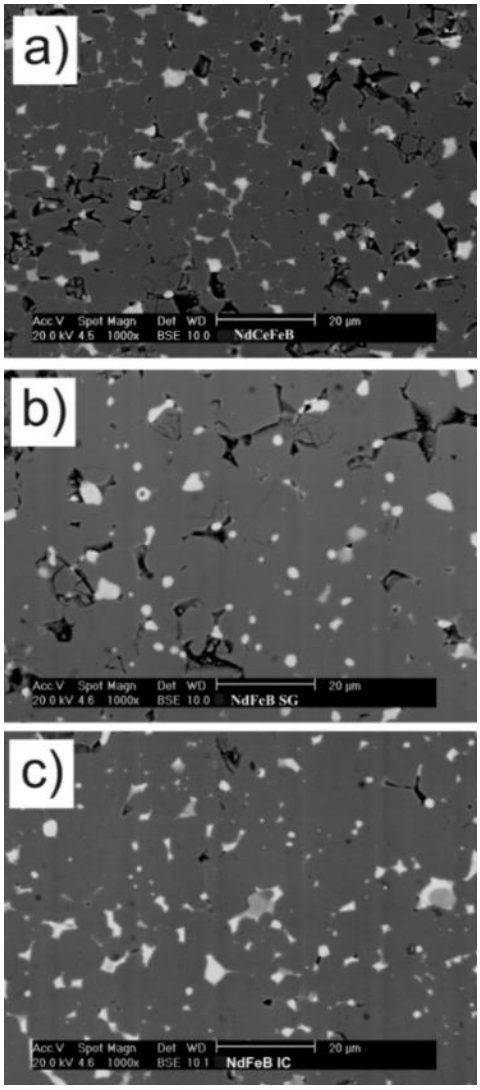

Figure 7. BSE-SEM images of a) Ce-alloyed magnet, b) SG reference and c) ICR reference magnets [Publication VI].

The effect of the differences in the composition between the magnet grades was evaluated using corrosion tests. In Publication I, HAST tests were conducted using two different test devices and seven as-received magnets, M1-M7 including magnets with cobalt contents of 0, 0.9, 2.3 and 2.4 wt.%. The average weight losses per area of the specimens were determined for all studied magnet grades. Although the absolute weight loss values differed significantly between the tests, with both tests devices the magnet grade M1 experienced the greatest weight losses (5.5 mg/cm^2 in HAST1 and 169 mg/cm^2 in HAST2). The tests showed the lowest weight losses for the magnet grades M5 and M7, 0.4 mg/cm^2 in HAST1 and 0 mg/cm^2 in HAST2 for both grades, indicating the best corrosion resistance. The weight losses for the magnet grades M4 and M6 amounted to 0.5 mg/cm^2 in HAST1 and 0.8 and 2.3 mg/cm^2 in HAST2.

The HAST tests included two magnet grades, M4 and M5 with 0.9 wt.% of cobalt and two grades with significantly higher amounts, M6 2.3 wt.% and M7 2.4 wt.% of cobalt. It is evident that Co-alloying lowers the weight loss of a magnet exposed to HAST. However, all cobalt containing magnets resulted in relatively equal weight losses so that no trend of ever-lowering losses with increasing amount of cobalt could be observed. Thereby, the exact amount of Co-addition, 0.9 or 2.3-2.4 wt.%, did not have a clear impact on the magnet weight losses, indicating that 0.9 wt.% may be a "sufficient" amount of added cobalt. This finding disagrees to some degree with the earlier observations by Fernengel *et al.* [82], where the cobalt content linearly correlated with the mass losses in HAST. It is assumed that information of the location and distribution of cobalt in the magnet would be needed for further understanding of the reason for the disagreement of the results.

The milder heat-humidity exposure in the 85/85 test, however, did not reveal any differences between the corrosion rates of the studied alloys. The corrosion performance of all three tested magnet grades, SG, IS and ICR, was practically the same in the 85/85 test [Publication III]. In the case of immersion in water [Publication III], the dissimilarities in the extent of the corrosion damage between the magnet grades were, similarly, relatively small and could not be attributed to the cobalt alloying or other compositional features. In the BCT tests, the magnets with Co-alloying resulted in the lowest weight losses [Publications III and VI], indicating improved stability of the Co-alloyed magnets in the BCT conditions, i.e., in the presence of pressurized saturated water vapor.

In the electrochemical measurements, the ICR magnet with the cobalt content of 2.5 wt.% showed the highest open circuit potential (OCP) among the studied magnet grades during the first half hour of immersion, but as the system stabilized, the OCP values of all magnet grades were similar [Publication III]. The EIS measurements performed for the magnets immersed in water revealed slight differences in the behavior between different magnet grades. In the electrochemical measurements performed in a NaCl solution, the magnets without cobalt additions had systematically lower corrosion potentials than those with the cobalt alloying [Publication I], implying that the cobalt-free grades were more active.

In the study of coated magnets in Publication II, an evident difference in the behavior between the specimens involving different substrate magnet grades was observed. The effect was significant in the immersion tests using nickel-coated magnets that were scratched prior to the exposure, as well as in the HAST tests. This finding is probably related to the Co alloying and will be explained in more detail in Chapter 4.1.3.

In Figure 8, the magnet grades M1-M7 are arranged in the order of decreasing corrosion resistance summarizing the effects of TRE and Co-contents. The rating is based on the parameters determined through polarization measurements and weight losses obtained in the

HAST tests. The magnet grades were sorted by the electrochemical values so that high E_{corr} and low i_{corr} indicated good corrosion resistance as did naturally low weight losses in the HAST tests. The columns in Figure 8 represent the amounts of TRE and Co in the magnets. Hence, the magnets with the best corrosion resistance were characterized by the highest or moderate cobalt alloying levels plus a low TRE content. The greatest weight losses in the HAST tests were experienced by the magnets with high TRE contents and no cobalt alloying. In turn, the poorest corrosion resistance was connected to the absence of cobalt alloying and a high overall TRE level. During the 96 hour HAST test in Publication IV, there were no measurable mass losses in any of the tested ICR magnets.

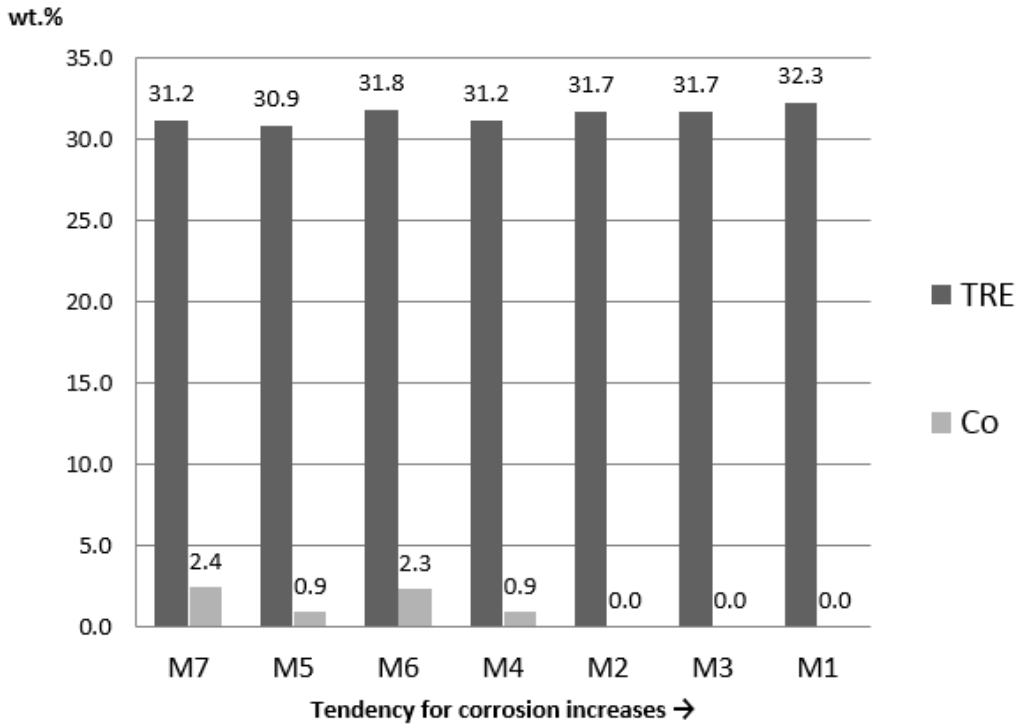

Figure 8. Magnet grades M1-M7 and their TRE and cobalt contents in the order of increasing corrosion tendency (based on the combined results from polarization measurements and HAST tests) [Publication I].

The Bulk Corrosion Test following the ASTM standard test method for permanent magnets was performed in order to accelerate the corrosion process with pressurized water vapor [Publication VI]. The average weight losses measured for the Ce-alloyed, SG and ICR magnets are presented in Table 4 together with the corresponding BCT grading (A-F) according to the ASTM standard. The magnitude of the weight losses fell in all cases in the BCT grade B category, which corresponds to specific weight losses from 1.1 to 3.9 mg/cm^2. The standard grading was the same for all three magnet grades, yet the Ce-alloyed magnets underwent slightly more weight losses than the two types of reference magnets.

Table 4. Weight losses for the three magnet grades in the BCT test. The BCT grading is done according to the ASTM standard using the scale A-F, where A is the most corrosion resistant alloy [Publication VI].

Specimen	Weight loss [mg/cm^2]	BCT grade
Ce-alloyed	3.8	B
SG	2.6	B
ICR	2.3	B

4.1.2 Surface finish

The initiation of corrosion is dependent on the behavior of the surface layer of the magnet, the area where the magnet is in contact with the surrounding atmosphere. The alloy composition influences the chemical nature of the surface layer, but also secondary factors, such as the surface roughness, may contribute to the corrosion rate of the magnet [Publication III]. Additional studies on the relationship between surface modifications and corrosion performance of Nd-Fe-B magnets were performed and published in the conference proceedings of EUROCORR [99]. In that study, four surface finishes of magnet grades M2 and M7 were compared in terms of corrosion resistance. The surfaces were either passivated, ground, polished or sandblasted. SEM-BSE images for the type M1 magnet with the four different surface finishes are presented in Figure 9. The corresponding images for the M7 magnets are not presented, as the differences in the chemical composition between the magnets did not result in any differences in the surface morphology.

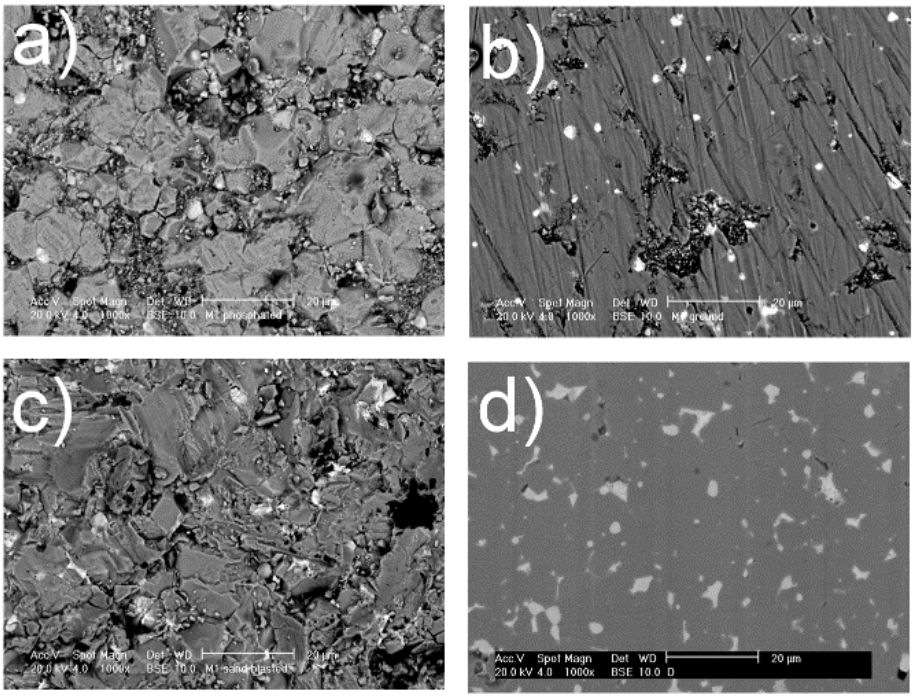

Figure 9. SEM-BSE images of M2 with a) passivated, b) ground, c) sand blasted and d) polished surface finish [99].

In the passivated magnet (Figure 9a), the grains of the matrix phase were slightly deformed by the preceding glass-bead blasting process, but in most areas separate matrix phase grains and GB phase could be observed. In some areas of the surface, the phases present were difficult to distinguish due to the surface deformation and roughness. The passivation treatment, including the glass-bead blasting and the following phosphate solution treatment, did not result in a phosphate layer detectable by SEM, but in the visual inspection the color of the surface was matt grey, while the other surface types where quite bright in color. This observation is consistent with the results by Martins *et al.* [7], who could not detect the corrosion hindering phosphate layer on the sintered Nd-Fe-B magnets by SEM but saw the color change with naked eye. The surface of the ground magnet (Figure 9b) was evidently smoother than that of the passivated magnet, but scratches from the grinding were evident. The morphology of the sand blasted magnet (Figure 9c) was quite similar to that of the passivated magnet, but the matrix grains were more flattened, indicating stronger forces of the mechanical bombarding. Also the contours between the phases were difficult to detect. The surface morphology of the polished magnet (Figure 9d) was very smooth and the relative amount of different phases corresponded to that in the bulk material. In applications, the polished surface is probably the most unlikely case of the studied surfaces, since the preparation of such smooth surface is laborious and thereby uneconomical. Additionally, if the magnets are, for example, glued, the adhesion properties are most likely better with rougher surfaces than with smooth ones.

The morphology of the studied surfaces was characterized also by using optical profilometry. 3D images showing the surface topographies together with the measured average arithmetic mean surface roughness, $R_{a,}$ values are provided in Figure 10. The passivated and ground surfaces had the most similar surface roughness values, 870 nm and 430 nm, respectively. The sand blasted surface had the highest surface roughness value, 2.5 µm, which is almost three times that of the passivated magnet. The polished surface was the smoothest with the surface roughness of 125 nm. The roughness of the surface may contribute to the wetting behavior [100]: in the case of condensation of water, the wetting behavior may have an effect on the corrosion performance of the magnet.

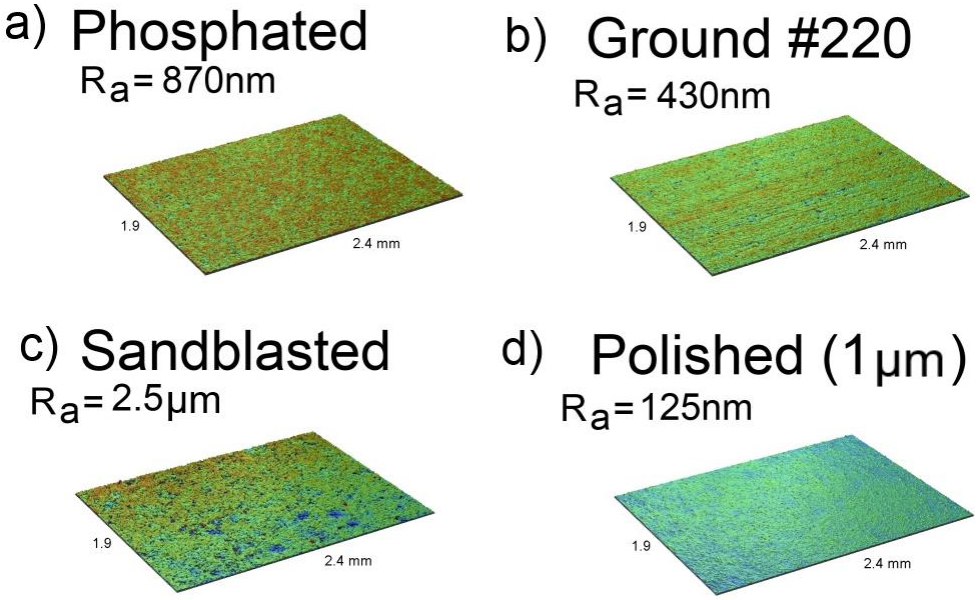

Figure 10. Arithmetic mean surface roughness (R_a) values and surface morphology 3D images of a) phosphated (i.e., passivated), b) ground, c) sand blasted and d) polished magnet surface [99].

An additional HAST test was performed in the study published in EUROCORR proceedings [99], where the focus was placed on comparing the changes in the surface morphology of the magnets, which are essentially connected to the prevailing corrosion mechanisms. Photographs of the magnets after the HAST test for 96 hours are shown in Figure 11. Again, the improved corrosion resistance of the magnet grade M2 alloyed with cobalt is evident. In visual inspection, all grade M2 magnets (Figure 11 a-d) were pulverized to some degree, whereas the surfaces of M7 magnets (Figure 11 e-h) did not contain any loose corrosion products. Both polished surfaces showed a slight violet tint, which may refer to the formation of an iron-oxide layer. Overall, the corrosion products on the M2 magnets were black in color and relatively loosely attached to the surface. However, small amounts of red rust were detected on the surfaces of the passivated and ground M7 grade magnet. The formation of red rust refers to the general corrosion of the iron-rich matrix phase [101]. Red rust was probably

formed also on the M2 grade magnets as a result of general corrosion, but in very low amounts. Therefore, pulverization by intergranular corrosion clearly dominated the corrosion process of the M2 grade magnet.

As the two magnet grades were tested in the same test set, it was evident that the cobalt alloying was the primary factor affecting the corrosion performance, but also the surface topography had a corrosion hindering role seen in the M2 samples. As may be detected in Fig. 11, the ground surface contained least corrosion products of the studied surfaces.

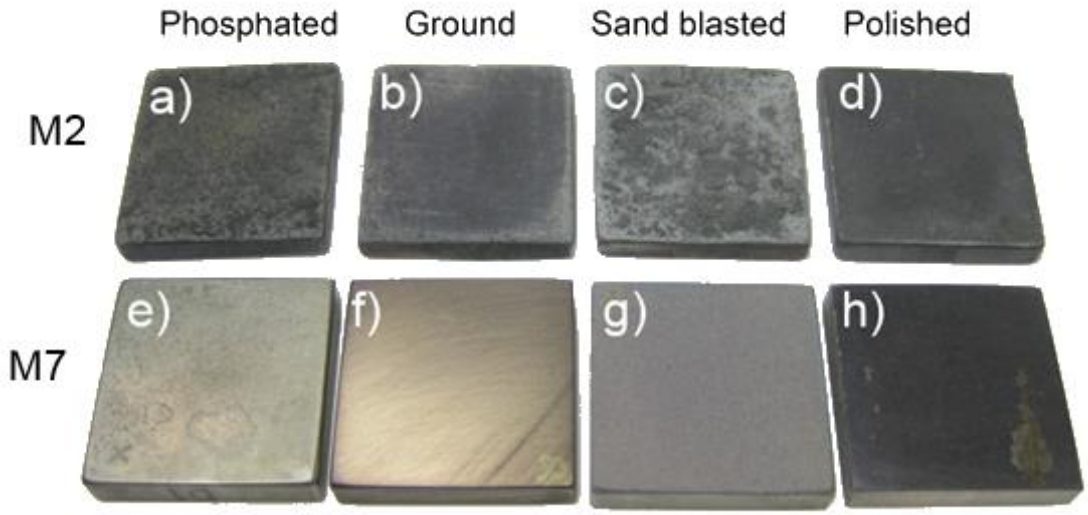

Figure 11. Photographs of magnets exposed to HAST for 96 hours with different surface finishing; a) phosphated (i.e., passivated) M2, b) ground M2, c) sand-blasted M2, d) polished M2, e) phosphated M7, f) ground M7, g) sand-blasted M7 and h) polished M7 magnet surface [99].

Roughness may act as a corrosion hindering feature, because the condensed droplets will wet the surface less [Publication III]. Therefore, interaction between a water droplet, which may originate for example from the condensed humidity, and the magnet surface was studied in Publication III for three types of surface finishes. Figure 12 from [Publication III] shows photographs of the specimens with three different surface finishes: passivated, ground and ground and polished after the 85/85 test together with the measured values of the surface roughness and the contact angles measured prior to testing. The wetting behavior examined by the contact angle analysis showed that the wetting was greatest in the case of the polished surface (contact angle 50.7°, R_a 125 nm), explaining partly also the formation of the well-adhered corrosion product layer on the surface of the polished magnet (Figure 12c) during the heat-humidity test. In turn, in the case of the ground surface (R_a 430 nm), the extent of corrosion was the lowest, as evaluated visually, and the contact angle was the highest (59.2°). These results demonstrate that although the wetting is not linearly connected to the roughness

of the surface (as the roughest surface had the middlemost contact angle) the surface roughness clearly has some role in the wetting behavior.

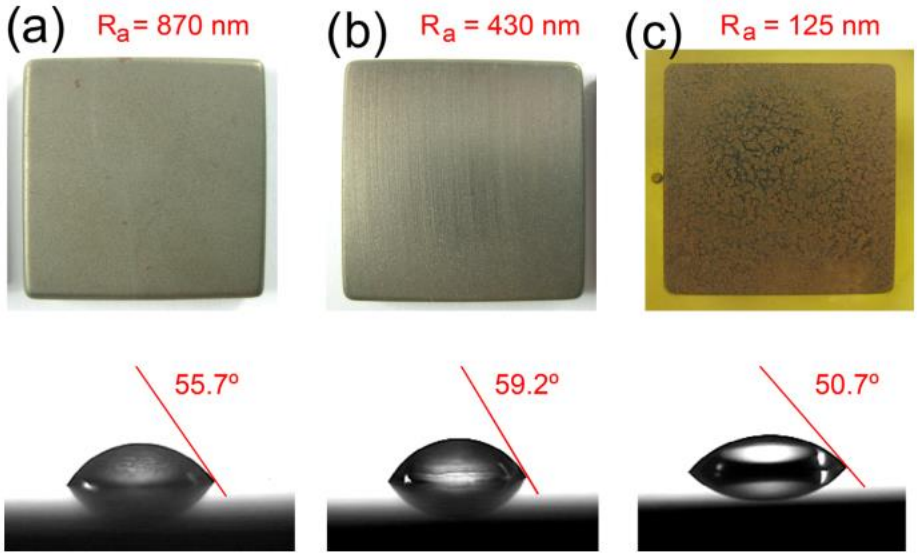

Figure 12. Photographs showing M1 (SG) magnets after the 85/85 tests together with the measured surface roughness values and contact angles: magnet with passivated (a), ground (b), and polished (c) surface [Publication III].

Both the harsh HAST test and the milder 85/85 heat-humidity test showed differences between the same magnet material with a different surface finish. In HAST, cobalt alloying was the primary factor affecting the corrosion performance, but also the optimized surface topography had a corrosion hindering role.

The passivation treatment used by the magnet manufacturer, including glass-bead blasting and phosphate solution immersion, did not provide the magnets with an efficient corrosion protection in, e.g., HAST. However, the treatment may provide protection for the surface in dry conditions and as such act as a corrosion protection method for example during transport or before installation, i.e., in very mild corrosion environments [102].

4.1.3 Coatings

Two electrochemically deposited metallic coatings were investigated in this work with respect to their corrosion protection properties for two substrate magnets, M1 and M8. Cross-sectional SEM images of the nickel-coated and tin-coated M1 magnets are shown in Figure 13. The nickel coatings had a layered structure, whereas the tin coatings featured a columnar cross-sectional morphology. Sub-surface cracks were detected in the fractured nickel-coated magnets in the near-surface regions. The cracks originated most likely from the hydrogen generation and the resulting magnet embrittlement during the plating process in the acidic bath. Similar challenges in the case of nickel-coated magnets were previously reported by Heng Xiu

et al. [103]. Also the mechanical properties of the coating, particularly ductility and hardness, may affect the crack propagation and fracturing behavior of the magnet.

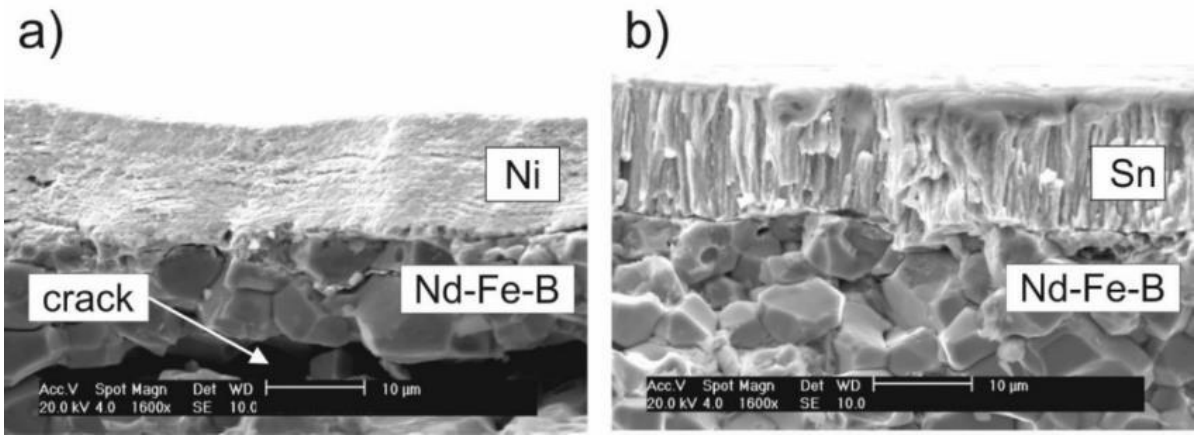

Figure 13. Cross-sectional SEM SE images of nickel (a) and tin (b) coated M1 grade Nd-Fe-B magnets [modified from Publication II].

As the coatings were applied on two magnet grades, M1 (Ref-A) and M8 (Ref-B), the possible role of two different substrate materials on the corrosion behavior was also investigated. The coated magnets were exposed to salt spray tests, 85/85 heat-humidity tests, and HAST tests. In addition, scratched specimens were immersed in a 3.5 wt.% NaCl solution for one week. A summary of the observations of the corrosion performance of the coated magnets in the tests is presented in Table 5.

The corrosion mechanisms between the tests varied greatly. The salt spray tests corroded the uncoated reference magnets so heavily that they were considered to have failed the test already after 24 hours. The surfaces were covered by a layer of red rust. The principal corrosion mechanism of the coated magnets was pitting. The corrosion resistance was directly related to the quality of the coating, because some of the specimens were retained intact during the tests, whereas some parallel specimens with poorer quality, e.g., those with pores and pinholes, contained several corrosion pits during the first days of exposure. When the test was prolonged to 480 hours, the corrosion pits had reached the substrate and thus the difference in the behavior between the magnet grades became evident. Both magnet grades were anodic compared to the metallic coatings, but as the grade Ref-A (M1) was less noble than Ref-B (M8), it formed a stronger galvanic pair with the coatings leading to higher corrosion rates.

To further simulate the stresses that the magnets may encounter in the applications, the resistance of the coated magnets to alternating elevated and low-temperature extremes was tested using thermal cycling tests. The nickel coating stayed intact, whereas in the tin coating small nodules and cracks were detected in the outermost parts of the coating layer after 100 cycles. Two replicas of grade M1 magnets with tin and nickel coatings that were first exposed

to thermal cycling were tested in the salt spray chamber for 96 hours. As stated earlier, the nickel coatings stayed intact in the thermal cycling, and therefore their behavior in the 96 hour salt spray tests did not differ from that of non-cycled specimens. In the tin-coated magnets, in turn, the observed changes in the microstructure resulted in poorer corrosion resistance than for the non-cycled specimens. Large areas of the coatings flaked and delaminated during the corrosion tests of the tin-coated magnets that had undergone thermal cycling.

The 85/85 heat-humidity test introduced a mild heat-humidity exposure for a relatively long exposure time. Both nicked-coated specimens were retained intact for the standard test duration of 500 hours. The tin-coated magnets with the M1 grade substrate underwent deterioration due to corrosion of the substrate. In addition, the color of the coatings turned from bright silvery to essentially golden with the increase of the test duration from 500 to 1000 hours.

The HAST tests revealed the intergranular corrosion tendency of the specimens and particularly the improvement in the corrosion resistance by the cobalt addition in the magnet grade M8 (Ref-B). The degree of pulverization and the corrosion damage depend both on the substrate and the coating material, as seen in Figure 14. In the presence of defects or pinholes in the coatings, the corrosion of the substrate magnet was drastically accelerated, particularly as the metallic coatings are cathodic to the magnets. The corrosion products that formed on the nickel- and tin-coated magnets were mainly corrosion products of the substrate.

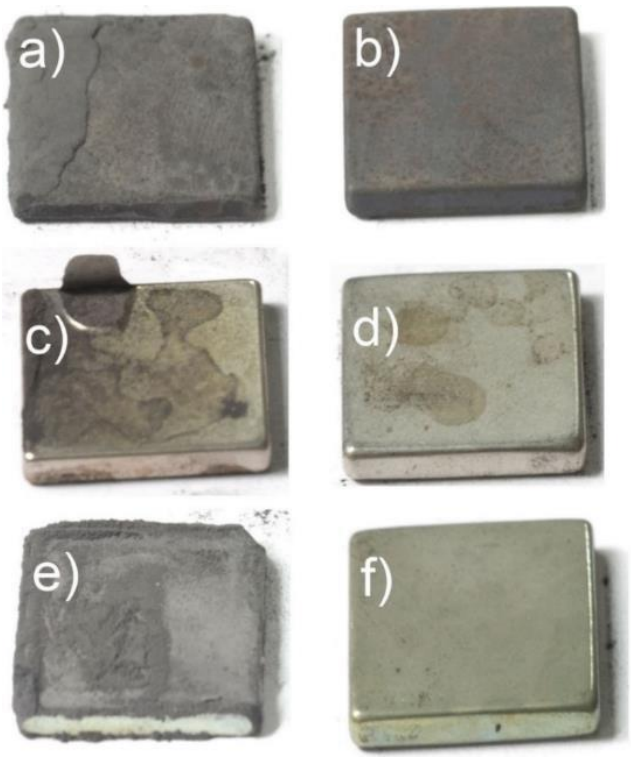

Figure 14. Uncoated magnets (a) M1 (Ref-A), (b) M8 (Ref-B), nickel-coated (c) Ni-A, (d) Ni-B, and tin-coated (e) Sn-A and (f) Sn-B after 10 days in HAST [Publication II].

Compared to the tin coatings, the nickel coatings provided a good protection for the Nd-Fe-B magnets against corrosion in the 85/85 and HAST tests. However, once corrosion was initiated, the strong galvanic coupling between the nickel coating and the magnet (Figure 15) and the loss of adhesion resulted in rapid peeling off of the coating.

The aim of immersing scratched specimens in a NaCl solution was to evaluate how the presence of coating defects, such as scratches, influences the corrosion damage and peeling off of the coating. The uncoated magnet corroded slightly by the formation of red rust, which did not form deep cavities, but only the outermost layer of the magnet was partly corroded. The scratches in the metallic coatings exposing the substrate and forming galvanic cells accelerated the corrosion of the magnet. Therefore, grade M1 (Ref-A) substrates were corroded to a greater extent than the grade M8 (Ref-B). The delamination around the scratch was less severe in the tin-coated magnets than in their nickel-coated counterparts. The most significant outcomes of the immersion tests were the following: In addition to the strength of the galvanic pairs (difference in E_{corr}) and the chemistry of the corrosion products, in the case of scratched coatings the loss of adhesion of the coating has an evident role in the corrosion resistance. Also, the total material losses of the uncoated reference magnets were actually less than those of the coated and scratched magnets due to the formation of new galvanic pairs between the coating and the substrate and, thus, acceleration of the corrosion reactions.

Table 5. General observations after the corrosion tests of uncoated (Ref-A and Ref-B), nickel coated (Ni-A and Ni-B) and tin coated (Sn-A and Sn-B) Nd-Fe-B magnets [Publication II].

Name	Salt spray 96 h	85/85 test 500 h	HAST 10 days	Immersion of scratched specimens 168 h (3.5 wt.% NaCl)
Ref-A	Red rust	Some red rust	Heavy pulverization	Some red rust
Ref-B	Red rust	Some red rust	Slight pulverization	Some red rust
Ni-A	Pits evolved	Intact	Some detachment and pulverization	Detachment of a large area of the coating
Ni-B	Pits evolved	Intact	Intact	Detachment of the coating near the scratch
Sn-A	Pits evolved	Heavily deteriorated coating, pulverization	Detachment of the coating, heavy pulverization	Detachment of the coating near the scratch
Sn-B	Pits evolved	Color change	Intact	Detachment of the coating near the scratch

The polarization behavior of the coated magnets and uncoated reference magnets were measured in a 3.5 wt.% NaCl solution. The behavior of the coated magnet was independent of the substrate. In Figure 15, typical polarization curves for all four cases are presented. Both of the coatings exhibited higher corrosion potentials than the uncoated magnets. The values for the corrosion potential and the corrosion current density shown in Table 6 were obtained by the Tafel extrapolation method. These results confirm that the coatings were more noble than the magnets.

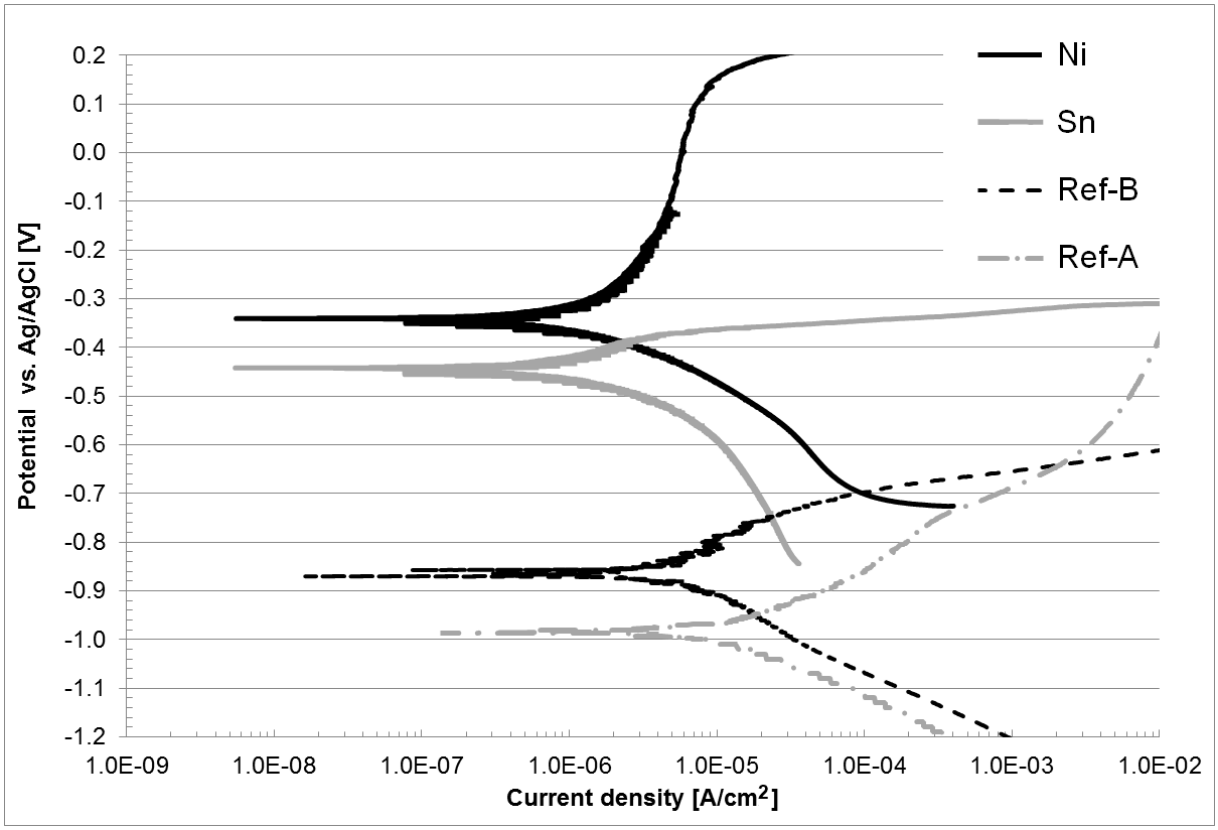

Figure 15. Polarization curves for the nickel and tin coatings on Nd–Fe–B magnets and for the bare substrates in a 3.5 wt.% NaCl solution [Publication II].

Table 6. Values for corrosion potential, E_{corr}, and corrosion current density, i_{corr}, of the magnets and coatings [Publication II].

	E_{corr} [mV]	i_{corr} [µA/cm^2]
M1, Ref-A	-996	12.02
M8, Ref-B	-875	1.24
Ni-coatings	-355	2.72
Sn-coatings	-443	1.65

To summarize the protection provided by the two metallic coatings for the sintered Nd-Fe-B magnets, nickel provided an overall higher corrosion protection for the sintered Nd-Fe-B magnets than the tin coatings. Both coating types were cathodic to the Nd-Fe-B magnets but, in addition, the tin coatings were sensitive to thermal stresses [Publication II]. In the presence of NaCl, i.e., a conducting electrolyte, a galvanic pair was created between the magnet and the coating.

4.1.4 Summary of the corrosion protection

Chapter 4.1 presented several methods to protect sintered Nd-Fe-B magnets from corrosion in different environments. In the case of uncoated magnets exposed to a corrosive environment, the composition of the magnet has a significant role in the corrosion performance of the magnet. In the presence of salts or pressurized water vapor, cobalt additions evidently increase the corrosion resistance by stabilization of the GB phase. In mild heat-humidity environments, the uncoated magnets may benefit from a ground surface finish so that the initiation of corrosion on the surface of the magnet is hindered.

In the case of coated magnets, the principal factor influencing the corrosion performance is the quality of the coating. With dense and defect-free coatings, sintered Nd-Fe-B magnets may tolerate very corrosive environments. In the case of coating failure or a defect, the properties of the substrate magnet material dominate. Figure 16 summarizes the findings for the corrosion protection strategies for sintered Nd-Fe-B magnets.

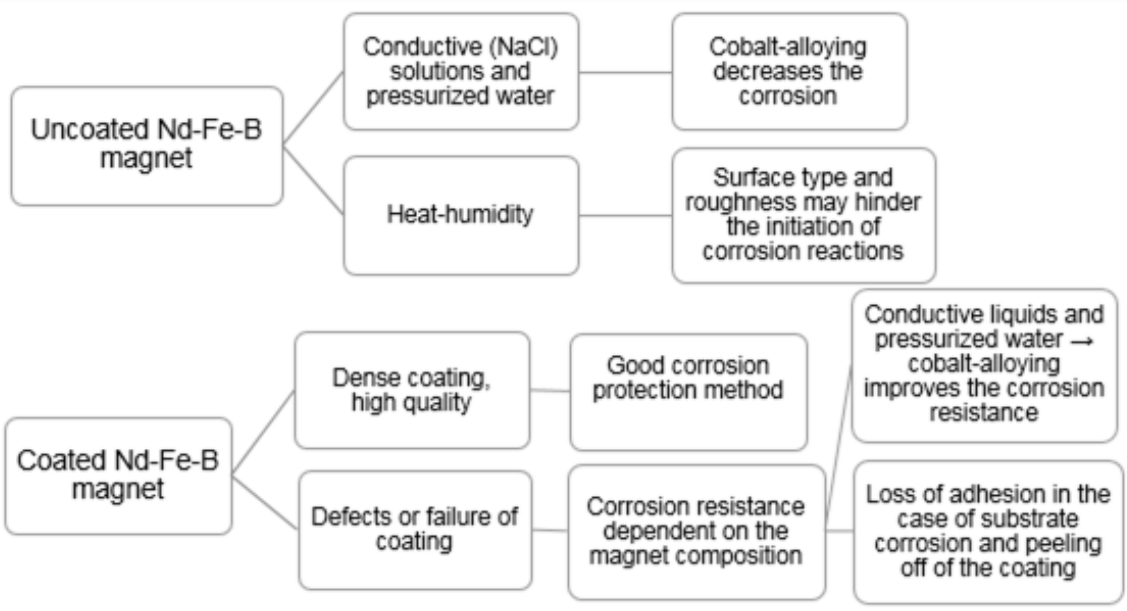

Figure 16. Corrosion protection strategies summarized for uncoated and coated Nd-Fe-B magnets.

4.2 Corrosion mechanisms and rates

Microstructural characterization of the corroded specimens aims to increase the understanding of the corrosion mechanisms and reactions. Characterization of the microstructures of the magnets was performed before and after the corrosion exposures. The comparison enabled to detect the degree and nature of the corrosion damage and thus to define the corrosion mechanisms, e.g., which of the phases corrodes and how the corrosion attack is distributed on the surface. This chapter summarizes the findings on the corrosion mechanisms during the heat-humidity exposures and the corrosion behavior of the magnets when immersed in liquid electrolytes.

4.2.1 Different mechanisms observed under heat-humidity exposure

The corrosion mechanisms were traced by inspecting the corroded surfaces after different corrosion tests. The mild heat-humidity exposure in the 85/85 test introduced general corrosion in all tested Nd-Fe-B magnets. The amount of corrosion was not dependent on the alloying elements, with negligible differences between the studied magnet grades being detected. In the case of the 85/85 test and the standard grade magnet M1, a part of the surface was evenly corroded and no preferential dissolution of any of the phases was observed. Here, the dominant corrosion mechanism was general corrosion. However, detailed SEM examination (Figure 17) disclosed the corrosion damage to occur in three ways or stages. First, the $Nd_2Fe_{14}B$ grains are protruding from the surface, probably due to the volume expansion of the surrounding GB phase (area marked by 1 in Figure 17a). This may be because of, e.g., formation of hydroxides (Equation 1). The second damage mechanism is an even dissolution of the surface without any particular phase being primarily attacked (area indicated by 2 in Figure 17a), i.e., the general corrosion mentioned above. Third, shallow (depth equal to multiple grain sizes) corrosion craters are formed due to the detachment of several grains (area 3 in Figure 17a). The damage in the first and third steps refers to the corrosion of the GB phase, which causes the disintegration of the $Nd_2Fe_{14}B$ grains, i.e., pulverization of the magnet. The damage caused by the second mechanism results from a uniform electrochemical dissolution reaction of the $Nd_2Fe_{14}B$ phase in the test environment (general corrosion of the matrix phase in some areas of the surface). A BSE image of the same examined area is provided in Figure 17b, where the contrast between the different phases of the magnet is evident, i.e., white for the GB phase, grey for the matrix, and black for the traces of the corrosion products.

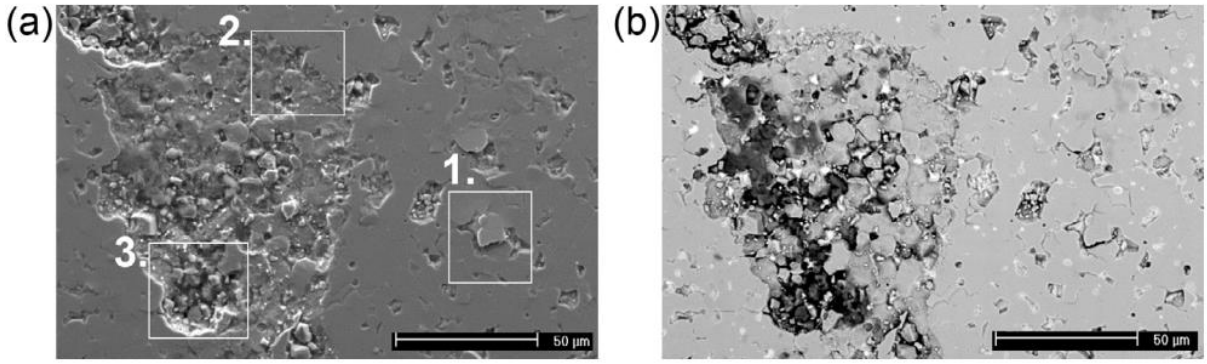

Figure 17. SEM SE (a) and BSE (b) images of the corroded surface of grade M1 magnet. After the 85/85 corrosion test for 96 h, three different types of morphological changes were observed, as marked in image (a) [Publication III].

The BCT and HAST tests were the most aggressive corrosion environments as they made use of pressurized water vapor. The lower relative humidity, RH 95 %, in HAST enables exposure to pure pressurized water vapor, whereas condensation is unavoidable in the BCT test with RH 100%. Indeed, the specimens characterized after the BCT tests showed a mixture of two corrosion mechanisms with most of the area of the magnet surface having undergone general corrosion in the form of formation of red rust, while some other areas had experienced a preferential dissolution of the GB phase (Figure 18). The HAST tests, in turn, introduced pure preferential dissolution of the GB phase and therefore revealed the most significant differences between the magnet grades with different chemical compositions. Indeed, the results indicate primarily the stability of the GB phase, which is generally directly related to the cobalt alloying. If cobalt was used as an additive only for improving the corrosion resistance of the magnets, more attention should be paid on targeting the cobalt into the GB phase. Based on these results, the presence of cobalt in the $Nd_2Fe_{14}B$ phase does not significantly affect the corrosion behavior of the magnet. However, cobalt alloying is not done only for the improved corrosion resistance but also to improve the temperature coefficient of remanence, i.e., the thermal stability of the magnets [104].

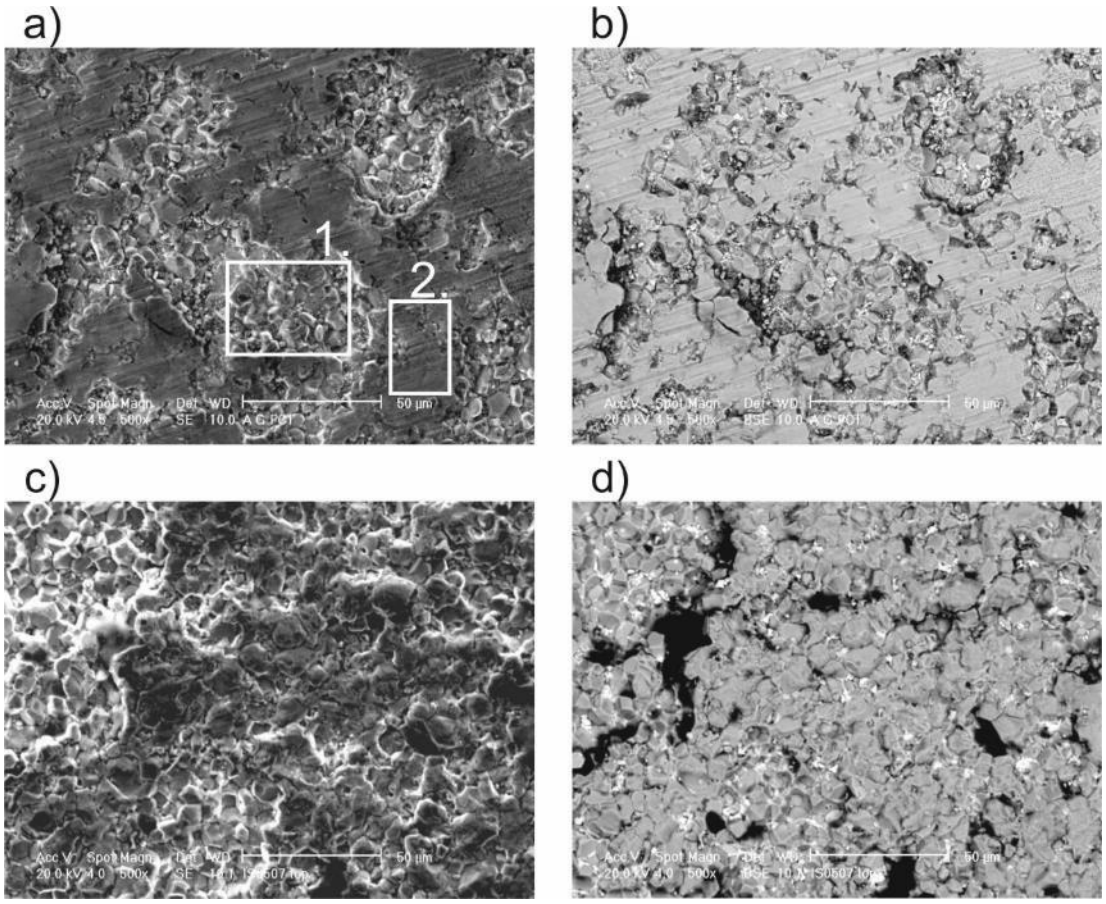

Figure 18. SEM SE a) and BSE b) images of the corroded surface of a grade M1 magnet after the BCT test for 96 h, c, d) after the HAST test for 240 hours. Pulverized (1) and undamaged or slightly corroded (2) areas detected in BCT tested magnets are marked in image a) [Unpublished].

The case of mixed corrosion mechanisms in the BCT tests was further studied by analyzing the surface and the corrosion products formed on a M1 magnet. The corrosion products were gently collected and visually categorized as black or red. In the SEM studies, two different areas were recognized: a pulverized area (Figure 19a) in the case of black corrosion products and an area where the surface was partially dissolved (Figure 19b) and contained red corrosion products (red rust). SEM images showing the morphologies and the formed corrosion products are presented in Figures 19 a-d. The elemental EDS analysis revealed that the black powder (Figure 19c) constituted mainly of the magnetic $Nd_2Fe_{14}B$ grains, both as large agglomerates and individual grains. In the former case, small amounts of the GB phase (seen white in the BSE-image) were naturally present between the matrix grains. The black corrosion product was a result of the pulverization process, as the grains were intact. The HAST tests in Publication V resulted in an identical corrosion product. The particles seen in the red rust sample had a spherical or equiaxed shape (Figure 19d), and based on the EDS spot analyses, they consisted mainly of iron and oxygen. The composition refers to iron oxides and/or

hydroxides, e.g., typical red rust similar to that of atmospheric corrosion of iron [105]. However, the composition was very heterogeneous and therefore the exact composition could not be identified based on EDS.

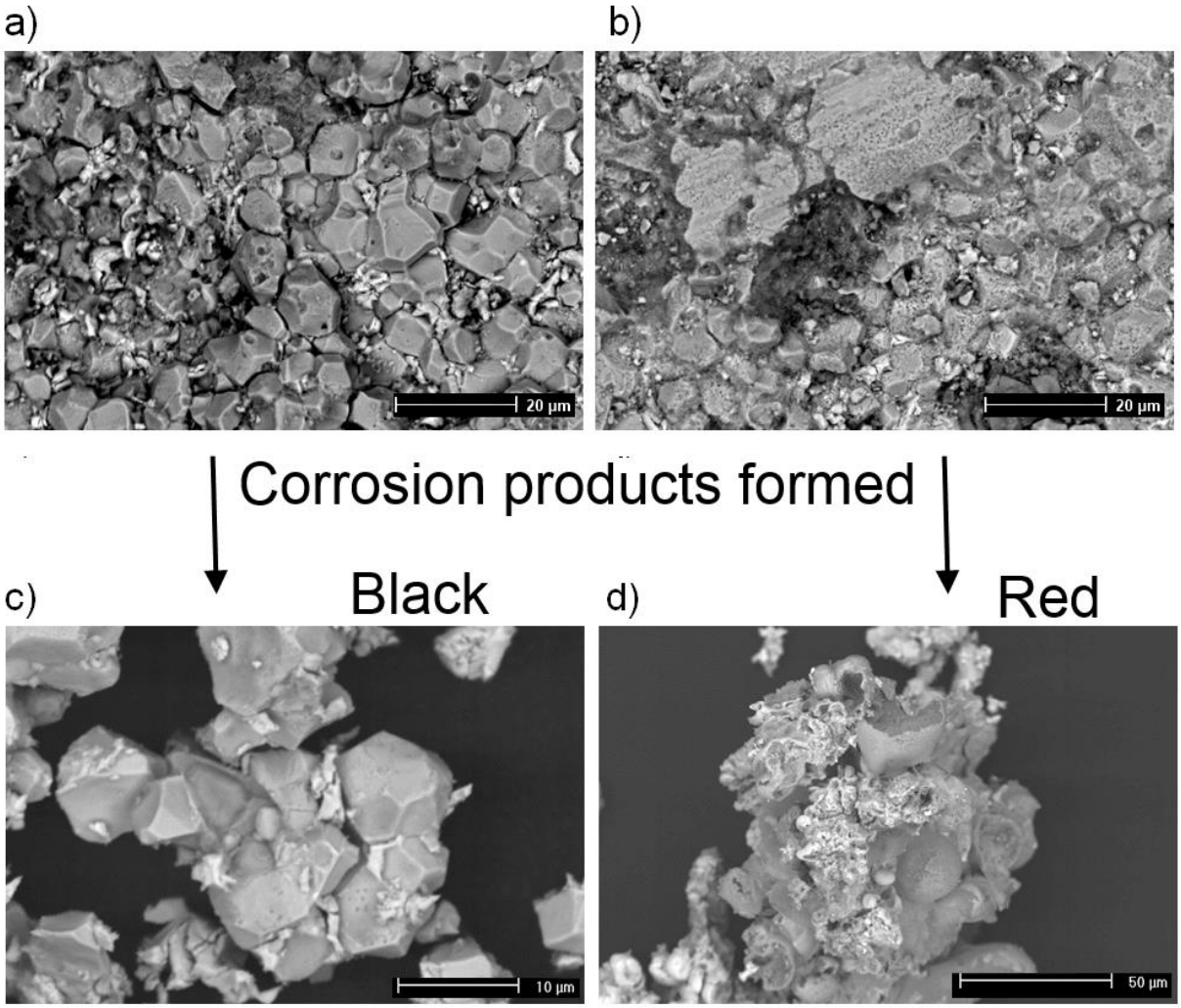

Figure 19. SEM BSE images of corroded magnets after the BCT test. Images of (a) pulverized area, (b) area with general corrosion as well as (c) red corrosion product and (d) black corrosion product collected from the SG grade specimens [Publication III – modified and corrected version].

4.2.2 Immersion

Immersion of the magnets in pure water introduced a corrosion morphology which, to the best of our knowledge, has not been reported before: locally the GB phase was retained intact, while the $Nd_2Fe_{14}B$ phase underwent dissolution. During the immersion test, the surfaces of the magnet, independently of the magnet grade, were covered by a layer of red corrosion products that was rinsed away when cleaning the specimens. Photographs of the magnet grade M3 immersed in water for 24 and 96 hours, and after a 96-hour test and removal of the

corrosion products, are shown in Figure 20. The polished mirror-like surface was partly intact, but the areas seen in black in the cleaned specimen (Figure 20c) disclosed a new type of corrosion morphology when examined with SEM. The behavior was observed with all three tested magnet grades, i.e., M1, M3 and M7.

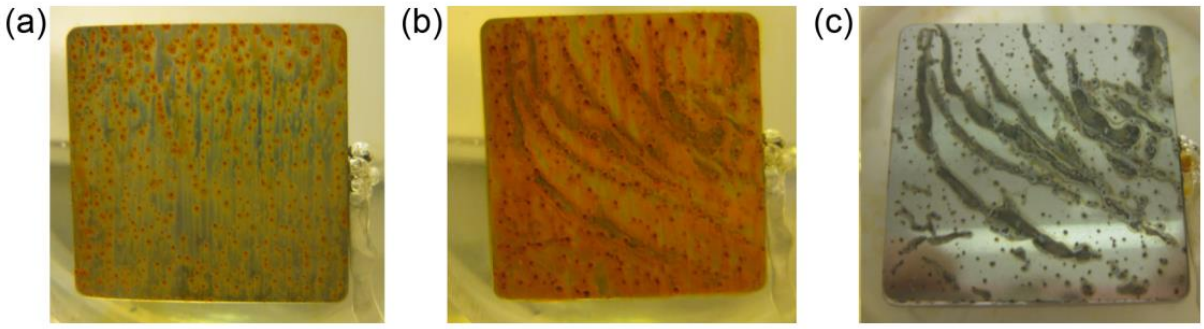

Figure 20. Photographs showing a polished immersion test specimen M3 and the formed corrosion product layer after (a) 24 h and (b) 96 h of immersion and (c) after cleaning the corrosion products from the specimen shown in b) [Publication III].

As in other exposures, an iron-rich corrosion product was formed on the magnet surfaces. Evidently the iron-rich $Nd_2Fe_{14}B$ phase had undergone oxidation in such areas. However, the Nd-rich GB phase did not dissolve or undergo any attack, as seen in the collection of SEM images in Figure 21. The GB phase formed a net-like structure protruding from the surface of each tested magnet. The GB areas were relatively thin to be accurately analyzed by EDS, but after numerous measurements their composition was disclosed to include 30–40 at.% oxygen the rest, i.e., 60–70 at.%, being neodymium or other rare-earth elements, which is a similar composition as in the as-received magnets. Water oxidized the $Nd_2Fe_{14}B$ grains, leaving the grain boundaries intact. An explanation for this could be a change in the electrochemical potentials of the phases by the change in the pH value, as predicted by the Pourbaix diagram [106]. Under immersion, the Nd-rich phases in the GB areas become cathodes and the nearby areas of the $Nd_2Fe_{14}B$ grains anodes. An earlier polarization study by Sueptitz *et al.* [107] showed that during the initial stages of immersion in distilled water, the pH level rises in front of the magnet surface and a temporary protective hydroxide layer is formed. In their study, the anodic polarization broke down the protective effect but here, as immersion was continued for 96 hours, the black areas could have been protected by such hydroxide film. The reason for the pH change near the surface could arise from the dissolution of Fe^{2+}, and as the surrounding water is stagnant, it stays near the magnet surface attracting negative charges. This theory is supported by additional tests, where such areas with preferential leaching of the matrix phase were not observed in stirred water.

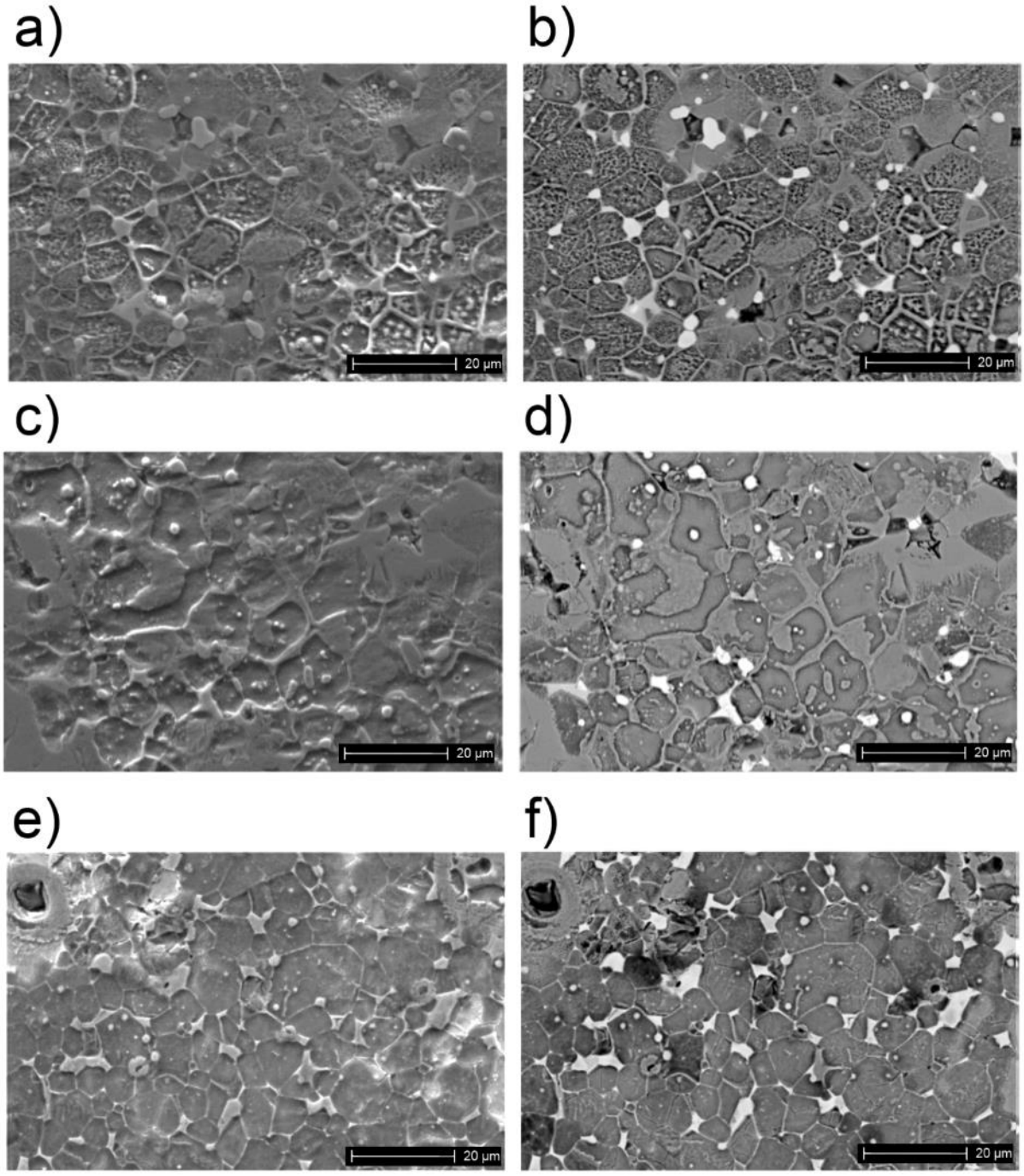

Figure 21. SEM images showing the morphology of the black areas on the surface of a magnet cleaned from the corrosion products after immersion for 96 hours in water. Both SE and BSE images of the same spot for grade M1 (a,b), M3 (c,d) and M7 (e,f) magnets are shown [Publication III].

The behavior of the magnets immersed in pure water was further studied through the open circuit potential records. Figure 22 shows the development of the OCP values during the first hour (Figure 22a) and the whole immersion period of 96 hours (Figure 22b). The OCP values

for all three magnet grades, M1, M3 and M7 (SG, IS and ICR), reached a steady-state value at the end of the 1 h stabilization period. Immediately after immersion in water, the open circuit potential of the M7 magnet was somewhat higher than the corresponding values for the M1 and M3 magnets, but it slightly decreased towards the end of the first hour of immersion, reaching the value of –435 mV after one hour. In the beginning of the immersion test, the OCP values for the M1 and M3 magnets first had a slightly decreasing trend, after which the OCP values rose again reaching the values of –416 mV for M1 and –560 mV for M3 at the end of the first hour. Based on these curves, evidence for the beneficial effect of cobalt alloying cannot be found.

During the 96 hours of immersion, all magnet grades showed fluctuations in the OCP value, but at the end of the measurement, the OCP levels of all magnet grades were within the range of 100 mV. The initial differences in the overall OCP level of the three magnets leveled off during the test period, referring to a relatively similar behavior and nature of the exposed surfaces after 96 h. It is assumed that most of the OCP fluctuations are related to the occurrence of corrosion, such as the build-up of corrosion products. As seen in Figure 20b, the corrosion product formation during 96 hours of immersion in water is evident. The fluctuations in OCP were somewhat fewer in the case of the M7 (ICR) magnet than in the case of the other two magnet grades, although measurable or visual differences in the corrosion product formation were not detected. This is supported by the SEM studies shown in Figure 21, where the corrosion behavior was similar independently of the magnet grade.

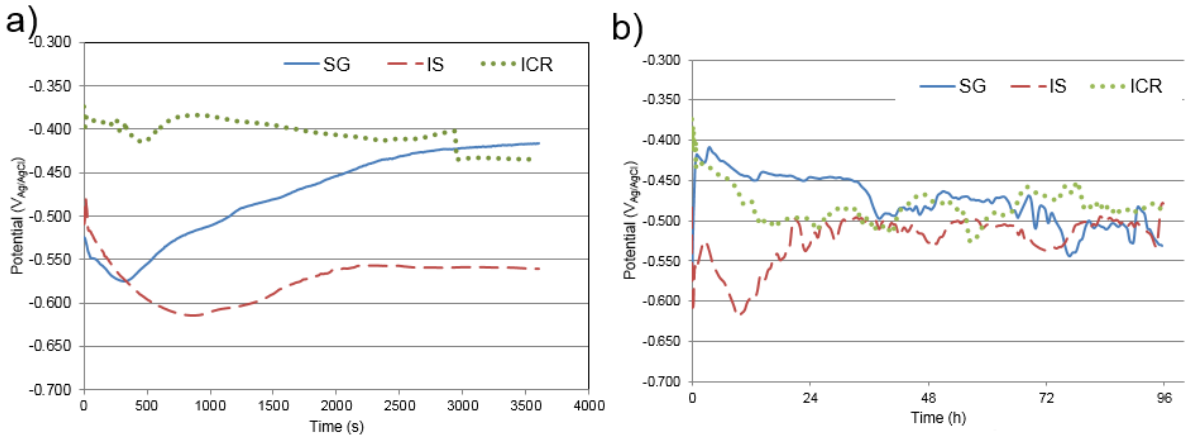

Figure 22. Open circuit potential records for magnet grades SG (M1), IS (M3) and ICR (M7) during a) the period of 1 h and b) 96 hours of immersion in water [Modified from Publication III].

The corrosion behavior of the magnets immersed in saline electrolyte was studied with polarization measurements and EIS [Publications I, II, III and VI]. The polarization curves were

Tafel extrapolated to deduce the values for the corrosion potential and the corrosion current density corresponding to the corrosion tendency and rate of each magnet grade.

The polarization measurements were performed for all magnet grades M1-M9. General observations common for all measurements can be summarized so that passivation of the magnets was not observed within the studied potential range. The magnets exhibited typical hydrogen evolution type polarization curves in the cathodic region, while the anodic sides were controlled by active dissolution. Typical polarization curves for M1, M7 and M9 are presented in Figure 23. Substitution of neodymium with cerium was not found to influence the electrochemical behavior significantly.

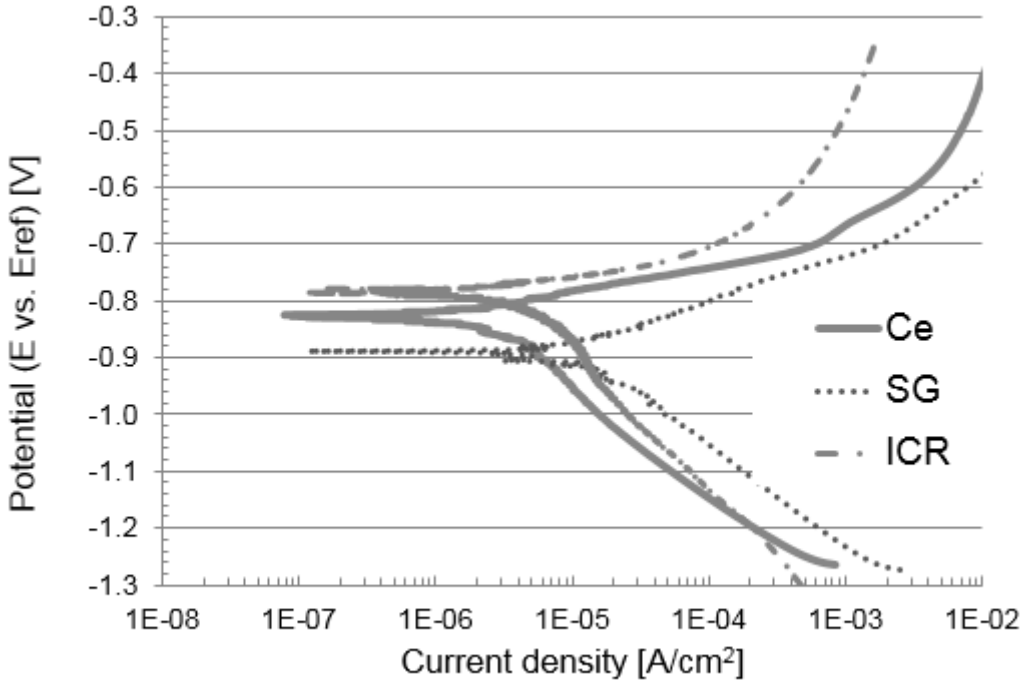

Figure 23. Potentiodynamic polarization curves for the grade M9 (Ce-alloyed), M1 (SG) and M7(ICR) magnets in NaCl solution. Potential values were determined with a Ag/AgCl reference electrode (E_{ref}) [Publication VI].

The corrosion potentials in the NaCl solution varied from -1010 to -790 mV so that the lowest values were measured for the magnet grades without cobalt alloying and the highest for the grade with the highest cobalt contents. The corrosion potential increase by the cobalt addition has been earlier reported by Sunada *et al.* [108]. The corrosion current densities deduced for the magnets varied from 1 to 61 µA/cm$^{2.}$ There was no direct correlation between the corrosion current density and any specific alloying element content, but the lowest current densities (implying lowest corrosion rate) were obtained for the cobalt-containing magnets and the highest values for those without cobalt. Some of the tested cobalt-alloyed magnets had a complex anodic branch in the polarization curve with several noses being detected. The

observed current peaks may indicate a temporary formation of a protective surface film or correspond to the presence of several corrosion reactions, most probably related to the different phases present in the microstructure.

The EIS measurements did not give simple answers concerning the corrosion resistance, especially the differences between the magnet grades. Compared to the polarization measurements, the test conditions of EIS are less aggressive due to the nearly open circuit conditions. According to the EIS studies performed on magnet grades M1-M7 in Publication I, the Nd-Fe-B magnets had several surface phenomena occurring during corrosion. Considerable variations between the replicate measurements in EIS were observed, which may be due to the reactive nature of the GB phase that affects the very small signals measured in the technique. It has been shown that the Nd-rich phase oxidizes even at room temperature [34], and it is most likely that this process is active during immersion, too.

In Publication II, the EIS measurements for two magnet grades (M1 and M7) with and without two metallic coatings were performed at increasing exposure times ranging from 30 minutes (only the stabilization period) to 168 hours of immersion in 3.5 wt.% NaCl solution. The corrosion resistance of both uncoated and coated magnets changed as a function of immersion time. In the case of uncoated magnets, the corrosion products formed on the magnet surface slowed down the corrosion process. After 30 minutes and 6 hours of immersion, the behavior of magnet grade M1 indicated lower corrosion resistance (charge transfer resistance) than that of magnet M7. After 24 hours of immersion, the difference between the magnet grades had vanished. In the case of metallic coatings, a temporary oxide film formation is suggested based on the results, but after longer immersion times in the electrolyte, pitting corrosion and thereby the exposed substrate dominate the corrosion behavior.

The EIS measurements were performed also for magnet grades M1, M3 and M7 (SG, IS and ICR) after immersion in water for 1 and 96 hours [Publication III]. Like in the case of NaCl solution, the differences in the charge transfer resistance of the magnet grades were essentially smaller after 96 hours of immersion.

The EIS measurements in Publication VI were performed for M1, M7 and M9 (SG, ICR and Ce-alloyed) at three different potentials; at 100 mV below OCP, at OCP, and at the potential 100 mV above OCP. The behavior of the ICR grade was the most stable at the studied potentials among the three studied magnet grades. The greatest differences between the three potentials were detected for the SG grade. The results suggest that alloying (Ce, Co) makes the surface processes more stable in near-OCP potential areas.

The Ce-alloyed magnets were examined with SEM again after the electrochemical measurements. SEM BSE images in Figure 24 show the surface morphology of the area

exposed to electrolyte after EIS (a) and polarization (b) experiments. Since the EIS measurement applied only 10 mV of AC, it is considered practically non-destructive. Therefore, the surface represents the same situation as if the magnet would have been immersed in a NaCl solution for about two hours. Most of the surface is similar to that of the as-polished magnets, but the areas with the GB phase seen with light grey contrast were corroded and $Nd_2Fe_{14}B$ grains therefore distinguishable. This implies a potential difference between the phases and the greatest activity of the GB phase with a light grey contrast. Anodic polarization (Figure 24b) resulted in the same mechanism, but in this case the GB phase was corroded throughout the specimen surface and dissolved completely leaving behind only the $Nd_2Fe_{14}B$ phase, which was also partially damaged (small pores) with the matrix phase loosened. The $Nd_2Fe_{14}B$ phase grains were only loosely attached to the substrate, the outermost layer of grains being already partly detached. Thereby, it can be stated that the NaCl solution as an electrolyte brings out intergranular corrosion in the Ce-alloyed magnet, similarly to the typical Nd-Fe-B magnets. Nevertheless, the oxides of neodymium are retained intact at the grain boundaries.

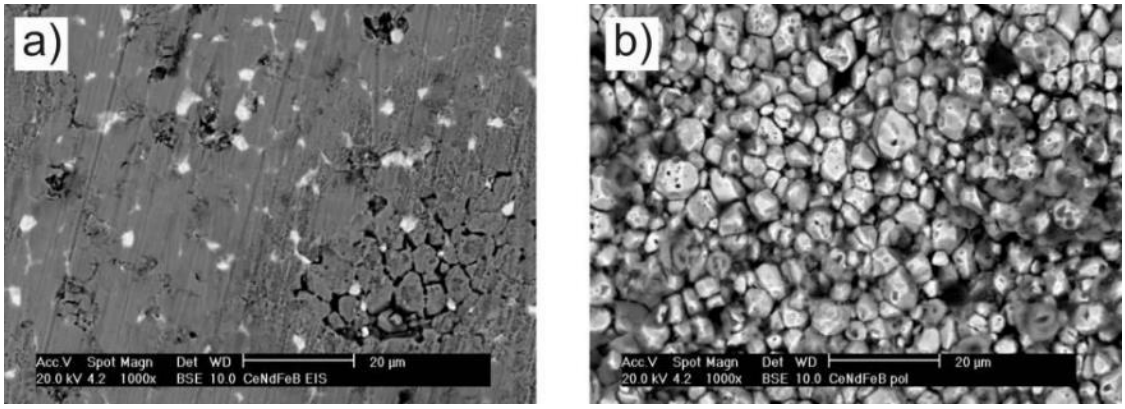

Figure 24. SEM BSE images of the Nd-Ce-Fe-B magnet subjected to EIS measurement at OCP (a) and potentiodynamic polarization (b) in 3.5 wt.% NaCl [Publication VI].

4.2.3 Summary of the corrosion mechanisms

As a summary, a schematic presentation of the corrosion mechanisms in two types of heat-humidity environments and in immersion in water is shown in Figure 25 [Publication III]. The simplified microstructure of the Nd–Fe–B magnet and the imposed environmental stresses are illustrated as the starting point for the corrosion reactions (0 hours), and the resulting microstructure after the exposure to the accelerated conditions for 96 hours is understood as the end result.

The presence of pure water vapor (Figure 25a) results in the general corrosion of the magnet and formation of a relatively thin layer of red rust. The corrosion damage is very moderate and does not result in significant material losses. In the case of pressurized water vapor (Figure

25b), the possibility of condensation of water on the magnet surface is included in the presentation. The situation can be regarded as a mixture of pressurized water vapor and liquid water and it is the most aggressive corrosion environment for the Nd–Fe–B magnets. In this case, both reported mechanisms of corrosion, i.e., selective corrosion of the GB phase and general corrosion of the $Nd_2Fe_{14}B$ grains, are present. Detachment of the $Nd_2Fe_{14}B$ phase grains, i.e., pulverization, follows the corrosion of the GB phase, but the magnet surface is also partly covered with red rust. The disintegration of the magnet structure is clearly accelerated by the applied pressure, which allows water vapor to penetrate the magnet along the grain boundaries and pores possibly present in the structure.

The detachment of individual grains and fragments of the magnet exposes new areas to the corrosive environment, which further enhances the disintegration of the magnet. The surface cannot passivate in the pressurized environment. In turn, the pressure enables the water vapor to penetrate deeper into the material.

Immersion in liquid water (Figure 25c) reveals a corrosion mechanism on the magnet surface that has not been reported before, i.e., the formation of a network of grain boundaries. Iron-rich corrosion products are detected in such areas where dissolution of the matrix phase occurs. The GB phase stays intact with the composition similar to the as-received magnets. This behavior is attributed to a formation of a weak protective hydroxide layer in stagnant water. The evaluated corrosion damage is significantly lower in the cases of exposure to the water vapor and immersion in water compared to that in pressurized water vapor.

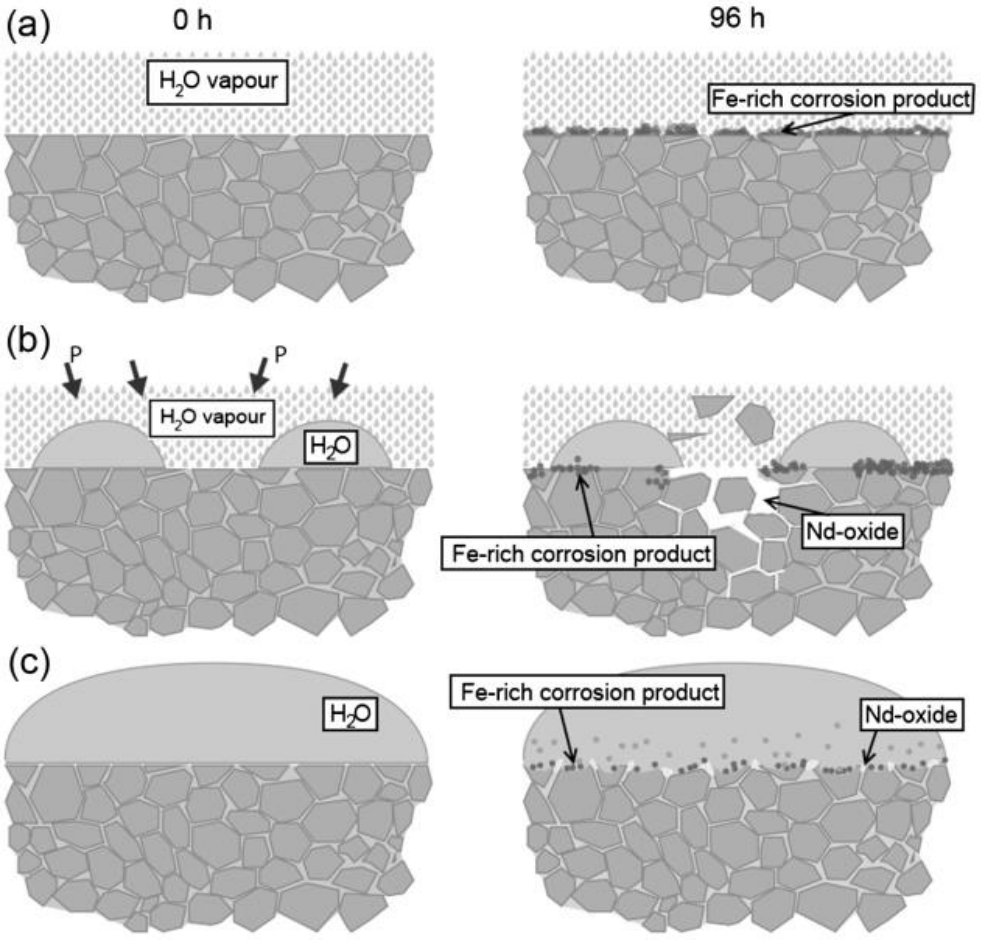

Figure 25. Schematic model for the corrosion mechanism under the three different accelerated conditions; (a) water vapor, (b) pressurized water vapor and condensation, and (c) immersion of the magnet in liquid water [Publication III].

4.3 Degradation of the magnetic properties due to corrosion

In order to understand the true corrosion losses, the weight and flux losses formed during the corrosion tests of Nd-Fe-B magnets were compared in this study. Such combined measurements of weight and flux losses related to the degradation of the magnets have not been done before. The two test durations used (96 and 240 hours) gave valuable information about the progress of corrosion. Here, not only the corrosion mechanism and the degree of corrosion were of interest, but also the knowledge of whether the degradation of the material will slow down or whether there is a risk of a total loss of the magnet at an accelerating rate. The few existing corrosion studies involving Nd-Fe-B magnets in the magnetized state have shown that the magnetization state can have a clear influence on the corrosion behavior [92–94]. Here, HAST was selected as the test method, as the corrosion mechanisms that occur

during HAST are well known, weight losses can be accurately quantified to enable the comparison between the specimens, and the magnetized state does not interfere with the test procedure (in contrast to, e.g., electrochemical measurements).

Due to the relatively high temperature of the HAST test, 130°C, the magnet grades for the tests were selected from those alloyed with dysprosium for increased stability at elevated temperatures. Otherwise, the thermal losses would dominate and the corrosion losses could not be separated from them. Grades M3 (IS) and M7 (ICR) were selected in order to compare the losses of non-cobalt containing and cobalt-containing magnet grades. The thermal stabilization treatment was performed for the magnets before the corrosion testing.

The Nd-Fe-B magnets show microcrystalline anisotropy due to the alignment of the grains during the manufacturing process. Due to the anisotropic nature, the geometry of the magnet is one of the key properties defining the produced magnetic field. Until now, the effect of magnet geometry has not been taken into account in the corrosion studies, although the anisotropic corrosion behavior in highly textured permanent magnets has been reported by Rada *et al.* [109]. In Publication V, magnets with two different geometries were tested in order to study if the corrosion behavior is affected by the geometry. All tested magnets had the passivated surface finishing and were in a magnetized state.

4.3.1 Thermal stabilization treatment

The HAST tests were performed at the temperature of 130ºC, while the thermal stabilization was performed by exposing the magnets to a slightly higher temperature of 150ºC. A similar approach and the scientific background of the stabilization treatment is described by Haavisto *et al*. [110]. The main idea of the treatment is to demagnetize the weakest domains of the magnet. Thereby, the domains that are not demagnetized by the stabilization treatment are assumed to be stable for a certain period of time when exposed to temperatures below the stabilization temperature. All tested magnets experienced flux losses in the thermal stabilization treatment. The treatment was performed in a similar manner in Publications IV and V. In Publication IV in Test Series 1, the average flux losses were 3.1±1.7% for grade IS magnets and 0.8±0.6% for grade ICR magnets. In Test Series 2, the average flux losses for IS grade magnets during the thermal stabilization treatment were 3.3±1.2%.

The focus of these studies is on the flux losses as a result of the corrosion of the magnets. Therefore, the losses caused by the temperature only had to be separated from those caused by corrosion in HAST. One set of reference magnets was placed in a laboratory furnace heated to the temperature of 130°C, while another set was left at room-temperature to study whether the magnets that were thermally stabilized at 150°C would suffer further flux losses. None of the reference samples kept at room temperature or in the furnace lost any of their magnetic

flux during the following 96 h. Thereby, it is assumed that all of the losses discussed in the following originated from the material degradation by corrosion. When discussing the flux losses resulting from corrosion, the flux value measured after the stabilization treatment is thus considered as the initial value of the magnetic flux, and all of the following flux losses are presented relative to it.

4.3.2 Corrosion of magnetized specimens

Parallel measurements of flux and weight losses were performed in Publications IV and V. The corresponding percentage weight losses were systematically smaller than the flux losses with the exception of one specimen, indicating that the total experienced flux losses do not originate from the material losses only. The percentage flux losses varied from 0.0 % to 45.6 % depending on the magnet grade and test duration. Differences in the losses between individual specimens of the same type were rather large. Two test sets were conducted. The losses of grade M7 (ICR) were negligible in Test series 1, and the following Test series 2 was conducted using grade M3 (IS) specimens only.

The heterogeneous corrosion behavior was detected visually as the preferential corrosion of the pole faces, in agreement with literature [109]. Indeed, the only measurable change in the sample dimensions in Publication IV was in the direction of the easy axis of the specimens, indicating the highest corrosion rate on the pole faces. The average thickness of the magnets after a 240 h HAST test was 3 mm, the original thickness being 4 mm. Figure 26 supports the finding of heterogeneous corrosion and shows the arrangement of the corrosion product in the magnetic field (Figure 26a), as well as the same specimen after the removal of the corrosion products (Figure 26b). The detached grains and the corrosion products on the magnet pole faces were captured and aligned to the magnetic field revealing their ferromagnetic nature. Test series 2 included flux measurements before and after the removal of the corrosion product. The results showed that the extent of flux losses increased with the removal of the corrosion products. Therefore, even if the material has detached from the magnet, it still acts as an intensifier of the produced magnetic field.

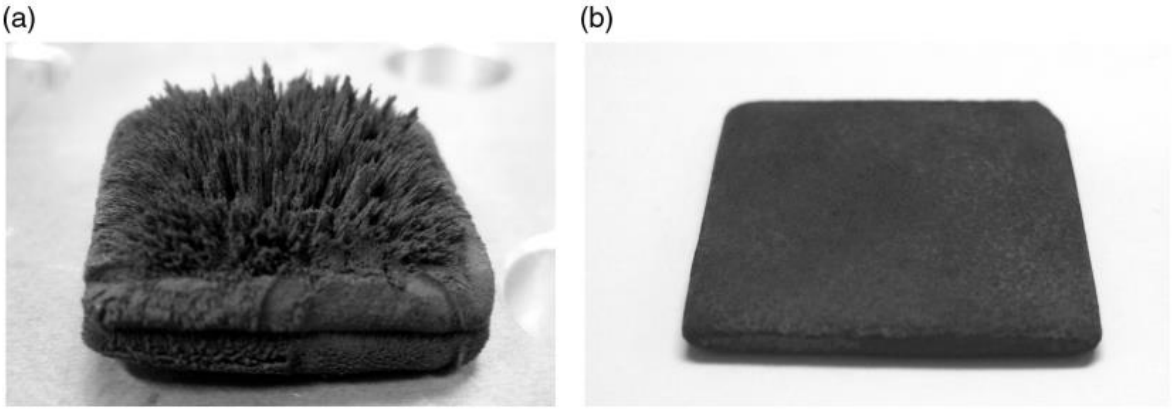

Figure 26. Heavily pulverized magnet M3 specimen (F) (a) immediately after 240 h of HAST corrosion testing conducted in the magnetized state and (b) after removal of the corrosion products [Publication IV].

In the SEM characterization of the exposed magnets, numerous subsurface cracks parallel to the surface were found in the cross-sectional specimens of grade M3 (IS) magnets, whereas no cracks were found in the M7 (ICR) magnets. The difference between the M3 (IS) magnets tested in the unmagnetized and magnetized states were further examined. The depth of the cracks varied locally. The most severe cracks, reaching to the depth of about 200 µm below the surface, were found in the specimens tested in the magnetized state. Therefore, the results suggest that cracking was more severe in the case of magnetized M3 (IS) grade magnets than in the case of the corresponding unmagnetized magnets. Figure 27 shows SEM SE and BSE cross-sectional images of a grade M3 (IS) magnet tested in the magnetized state in HAST for 240 hours. The images were taken in the BSE mode so that the $Nd_2Fe_{14}B$ phase (seen with grey contrast) and the grain-boundary phase (white contrast) are clearly distinguished. It was observed that the regions of the $Nd_2Fe_{14}B$ phase near the major cracks showed an essentially darker contrast than elsewhere in the structure, especially in the BSE images (Figure 27d). The EDS analyses disclosed that the dark regions were enriched with oxygen. Previously, similar microstructural changes due to the oxidation of the $Nd_2Fe_{14}B$ phase have been reported [111,112], but in the temperature range of 250°C to 500 °C.The mechanical degradation plays a significant role in the overall degradation process. The cracks evolved in the sub-surface regions act as pathways for the water vapor and oxygen to penetrate deeper into the structure. Oxidation of the $Nd_2Fe_{14}B$ phase probably increases the volume of the oxidized areas, resulting in higher mechanical stresses and further cracking of the structure.

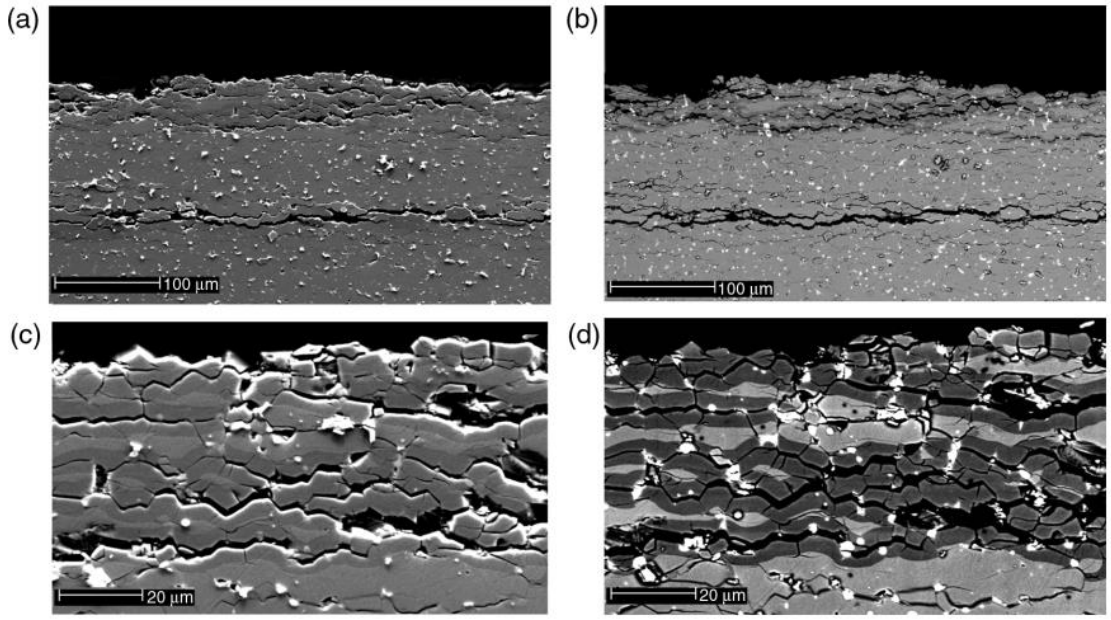

Figure 27. SEM images of the cross-section of a corroded M3 magnet (HAST 240h) at two different magnifications. The original surface of the magnet was passivated [Publication IV].

Corrosion tests of magnets with a flat and cube geometry were performed using grade M3 magnets to study the influence the different geometry of magnets and, thus, the different magnetic field they produce have on the overall corrosion behavior [Publication V]. Although the flat magnets had relatively more pole face surface compared to the cube magnets, the total losses of the flat magnets were smaller than those of the cube magnets. In both cases, the side faces were essentially intact. Therefore, it is evident that the presence and strength of the magnetic field has an impact on the corrosion performance of the magnets. The optical profilometry studies of the pole faces performed after the removal of the corrosion products verified the visual observations that the pole faces of the cube magnets corroded quite evenly (Figure 28a), whereas in the case of flat magnets (Figure 28b) the most severe (corrosion) degradation took place in the areas near the edges of the pole face surfaces. This behavior may be partly a result of the magnetic flux density distribution on the pole face surface [94]. With FEM modeling it can be explained how the geometry of the magnet influences the initial flux density on the surface: the flat magnets have a gradient flux density on the pole face as compared to the more even flux density of the magnets with a cube geometry.

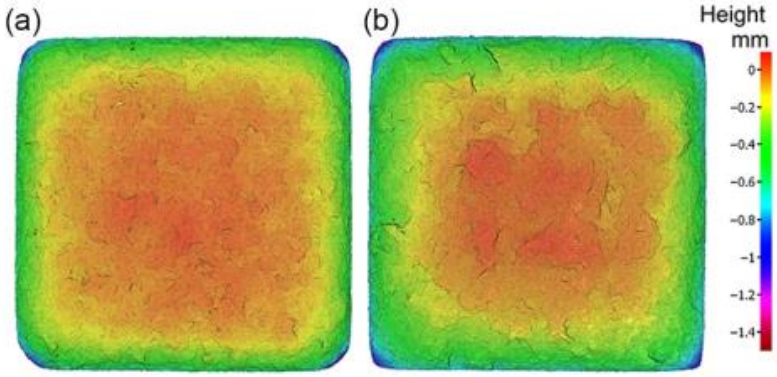

Figure 28. Optical profilometer images of the pole faces of (a) cube (10 x 10 x 10 mm) and (b) flat (10 x 10 x 5 mm) M3 magnets after 240 hour corrosion tests, demagnetization, and removal of the corrosion products [Publication V].

The depth profiles of the M3 magnets corroded in HAST for 240 hours were measured with an optical profilometer. The profiles plotted together with the demagnetization factor (DMF) are presented in Figure 29. The DMF values for the original pole faces for both magnet geometries were constructed with FEM for the same diagonal direction as the depth profiles from the profilometer measurements in Publication V. It can be seen that the two parameters correlate, i.e., in the cube magnets both DMF and the corrosion depth of the surface are quite even, whereas in flat magnets DMF falls dramatically from the center of the pole face to the corners, which is consistent with the increasing corrosion losses toward the corners.

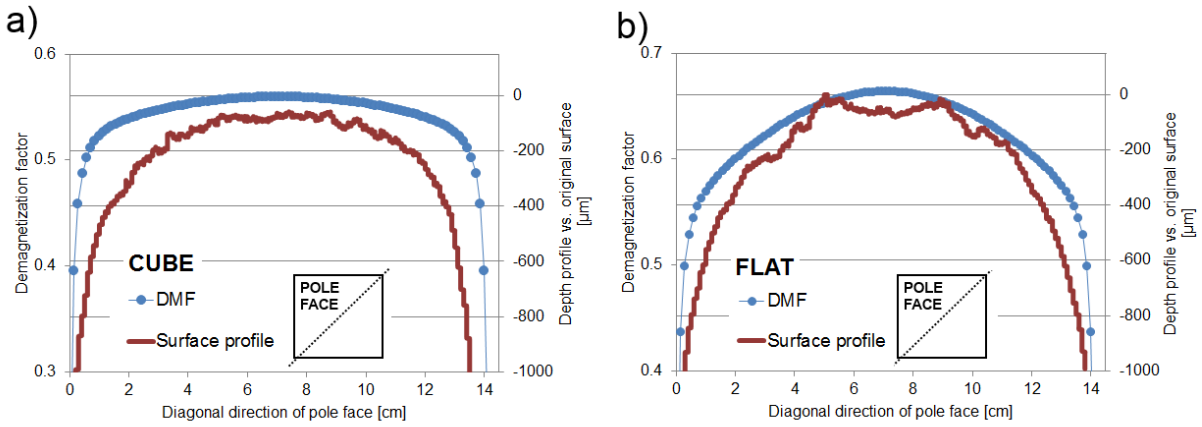

Figure 29. Variations in the modeled DMF and the measured depth profile of corroded M3 magnets along the diagonal cut of the pole face for (a) cube and (b) flat magnet geometries [Publication V].

It is evident that when exposing magnets to the corrosion of the GB phases in the magnetized state, the $Nd_2Fe_{14}B$ grains in the outermost layers of the pole faces of the magnets are attracted by the magnetic field and pulled away from the surface. The initial stage of the corrosion mechanism with both specimen geometries was similar, but the stronger magnetic

field in the case of the cube magnets due to the larger volume and total flux accelerated the corrosion as a function of time. The shape of the magnet was relevant also because the distribution of the flux density on the surface was different in the two studied cases and uneven thinning of the flat specimens was observed.

Based on these observations, the magnetic field due to the magnet itself may contribute to the detachment of the grains and, thus, to the degradation process of the magnet. These observations on the influence of the magnetic fields on the overall corrosion performance should be known when evaluating the corrosion risks of permanent magnet materials. In practice, permanent magnets are always used as part of a larger entity forming a magnetic circuit. The accelerated laboratory corrosion tests are, however, performed in so-called open magnetic circuit environments. In order to simulate the corrosion behavior in actual motor and generator applications, other components of the circuit should be taken into account in the future studies.

4.3.3 Development of the losses in the magnetic flux

The two measurement points enabled the examination of the formation of flux losses as a function of time. The development of the remaining magnetic flux of each tested grade M3 (IS) magnet (A-N) in Test series 2 are presented in Figure 30. The HH-points refer to the Helmholz coil measurements for the determination of the remaining flux (process presented in Figure 3). All flux values are expressed as percentage values of the original flux. Instead of using the average value for all specimens, the development of the flux values of each specimen is presented. The deviation between the flux values of parallel specimens is evident.

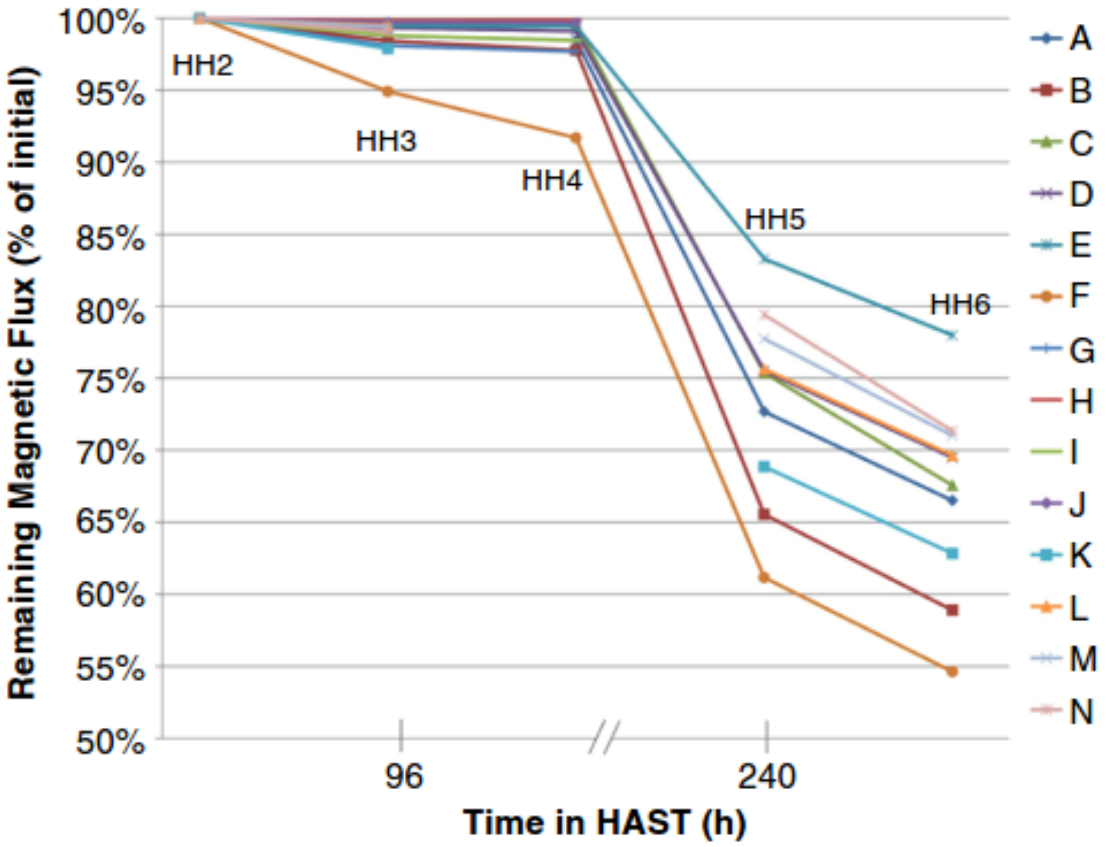

Figure 30. Development of flux values of 14 grade M3 (IS) magnets (designated by letters A through N) during the exposure to HAST in Test Series 2. The results are scaled so that the initial flux (after thermal stabilization) corresponds to 100 % [Publication IV].

When the flux loss results were analyzed as a function of time, it could be observed that the development of losses accelerated after the 96-hour measurement point. If the losses would progress linearly, the formation of flux losses during the first 96 hour-period resulted in average loss amounts between 0% and 2% per day, whereas during the last 6 days of the test (from 96 hours to 240 hours) the flux losses evolved at a daily rate of 2% to 7%. Hence, it can be safely stated that corrosion was accelerated as the test proceeded.

4.3.4 Summary of the flux losses

The corrosion testing of magnetized specimens revealed new features influencing the observed corrosion mechanism and enabled to measure the losses in magnetization. The corrosion test used, HAST, caused pulverization of the magnets without cobalt alloying. The loosened powder detached from the surface is ferromagnetic, and the magnetic field of the magnet captured the loosened powder, i.e., the detached $Nd_2Fe_{14}B$ grains near the pole surface. Sub-surface cracking resulted in the oxidation of the $Nd_2Fe_{14}B$ phase. The volume expansion due to oxidation further promotes cracking and thus accelerates the degradation.

Cobalt addition is not directly related to the amount of this mechanical degradation, but as it evidently prevents the first step of the corrosion process, i.e., corrosion of the GB phases, corrosion does not proceed to the cracking phase. Therefore, Co-alloyed magnets showed almost negligible losses.

Differences in the losses between individual specimens of the same type were large mainly due to the differences in the initiation of the corrosion process on the surface of the magnet [Publication IV]. Once corrosion initiated on the surface of a Nd-Fe-B magnet in the accelerated test, the following material removal was fairly quick and accelerated towards the end of the 10-day test. The volume and geometry of the magnet affect the strength of the magnetic field and the distribution of the flux density on the pole surface. These features were shown to affect the corrosion, as uneven thinning of the flat specimens was observed, whereas the cubic specimen shape resulted in higher weight losses with less localized corrosion. The flux losses formed during the tests were significant: such losses would probably result in a malfunction of the machine.

5 CONCLUDING REMARKS

Sintered Nd-Fe-B magnets are essential components of many modern machines. In order to build reliable motors, generators and other magnet-based systems also in the future, the corrosion behavior of the magnets has to be predictable and suitable protection needs to be applied. The development of sintered Nd-Fe-B magnets is aiming at stronger magnets with good thermal stability using less expensive and more sustainable raw materials. The corrosion resistance should not be the limiting factor in the use of permanent magnets in new potential applications and, thus, the methods to improve the corrosion stability need to be understood in more detail.

5.1 Novel scientific conclusions

The aim of this study was to achieve a deeper understanding of the corrosion behavior of sintered Nd-Fe-B magnets and thus to facilitate the development and selection of proper corrosion protection methods. The results obtained in this thesis enable the following conclusions to be drawn.

I. The level of corrosion protection needed is dependent on the corrosive environment as it largely determines the dominant corrosion mechanism. The test methods chosen for this study were selected to describe the most potential corrosive media around the magnets, mainly pure water (e.g., condensation), humidity, and saline solution (sea water environment). Already within these environments, the role of different methods to improve the corrosion resistance varied.

II. The GB phase of sintered Nd-Fe-B magnets is not inevitably the anodic phase, which will corrode first. Immersion in stagnant pure water introduced a new type of corrosion mechanism, where the matrix phase was preferentially corroded. Although the found mechanism is not the most probabilistic or severest form of corrosion in applications causing failure of magnet components, the finding emphasises that the principal corrosion mechanism may change even by small alterations in the prevailing conditions in water.

III. The measurement of the losses in the magnetic flux reveal the true functional losses and enhance the understanding of the corrosion failure mechanisms. Typically, most of the information concerning corrosion gained with material characterization is concentrated on the chemical and electrochemical reactions and their result on the surface layer. Here, measuring and understanding the development of the flux losses during corrosion tests showed the accelerating nature of microstructural degradation. In order to simulate the corrosion in

applications, magnets should be tested in the magnetized state. This is recommended not only because the loss measurements could then be done with respect to the magnetic properties, but also because the state of magnetization and flux density variations affect the amount and type of corrosion damage.

5.2 Research questions revisited

The research questions stated in Chapter 2 can be now answered as follows:

1. What corrosion protection method should be prioritized in motor and generator applications?

The potential of PMs in motor and generator applications should not be limited by corrosion resistance, if the humidity of the environment can be kept low and a protective coating layer is applied. The coating layer acts as the principal protection mechanism in normal service conditions, but cobalt alloying increases the reliability in the case of coating failures. The needed corrosion protection must be deduced according to the requirements of the application in question by studying both the magnet material and the corrosion environment. Thereby, knowing the possible corrosion mechanisms and selecting the most reasonable corrosion protection strategies, decent corrosion resistance will be achieved and the reliability of the PM machines can be assured.

Cobalt alloying inhibits the selective corrosion of the GB phase. Effective inhibition is reached with about 1 wt.% addition of cobalt. From the viewpoint of risk management, adding cobalt is a very reasonable method to prevent the rapid degradation in critical applications, such as in wind turbines, where the maintenance interval should be long. In mild corrosion environments, such as those of only moderate humidity, corrosion of the magnet is mainly general corrosion of the iron-rich matrix phase and, hence, addition of the stabilizing elements does not contribute to the prevention of the corrosion risks significantly. Instead, the surface modification by altering the roughness and morphology of the surface may act as a corrosion hindering feature in mild heat-humidity environments.

Coatings provide protection against the corrosion of sintered Nd-Fe-B magnets as long as the barrier effect is total and the coating layer is flawless or hermetic. In that case, the corrosion risks are negligible even in very harsh environments. However, in the presence of pores or other defects, whether they originate from the coating process or are formed during the use, secondary factors, such as rapid loss of adhesion between the corroded substrate and coating, will take a more important role in the overall corrosion resistance. With coated magnets, the volume expansion due to the formation of the corrosion products may further accelerate the coating delamination, exposing more of the magnet to the corrosive environment. The

corrosion resistance of the substrate magnet will play a role in the overall corrosion protection. As observed in the corrosion testing of magnet-coating pairs, those with a more active substrate material were highly damaged by corrosion when the coating failed, whereas when the substrate material was cobalt-alloyed (i.e., more corrosion resistant), the total corrosion damage was essentially less severe.

2. What are the relevant corrosion mechanisms in sintered Nd-Fe-B magnets in typical applications?

The HAST test was used to measure the stability of the GB phase. Thus, the results from these tests do not reflect the corrosion risks in moderate corrosion environments without the presence of pressurized humidity. However, it is realized that the corrosion mechanism that pressurized water vapor initiates is very severe, leading to the pulverization of the whole magnet (vs. formation of a corrosion product layer on the surface). A very similar corrosion mechanism but with minor damage was observed when the magnets were immersed in a NaCl solution. Therefore, the risk must be taken into account in demanding environments, such as offshore applications.

The examined corrosion mechanisms and the modifications of the surfaces described mainly the initial stages of the corrosion events, which are crucial for the subsequent degradation of the material. The sequence of the corrosion events and the resulting losses were further explained by the measurement of losses in the magnetization, which were found relatively higher than the corresponding weight losses. The large scatter between parallel magnet specimens that was detected in the results, especially in the measured magnetic losses during the corrosion tests with the duration of days, asserts the theory that the initiation stage of corrosion might differ between nominally identical magnets. Once initiated, (pulverization) corrosion proceeds rapidly through the grain boundaries. The sub-surface cracks parallel to the surface of the pole face developed in the near-surface regions play an important role in the further degradation as they detach larger fragments of material and also act as paths for the corrosive species to enter deeper into the material. Evidence of the oxidation of the $Nd_2Fe_{14}B$ phase along the cracks was found. The magnetized specimens showed that the microcrystalline anisotropy resulted in heterogeneous corrosion, where the pole faces degraded preferentially to the side faces.

3. What are the parameters that would best represent the true corrosion losses and could be reliably measured when evaluating the corrosion resistance of magnets?

The corrosion evaluation of magnets should be based on the losses in the magnetization during the corrosion exposure, i.e., operation. This may be done by measuring the flux losses. The results showed that the losses in the magnetization were detected prior to other physical

changes, such as weight losses or changes in the appearance. The measurements of flux losses could be used in the condition monitoring of applications (generators, motors), because they enable the corrosion detection under the coating and possibly under embedding resin.

5.3 Suggestions for future work

Future work on the sequence of events after the corrosion of the surface layers could be useful. The evolution of magnetic losses as a function of time was followed here, but more could be done by building models for the long-term corrosion performance of the magnets. New substitutes and alloying elements that are introduced due to either higher performance or lower cost requirements may change the potential of the phases. Replacing some of the critical rare-earth elements with the most promising low-cost substitute material, cerium, did not deteriorate the corrosion properties. Modern magnets also go towards smaller grain sizes and more even distribution of the GB phase, which will change the relationship of the anodic and cathodic areas on the magnet surface. Therefore, the corrosion tests should be continued and included in the development projects of new magnet materials.

REFERENCES

[1] J.M.D. Coey, Magnetism and Magnetic Materials, Cambridge University Press, 2009.

[2] M. Sagawa, S. Fujimura, N. Togawa, H. Yamamoto, Y. Matsuura, New material for permanent magnets on a base of Nd and Fe (invited), J. Appl. Phys. 55 (1984) 2083–2087.

[3] O. Gutfleisch, M. a Willard, E. Brück, C.H. Chen, S.G. Sankar, J.P. Liu, Magnetic materials and devices for the 21st century: stronger, lighter, and more energy efficient., Adv. Mater. 23 (2011) 821–842. doi:10.1002/adma.201002180.

[4] Vacuumschmelze GmbH &Co., Rare-earth permanent magnets VACODYM · VACOMAX, (2007). http://www.vacuumschmelze.com/index.php?id=1039&L=2.

[5] S.M. Lu, A review of high-efficiency motors: Specification, policy, and technology, Renew. Sustain. Energy Rev. 59 (2016) 1–12. doi:10.1016/j.rser.2015.12.360.

[6] M. Leijon, O. Danielsson, M. Eriksson, K. Thorburn, H. Bernhoff, J. Isberg, J. Sundberg, I. Ivanova, E. Sjöstedt, O. Ågren, K.E. Karlsson, A. Wolfbrandt, An electrical approach to wave energy conversion, Renew. Energy. 31 (2006) 1309–1319. doi:10.1016/j.renene.2005.07.009.

[7] N. Blažauskas, A. Pašilis, A. Knolis, Potential applications for small scale wave energy installations, Renew. Sustain. Energy Rev. 49 (2015) 297–305. doi:10.1016/j.rser.2015.04.122.

[8] G.W. Warren, K. Chang, B. Ma, C.O. Bounds, Corrosion behavior of NdFeB with Co and V additions, J. Appl. Phys. 73 (1993) 6479–6481.

[9] N.C. Ku, C. Qin, C.C. Yu, D.H.L. Ng, Corrosion resistance of NdFeB magnets coated by Al, IEEE Trans. Magn. 32 (1996) 4407–4409. doi:10.1109/20.538884.

[10] H.-H. Strehblow, P. Marcus, Fundamentals of Corrosion, in: P. Marcus (Ed.), Corros. Mech. Theory Pract., 3rd ed., CRC Press, 2012: p. 502.

[11] D.A. Jones, Principles and Prevention of Corrosion, 2nd ed., Prentice-Hall, New York, 1996.

[12] M. Arponen, Lecture, AEL Insko Seminar. Teknillis-taloudellinen materiaalinvalintaprosessi, (2015).

[13] S.D. Cramer, B.S.J. Covido, eds., ASM Handbook 13A, Corrosion: Fundamentals, Testing and Protection, ASM Handbook Committee, 2003.

[14] S. Sugimoto, Current status and recent topics of rare-earth permanent magnets, J. Phys. D. Appl. Phys. 44 (2011) 64001. doi:10.1088/0022-3727/44/6/064001.

[15] W. Rodewald, Magnets : Sintered, in: Encycl. Mater. Sci. Technol., Elsevier Science Ltd, 2001: pp. 5126–5130.

[16] W. Rodewald, Rare Earth-Transition Metal Magnets, in: H. Kronmüller, S. Parkin (Eds.), Handb. Magn. Adv. Magn. Mater., 2007. doi:10.1051/jphyscol:1985637.

[17] D. Brown, B.-M. Ma, Z. Chen, Developments in the processing and properties of NdFeB-type permanent magnets, J. Magn. Magn. Mater. 248 (2002) 432–440. doi:10.1016/S0304-8853(02)00334-7.

[18] B.E. Davies, R.S. Mottram, I.R. Harris, Recent developments in the sintering of NdFeB, Mater. Chem. Phys. 67 (2001) 272–281. doi:10.1016/S0254-0584(00)00450-8.

[19] J. Fidler, D. Suess, T. Schrefl, Rare-earth Intermetallics for Permanent Magnet Applications, in: Handb. Magn. Adv. Magn. Mater., 2007.

[20] P. Zhang, T. Ma, L. Liang, X. Liu, X. Wang, J. Jin, Y. Zhang, M. Yan, Improved corrosion resistance of low rare-earth Nd-Fe-B sintered magnets by Nd6Co13Cu grain boundary restructuring, J. Magn. Magn. Mater. 379 (2015) 186–191. doi:10.1016/j.jmmm.2014.12.044.

[21] M.O. Wenjian, Z. Lanting, L.I.U. Qiongzhen, S. Aidang, Microstructure and corrosion resistance of sintered NdFeB magnet modified by intergranular additions of MgO and ZnO, J. Rare Earths. 26 (2008) 268–273. doi:10.1016/S1002-0721(08)60079-4.

[22] J.M.D. Coey, Permanent magnets: Plugging the gap, Scr. Mater. 67 (2012) 524–529. doi:10.1016/j.scriptamat.2012.04.036.

[23] K. Bourzac, The rare-earth crisis, Technol. Rev. 114 (2011) 58. https://www.technologyreview.com/s/423730/the-rare-earth-crisis/.

[24] S. Massari, M. Ruberti, Rare earth elements as critical raw materials: Focus on international markets and future strategies, Resour. Policy. 38 (2013) 36–43. doi:10.1016/j.resourpol.2012.07.001.

[25] K. Hono, H. Sepehri-Amin, Strategy for high-coercivity Nd–Fe–B magnets, Scr. Mater. 67 (2012) 530–535. doi:10.1016/j.scriptamat.2012.06.038.

[26] S. Hoenderdaal, L. Tercero Espinoza, F. Marscheider-Weidemann, W. Graus, Can a dysprosium shortage threaten green energy technologies?, Energy. 49 (2013) 344–355. doi:10.1016/j.energy.2012.10.043.

[27] R. Goto, M. Matsuura, S. Sugimoto, N. Tezuka, Y. Une, M. Sagawa, Microstructure evaluation for Dy-free Nd-Fe-B sintered magnets with high coercivity, J. Appl. Phys. 111 (2012) 2010–2013. doi:10.1063/1.3680190.

[28] P. Mcguiness, O. Akdogan, a. Asali, S. Bance, F. Bittner, J.M.D. Coey, N.M. Dempsey, J. Fidler, D. Givord, O. Gutfleisch, M. Katter, D. Le Roy, S. Sanvito, T. Schrefl, L. Schultz, C. Schwöbl, M. Soderžnik, S. Šturm, P. Tozman, K. Üstüner, M. Venkatesan, T.G. Woodcock, K. Žagar, S. Kobe, Replacement and Original Magnet Engineering Options (ROMEOs): A European Seventh Framework Project to Develop Advanced Permanent Magnets Without, or with Reduced Use of, Critical Raw Materials, Jom. (2015). doi:10.1007/s11837-015-1412-x.

[29] K. Löewe, C. Brombacher, M. Katter, O. Gutfleisch, Temperature-dependent Dy diffusion processes in Nd–Fe–B permanent magnets, Acta Mater. 83 (2015) 248–255. doi:10.1016/j.actamat.2014.09.039.

[30] A.K. Pathak, M. Khan, K. a. Gschneidner, R.W. McCallum, L. Zhou, K. Sun, K.W. Dennis, C. Zhou, F.E. Pinkerton, M.J. Kramer, V.K. Pecharsky, Cerium: An Unlikely Replacement of Dysprosium in High Performance Nd-Fe-B Permanent Magnets, Adv. Mater. 27 (2015) 2663–2667. doi:10.1002/adma.201404892.

[31] S. Huang, H. Feng, M. Zhu, A. Li, Y. Li, Y. Sun, Y. Zhang, W. Li, Optimal design of sintered Ce9Nd21FebalB1 magnets with a low-melting-point (Ce,Nd)-rich phase, Int. J. Miner. Metall. Mater. 22 (2015) 417–422. doi:10.1007/s12613-015-1088-9.

[32] M. Hussain, L.Z. Zhao, C. Zhang, D.L. Jiao, X.C. Zhong, Z.W. Liu, Composition-dependent magnetic properties of melt-spun La or/and Ce substituted nanocomposite NdFeB alloys, Phys. B Condens. Matter. 483 (2016) 69–74. doi:10.1016/j.physb.2015.12.033.

[33] M. Zakotnik, I.R. Harris, a. J. Williams, Possible methods of recycling NdFeB-type sintered magnets using the HD/degassing process, J. Alloys Compd. 450 (2008) 525–531. doi:10.1016/j.jallcom.2007.01.134.

[34] J.P. Meakin, J.D. Speight, R.S. Sheridan, A. Bradshaw, I.R. Harris, A.J. Williams, A. Walton, 3-D Laser Confocal Microscopy Study of the Oxidation of NdFeB Magnets in Atmospheric Conditions, Appl. Surf. Sci. 378 (2016) 540–544. doi:10.1016/j.apsusc.2016.03.182.

[35] W. Rodewald, B. Wall, W. Fernengel, Grain Growth Kinetics in Sintered Nd-Fe-B Magnets, IEEE Trans. Magn. 33 (1997) 3841–3843.

[36] J. Fidler, On the role of the Nd-rich phases in sintered Nd-Fe-B magnets, IEEE Trans. Magn. 23 (1987) 2106–2108.

[37] X. Fu, X. Han, Z. Du, H. Feng, Y. Li, Microstructural investigation of Nd-rich phase in sintered Nd-Fe-B magnets through electron microscopy, J. Rare Earths. 31 (2013) 765–771. doi:10.1016/S1002-0721(12)60355-X.

[38] T.G. Woodcock, Y. Zhang, G. Hrkac, G. Ciuta, N.M. Dempsey, T. Schrefl, O. Gutfleisch, D. Givord, Understanding the microstructure and coercivity of high performance NdFeB-based magnets, Scr. Mater. 67 (2012) 536–541. doi:10.1016/j.scriptamat.2012.05.038.

[39] W. Mo, L. Zhang, Q. Liu, A. Shan, J. Wu, M. Komuro, Dependence of the crystal structure of the Nd-rich phase on oxygen content in an Nd–Fe–B sintered magnet, Scr. Mater. 59 (2008) 179–182. doi:10.1016/j.scriptamat.2008.03.004.

[40] T.G. Woodcock, O. Gutfleisch, Multi-phase EBSD mapping and local texture analysis in NdFeB sintered magnets, Acta Mater. 59 (2011) 1026–1036. doi:10.1016/j.actamat.2010.10.033.

[41] Y. Shinba, T.J. Konno, K. Ishikawa, K. Hiraga, M. Sagawa, Transmission electron microscopy study on Nd-rich phase and grain boundary structure of Nd–Fe–B sintered magnets, J. Appl. Phys. 97 (2005) 53504. doi:10.1063/1.1851017.

[42] V. Raghavan, B-Fe-Nd (Boron-Iron-Neodymium), J. Phase Equilibria. 24 (2003) 451–454.

[43] J. Fidler, T. Schrefl, D. Suess, Grain boundaries in high performance magnets, reasons for poor or excellent properties?, in: I.R. Harris, I.P. Jones (Eds.), Proc. Work. Grain Boundaries, Inst. Mater. Univ. Birmingham, 2001: pp. 147–163.

[44] Z. Hu, G. Liu, H. Wang, Effect of niobium on thermal stability and impact toughness of Nd-Fe-B magnets with ultra-high intrinsic coercivity, J. Rare Earths. 29 (2011) 243–246. doi:10.1016/S1002-0721(10)60439-5.

[45] R.S. Mottram, A.J. Williams, I.R. Harris, The effects of blending additions of copper and cobalt to Nd16Fe76B8 milled powder to produce sintered magnets, J. Magn. Magn. Mater. 234 (2001) 80–89. doi:/10.1016/S0304-8853(01)00067-1.

[46] W. Cheng, W. Li, C. Li, S. Dong, The magnetic properties , thermal stability and microstructure of Nd – Fe – B / Ga sintered magnets prepared by blending method, J. Magn. Magn. Mater. 234 (2001) 274–278.

[47] W. Fernengel, W. Rodewald, R. Blank, P. Schrey, M. Katter, B. Wall, The influence of Co on the corrosion resistance of sintered N d - F e - B magnets, J. Magn. Magn. Mater. (1999) 9–11.

[48] W. Liu, C. Sun, M. Yue, H. Sun, D. Zhang, J. Zhang, X. Yi, J. Chen, Improvement of coercivity and corrosion resistance of Nd-Fe-B sintered magnets by doping aluminium nano-particles, J. Rare Earths. 31 (2013) 65–68. doi:10.1016/S1002-0721(12)60236-1.

[49] R.S. Mottram, A.J. Williams, I.R. Harris, Blending additions of cobalt to Nd Fe B milled powder to produce sintered magnets, J. Magn. Magn. Mater. 217 (2000) 27–34.

[50] R.S. Mottram, A.J. Williams, I.R. Harris, Blending additions of aluminium and cobalt to Nd Fe B milled powder to produce sintered magnets, 222 (2000) 305–313.

[51] A.S. Kim, F.E. Camp, Effect of Minor Grain Boundary Additives on the Magnetic Properties of NdFeB Magnets, IEEE Trans. Magn. 31 (1995) 3620–3622.

[52] A.S. Kim, Effect of oxygen, carbon, and nitrogen contents on the corrosion resistance of Nd-Fe-B magnets, Trans. Magn. 26 (1990) 1936–1938.

[53] W. Kaszuwara, M. Leonowicz, Long-term corrosion tests on Nd – Fe – B sintered magnets, Mater. Lett. (1999) 18–22.

[54] Q. Zhou, Z.W. Liu, X.C. Zhong, G.Q. Zhang, Properties improvement and structural optimization of sintered NdFeB magnets by non-rare earth compound grain boundary diffusion, Mater. Des. 86 (2015) 114–120. doi:10.1016/j.matdes.2015.07.067.

[55] P. Zhang, L. Liang, J. Jin, Y. Zhang, X. Liu, M. Yan, Magnetic properties and corrosion resistance of Nd-Fe-B magnets with Nd64Co36 intergranular addition, J. Alloys Compd. 616 (2014) 345–349. doi:10.1016/j.jallcom.2014.07.085.

[56] NdFeB-Info.com, Coatings, (n.d.). http://www.ndfeb-info.com/coatings.aspx.

[57] A.S. Kim, Permanent Magnets: Corrosion Properties, in: Encycl. Mater. Sci. Technol., Elsevier Science Ltd., 2001: pp. 6812–6815.

[58] A. Walton, J.D. Speight, A.J. Williams, I.R. Harris, A zinc coating method for Nd–Fe–B magnets, J. Alloys Compd. 306 (2000) 253–261. doi:10.1016/S0925-8388(00)00773-8.

[59] R. Hilzinger, W. Rodewald, Magnetic Materials - Fundamentals, Products, Properties, Applications, Publicis Publishing, Erlangen, 2013.

[60] T. Xie, S. Mao, C. Yu, S. Wang, Z. Song, Structure, corrosion, and hardness properties of Ti/Al multilayers coated on NdFeB by magnetron sputtering, Vacuum. (2012). doi:10.1016/j.vacuum.2012.03.019.

[61] X.K. Yang, Q. Li, S.Y. Zhang, X.K. Zhong, Y. Dai, F. Luo, Electrochemical corrosion behaviors and protective properties of Ni-Co-TiO2 composite coating prepared on sintered NdFeB magnet, Mater. Corros. 61 (2010) 618–625. doi:10.1002/maco.200905449.

[62] A. Ali, A. Ahmad, K.M. Deen, Multilayer ceramic coating for impeding corrosion of sintered NdFeB magnets, J. Rare Earths. 27 (2009) 1003–1007. doi:10.1016/S1002-0721(08)60357-9.

[63] I. Rampin, F. Bisaglia, M. Dabalà, Corrosion Properties of NdFeB Magnets Coated by a Ni/Cu/Ni Layer in Chloride and Sulfide Environments, J. Mater. Eng. Perform. 19 (2010) 970–975. doi:10.1007/s11665-009-9568-6.

[64] Y. Huang, H. Li, M. Zuo, L. Tao, W. Wang, J. Zhang, Q. Tang, P. Bai, Corrosion resistance of sintered NdFeB coated with SiC/Al bilayer thin films by magnetron sputtering, J. Magn. Magn. Mater. 409 (2016) 39–44. doi:10.1016/j.jmmm.2016.02.006.

[65] J. Li, S. Mao, K. Sun, X. Li, Z. Song, AlN/Al dual protective coatings on NdFeB by DC magnetron sputtering, J. Magn. Magn. Mater. 321 (2009) 3799–3803. doi:10.1016/j.jmmm.2009.07.039.

[66] F. Liu, Q. Li, X.K. Yang, Y. Dai, F. Luo, S.Y. Wang, H.X. Zhang, Corrosion resistance of environment-friendly sealing layer for Zn-coated sintered NdFeB magnet, Mater. Corros. 62 (2011) 1141–1148. doi:10.1002/maco.201006039.

[67] X. Yang, Q. Li, S. Zhang, F. Liu, S. Wang, H. Zhang, Microstructure characteristic and excellent corrosion protection properties of sealed Zn–TiO2 composite coating for sintered NdFeB magnet, J. Alloys Compd. 495 (2010) 189–195. doi:10.1016/j.jallcom.2010.01.117.

[68] L. Song, Y. Wang, W. Lin, Q. Liu, Primary investigation of corrosion resistance of Ni-P/TiO2 composite film on sintered NdFeB permanent magnet, Surf. Coatings Technol. 202 (2008) 5146–5150. doi:10.1016/j.surfcoat.2008.05.025.

[69] M. Yan, H.G. Ying, T.Y. Ma, Preparation of coatings with high adhesion strength and high corrosion resistance on sintered Nd–Fe–B magnets through electroless plating, Mater. Chem. Phys. 113 (2009) 764–767. doi:10.1016/j.matchemphys.2008.08.048.

[70] S. Attanasio, Corrosion of rapidly solidified neodymium-iron-boron (Nd_Fe_B) permanent magnets and protection via sacrificial zinc coatings, Mater. Sci. Eng. A. 198 (1995) 25–34. doi:10.1016/0921-5093(95)80055-Y.

[71] J.L. Xu, Z.C. Zhong, Z.X. Huang, J.M. Luo, Corrosion resistance of the titania particles enhanced acrylic resin composite coatings on sintered NdFeB permanent magnets, J. Alloys Compd. 570 (2013) 28–33. doi:10.1016/j.jallcom.2013.03.033.

[72] Handbook of Chemistry and Physics, 72nd ed., CRC Press, USA, 1991.

[73] F.T. Cheng, H.C. Man, W.M. Chan, C.W. Cheng, W.O. Chan, Corrosion protection of Nd–Fe–B magnets by bismaleimide coating, J. Appl. Phys. 85 (1999) 5690. doi:10.1063/1.369842.

[74] J.L. Xu, Z.X. Huang, J.M. Luo, Z.C. Zhong, Effect of titania particles on the microstructure and properties of the epoxy resin coatings on sintered NdFeB permanent magnets, J. Magn. Magn. Mater. 355 (2014) 31–36. doi:10.1016/j.jmmm.2013.11.050.

[75] P.R. Roberge, Corrosion Engineering, Principles and Practice, 1st ed., McGraw-Hill Companies, Inc., USA, 2008.

[76] M.M. Codescu, W. Kappel, M. Dumitrache, D. Popa, Corrosion tests on alloys and permanent magnets based on NdFeB, used in aerospace industry, J. Optoelectron. Adv. Mater. 10 (2008) 790–793.

[77] C.W. Cheng, H.C. Man, F.T. Cheng, Magnetic and Corrosion characteristics of Nd-Fe-B magnet with various surface coatings, IEEE Trans. Magn. 33 (1997) 3910–3912.

[78] T. Minowa, M. Yoshikawa, M. Honshimn, Improvement of the corrosion resistance on Nd-Fe-B magnet with nickel plating, IEEE Trans. Magn. 25 (1989) 3776–3778.

[79] J.R. Scully, J.A. Ellor, J. Repp, Section IV: Testing for Corrosion Types Uniform Corrosion, in: R. Baboian (Ed.), Corros. Tests Stand. Appl. Interpret. (2nd Ed. (MNL 20), ASTM International,

2005.

[80] R. Singleton, Cabinet Testing, in: S.D. Cramer, B.S.J. Covino (Eds.), ASM Handbook, Vol. 13A - Corros. Fundam. Testing, Prot., ASM International, 2003: pp. 471–477.

[81] A.S. Kim, F.E. Camp, T. Lizzi, Hydrogen induced corrosion mechanism in NdFeB magnets, J. Appl. Phys. 79 (1996) 4840–4842. doi:10.1063/1.361626.

[82] M. Katter, L. Zapf, R. Blank, W. Fernengel, W. Rodewald, Corrosion Mechanism of RE–Fe–Co–Cu– Ga–Al–B Magnets, IEEE Trans. Magn. 37 (2001) 2474–2476. doi:10.1109/20.951207.

[83] M. Haavisto, Studies on the Time-Dependent Demagnetization of Sintered NdFeB Permanent Magnets, Doctoral Thesis, Tampere University of Technology, Tampere, 2013. https://dspace.cc.tut.fi/dpub/handle/123456789/21839.

[84] C. Gaona-Tiburcio, F. Almeraya-Calderon, J.G. Chacon-Nava, J.A. Matutes-Aquino, A. Martinez-Villafane, Electrochemical response of permanent magnets in different solutions, J. Alloys Compd. 369 (2004) 78–80. doi:10.1016/j.jallcom.2003.09.050.

[85] H. Xie, J. Zhao, Y. Yu, New Achievements in NdFeB Mass Production, J. Iron Steel Res. Int. 13 (2006) 324–330. doi:10.1016/S1006-706X(08)60203-4.

[86] N. Sinnadurai, The use and abuse of HAST, in: Proc. Third ESA Electron. Conf., Noordwijk, 1997: pp. 375–379.

[87] J.J. Licari, Coating Materials for Electronic Applications - Polymers, Processes, Reliability, Testing, William Andrew Publishing/Noyes, 2003. http://app.knovel.com/hotlink/toc/id:kpCMEAPPR1/coating-materials-electronic/coating-materials-electronic (accessed April 13, 2016).

[88] W. Rodewald, R. Blank, B. Wall, G.W. Reppel, H.D. Zilg, Production of Sintered Nd-Fe-B Magnets with a Maximum Energy Density of 53 MGOe, in: Proc. 16th Int. Work. RE Magnets Their Appl. Sendai, Japan, 2000: pp. 119–126.

[89] S. Hirosawa, H. Tomizawa, S. Mino, K. Tokuhara, Improvements of Coercivity and Corrosion Resistance in Nd-Fe-Co-B Sintered Magnet by Addition of V or Mo, IEEE Traslation J. Magn. Japan. 6 (1991) 901–907. doi:0882-4959/91/$12.00.

[90] G. Yan, A.J. Williams, I.R. Harris, The effect of density on the corrosion of NdFeB magnets, J. Alloys Compd. 292 (1999) 266–274. doi:10.1016/S0925-8388(99)00443-0.

[91] ASTM International, A1071/A1071M, Standard Test Method for Evaluating Hygrothermal Corrosion Resistance of Permanent Magnet Alloys, (2011). doi:10.1520/A1071.

[92] M. Moore, R. Sueptitz, A. Gebert, L. Schultz, O. Gutfleisch, Impact of magnetization state on the corrosion of sintered Nd-Fe-B magnets for e-motor applications, Mater. Corros. 65 (2014) 891–896. doi:10.1002/maco.201206978.

[93] I. Costa, M.C.L. De Oliveira, H.G. de Melo, R.N. Faria, The effect of the magnetic field on the corrosion behavior of Nd-Fe-B permanent magnets, J. Magn. Magn. Mater. 278 (2004) 348–358. doi:10.1016/j.jmmm.2003.12.1320.

[94] R. Sueptitz, K. Tschulik, M. Uhlemann, M. Katter, L. Schultz, A. Gebert, Effect of magnetization state on the corrosion behaviour of NdFeB permanent magnets, Corros. Sci. 53 (2011) 2843–2852. doi:10.1016/j.corsci.2011.05.022.

[95] JEDEC Solid State Technology Association, JESD22-A101C Steady State Temperature Humidity Bias Life Test, Standard. (2009).

[96] International Organization for Standardization (ISO), ISO 9227:2012 - Corrosion tests in artificial atmospheres. Salt spray tests, (2012).

[97] JEDEC Solid State Technology Association, JESD22-A104D Temperature Cycling, Test. (2005).

[98] E.N. Kablov, A.F. Petrakov, V.P. Piskorevskii, R.A. Valeev, E.B. Chabina, Effect of cerium and yttrium on the magnetic properties and phase composition of materials of the Nd-Dy-Fe-Co-B system, Met. Sci. Heat Treat. 47 (2005) 462–466. doi:10.1007/s11041-006-0011-4.

[99] E. Isotahdon, E. Huttunen-Saarivirta, V.-T. Kuokkala, The role of surface modification by phosphating in corrosion protection of sintered Nd-Fe-B magnets, in: EUROCORR Conf. Proc., 2014.

[100] N.A. Patankar, Mimicking the lotus effect: Influence of double roughness structures and slender pillars, Langmuir. 20 (2004) 8209–8213. doi:10.1021/la048629t.

[101] E. Isotahdon, E. Huttunen-Saarivirta, V.-T. Kuokkala, M. Paju, Competing corrosion mechanisms in sintered Nd-Fe-B magnets, in: S. Tuominen, M. Haavisto (Eds.), Proc. Appl. Magn. Mater. 2013 Conf., Pori, 2013: pp. 6–11.

[102] J. Liu, Some Design Considerations Using Permanent Magnets, Magn. - Bus. Technol. (2016). http://www.magneticsmagazine.com/main/articles/some-design-considerations-using-permanent-magnets/.

[103] Y. Heng Xiu, D. Yong, S. Zhen Lun, The analysis of adhesion failure between Ni-coating and sintered NdFeB substrate, J. Phys. Conf. Ser. 266 (2011) 12053. doi:10.1088/1742-6596/266/1/012053.

[104] M. Sagawa, S. Fujimura, H. Yamamoto, Y. Matsuura, K. Hiraga, Permanent magnet materials based on the rare earth-iron-boron tetragonal compounds, IEEE Trans. Magn. 20 (1984) 1584–1589. doi:10.1109/TMAG.1984.1063214.

[105] C. Leygraf, Atmospheric Corrosion, in: P. Marcus (Ed.), Corros. Mech. Theory Pract., CRC Press, 2012: p. 502.

[106] M. Pourbaix, Atlas of electrochemical equilibria in aqueous solutions, Pergamon Press Ltd, Great Britain, 1966.

[107] R. Sueptitz, M. Uhlemann, a. Gebert, L. Schultz, Corrosion, passivation and breakdown of passivity of neodymium, Corros. Sci. 52 (2010) 886–891. doi:10.1016/j.corsci.2009.11.008.

[108] S. Sunada, K. Majima, Y. Akasofu, Y. Kaneko, Corrosion assessment of Nd–Fe–B alloy with Co addition through impedance measurements, J. Alloys Compd. 412 (2006) 1373–1376. doi:10.1016/j.jallcom.2005.04.039.

[109] M. Rada, a. Gebert, I. Mazilu, K. Khlopkov, O. Gutfleisch, L. Schultz, W. Rodewald, Corrosion studies on highly textured Nd–Fe–B sintered magnets, J. Alloys Compd. 415 (2006) 111–120. doi:10.1016/j.jallcom.2005.07.063.

[110] M. Haavisto, H. Kankaanpää, T. Santa-Nokki, S. Tuominen, M. Paju, Effect of Stabilization Heat Treatment on Time-Dependent Polarization Losses in Sintered Nd-Fe-B Permanent Magnets, EPJ Web Conf. 40 (2013) 6001. doi:10.1051/epjconf/20134006001.

[111] I. Skulj, H.E. Evans, I.R. Harris, Oxidation of NdFeB-type magnets modified with additions of Co, Dy, Zr and V, J. Mater. Sci. 43 (2008) 1324–1333. doi:10.1007/s10853-007-2229-y.

[112] Y. Li, H.E. Evans, I.R. Harris, I.P. Jones, The Oxidation of NdFeB Magnets, Oxid. Met. 59 (2003) 167–182. doi:10.1023/A:1023078218047.

Tampereen teknillinen yliopisto
PL 527
33101 Tampere

Tampere University of Technology
P.O.B. 527
FI-33101 Tampere, Finland

ISBN 978-952-15-3911-4
ISSN 1459-2045